Interpreting plant-sampled $\Delta^{14}CO_2$ to study regional anthropogenic CO_2 signals in Europe

D. N. Bozhinova

Interpreting plant-sampled $\Delta^{14}CO_2$ to study regional anthropogenic CO_2 signals in Europe

D. N. Bozhinova

Thesis
submitted in fulfilment of the requirements for the degree of doctor
at Wageningen University
by the authority of the Rector Magnificus
Prof. Dr A.P.J. Mol,
in the presence of the
Thesis Committee appointed by the Academic Board
to be defended in public
on Wednesday 21 October 2015
at 1:30 p.m. in the Aula.

Contents

1
Introduction

Anthropogenic activities are changing our environment. Gaseous and particulate man-made emissions to the atmosphere modify its composition, chemistry, and dynamical behavior (IPCC, 2013). The burning of fossil fuels is a prominent process, which contributes significantly to these changes. Fossil fuel combustion releases large quantities of CO_2 into the air, perturbing the natural carbon cycle from its average pre-industrial atmospheric concentrations of about 280±10 ppm (Smith et al., 1999; Indermuhle et al., 1999) to just around 400 ppm nowadays. The consequences for the Earth system are ranging from the global scale with the changes in the climate system, down to local effects on plant species through CO_2 fertilization effects. The monitoring and forecast of the atmospheric CO_2 concentrations are at the foundation of any plan to mitigate and adapt to the large spectrum of future impacts expected from the continuously rising CO_2 levels. Top-down verification of existing inventory-based anthropogenic emission maps is still a challenge for the scientific community, especially on the regional and national scales. Thus, there is a continuous search for new experimental techniques that could provide useful and independent data that helps to disaggregate the carbon cycle into its natural and anthropogenic components.

In this thesis, I explore the possible use and quantitative interpretation of the radiocarbon (^{14}C) content in plants as a measure of the fossil fuel CO_2 levels in the regional atmosphere. In this introduction, I present first the different components of the carbon cycle and their importance over Europe. Next I introduce the $^{14}CO_2$ cycle and its relevance to the fossil fuel CO_2 content in the atmosphere. I discuss the advantages and disadvantages of the plant-sampling technique among other alternatives employed to observe the relative atmospheric

$^{14}CO_2$ content (denoted hereafter as $\Delta^{14}CO_2$). After this, I outline the important role played by numerical models for the accurate estimation of atmospheric and plant $\Delta^{14}CO_2$. Finally, I present the research questions that are addressed in this dissertation.

1.1 The carbon cycle

The carbon cycle is a natural mechanism, in which carbon atoms are transported between the atmosphere, biosphere, hydrosphere and lithosphere through various biochemical and physical processes (Figure 1.1). The rate of the exchange between these carbon "pools", in combination with their size, defines the average residence time of carbon in a specific pool. For instance, the atmosphere currently holds 800 PgC and the average residence time of carbon in it is less than 4 years. The different sizes and time-scales of the various carbon pools have important consequences for the dynamics of the carbon cycle and its ability to react to changes in the connected system. For example, far more carbon is stored in the deep ocean than in the atmosphere, biosphere and the surface ocean combined, and this pool has the capacity to absorb even more. However, its exchange rate with the surface ocean is quite slow, meaning that even though the two pools are connected, an increase in the CO_2 content in the surface waters will propagate much slower to the deep ocean than it will to the atmosphere.

Due to the large interactions with the biosphere and surface oceans, the atmosphere is the pool with the shortest residence time in the carbon cycle. Every year more than 25% of its total carbon content is transported through photosynthesis, soil and plant respiration and air-sea gas exchange in and out of the atmosphere. In the pre-industrial era the net of the natural flux of CO_2 to the atmosphere was close to zero and for thousands of years the atmospheric levels of CO_2 were relatively stable at around 280 ppm. In more recent times, human activities, characterized by e.g. land-use change and combustion of fossil fuels, have initiated an additional "anthropogenic" flux of CO_2 to the atmosphere, which has perturbed the natural balance of the system.

Using the conservation of mass, the changes in the atmospheric CO_2 content can be described through the contributions of the net mass fluxes from different sources and sinks, resulting in a mass balance equation like Equation 1.1.

$$\frac{dC}{dt} = F_{ocean} + F_{biosphere} + F_{anthropogenic} \tag{1.1}$$

On the global and annual scale, the fluxes are commonly reported in PgC/year. A more complete expression splits the net fluxes into their gross contributions (e.g. $F_{ocean} = F_{ocean}^{out} - F_{ocean}^{in}$),
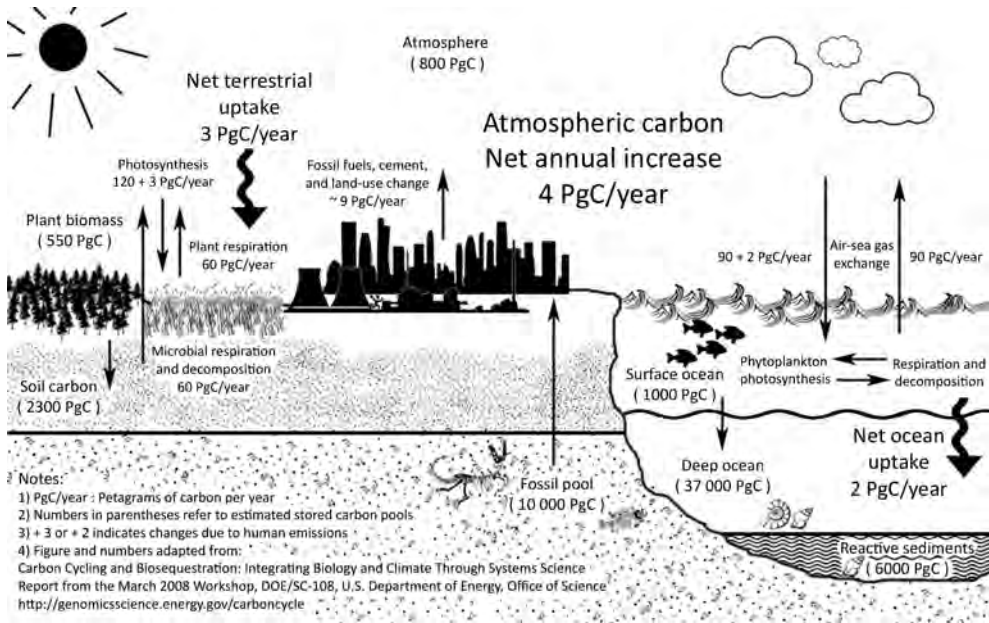
Figure 1.1: Simplified representation of the global carbon cycle. Figure adapted from http://genomicsscience.energy.gov/carboncycle/report.

which are illustrated in Figure 1.1. This transforms Equation 1.1 in Equation 1.2:

$$C(t) = C_0 + (F_{ocean}^{out} - F_{ocean}^{in} + F_{biosphere}^{out} - F_{biosphere}^{in} + F_{anthropogenic}) \cdot \Delta t \qquad (1.2)$$

Here with C_0 we indicate the initial carbon content at start of the investigated time period (t_0) with length Δt ($t = t_0 + \Delta t$), and with F^{in} and F^{out} the corresponding gross fluxes going in or out of a particular carbon pool. Thus, for instance, the F_{ocean}^{out} is the outgoing carbon flux from the ocean pool due to outgassing processes that add carbon to the atmosphere, as also indicated by the positive sign in front of this term. The anthropogenic flux is only a source of carbon for the atmospheric balance and as such has only positive component in this equation.

The atmospheric CO_2 mole fractions have risen from 280 ppm in 1850 to about 400 ppm nowadays in an unprecedented and increasing rate. Only half of the accumulated anthropogenic flux to the atmosphere is required to account for this increment, with the other half being taken up by the biosphere and the surface ocean. The assimilation of the additional CO_2 has been quite consistent in the past century, but not without consequences for the pools themselves. The slow exchange rate with the deep ocean and the final burial as carbonate material cannot compensate for the elevated pCO_2 levels in the surface ocean. The additional dissolved CO_2 molecules increase the hydrogen ions in the water and as a result the acidity of

surface ocean is rising. If this increase continues in the future, it will have dire consequences for the marine life and ecosystem (Ridgwell et al., 2007). On the other hand, increased atmospheric CO_2 levels are considered generally beneficial for the biosphere as it means larger and faster growth through the enhanced photosynthesis (CO_2 fertilization effect, Strain and Cure (1985)) . Still, the complete effects on the plant biology are largely unknown, with studies finding that even the fine cellular structure of the plants that grew in CO_2 enriched conditions is altered, with currently still poorly understood consequences for the plant energy balance (Griffin et al., 2000).

Besides the direct impact of the anthropogenically elevated atmospheric CO_2 levels, the arguably more important consequences are connected with the effects on the climate system. The radiative forcing supplied by the increased atmospheric CO_2 is the single largest forcing on the climate system (IPCC, 2013). As such, constraining the future increase of the CO_2 in the atmosphere is in the center of most attempts to mitigate climate change. There are still challenges, however, in attributing observed CO_2 mole fraction changes to the exact sources and sinks, natural or anthropogenic, especially at the smaller temporal and spatial scales. This thesis focuses on the investigation of the anthropogenic CO_2 emissions on a regional scale and seasonal time frame, which are discussed in more detail next.

1.2 Anthropogenic fossil fuel CO_2 emissions

Anthropogenic CO_2 emissions are continuously increasing on the global scale and for the last decade (2003-2012) their average annual total is estimated at 8.6±0.4 PgC y^{-1}, with an estimated emission total of 9.7±0.5 PgC y^{-1} in the year 2012 alone (Quéré et al., 2014). More than 50% of these emissions were due to the world top three contributors - China, USA and the European Union (EU). In total, the EU accounts for about 11% of the annual global anthropogenic CO_2 emissions, with more than half of these located in the area between France, Germany and the United Kingdom. In the center of this zone is the Netherlands, with one of the highest per capita emissions in the EU and more than two times the world average (Boden et al., 2010) (Figure 1.2). All these factors, combined with the EU commitment to the Kyoto Protocol to reduce its emissions by 20% of their 1990 values by the year 2020, make this a region of particular interest.

A recent study (Friedlingstein et al., 2014) suggests that the EU is the only of the top four emitters that has accomplished a persistent decrease in annual emissions, however, the information about the anthropogenic CO_2 emissions is available largely through the energy statistics of fossil fuel production and trade. These provide relatively good annual and global estimates that are known within a 2-σ uncertainty of 8.4% (Andres et al., 2014). Information on their temporal variability is usually inferred from monthly, weekly and diurnal pro-
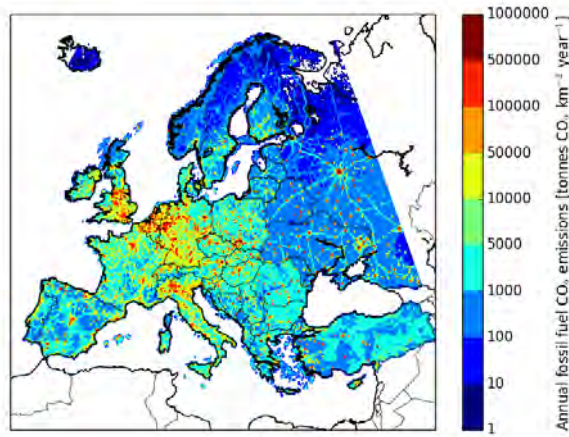
Figure 1.2: Anthropogenic CO$_2$ emissions of Europe (Institute for Energy Economics and the Rational Use of Energy, University Stuttgart)

files based on statistical data for different emission categories (e.g. road traffic peak hours, weekday-weekend production patterns and power used for heating throughout the year). These bottom-up inventories are more unreliable on the national level, where broader and more locally specific information is needed to estimate the fuel consumption. At finer spatial scales of <200 km uncertainties can be as high as 60% of the annual mean anthropogenic flux even for developed industrialized countries like the 25 member states of EU (Ciais et al., 2010). The national and regional scales, however, are exactly the scales on which emission reducing policies are applied and where the evaluation of their effectiveness is needed.

An alternative method to verify surface emissions is to use atmospheric observations in the so-called "top-down" approach (Ciais et al., 2014). Traditionally, numerical models that simulate the weather and atmospheric transport are used in combination with inventory-based emissions to calculate the atmospheric concentrations of a certain pollutant ("forward modeling", e.g. Pillai et al. (2011)). If independent atmospheric observations are available, these can be used to evaluate the model and seek the original emissions that would lower the mismatch between model and observations ("inverse modeling", e.g. Shiga et al. (2014)). The main problem in applying this approach to fossil fuel emissions is that atmospheric CO$_2$ observations alone do not contain the information to identify solely the anthropogenic CO$_2$ sources: a CO$_2$ molecule from fossil fuel combustion does not differ from a CO$_2$ molecule released from respiring plant material. In general, the contribution of natural fluxes to the atmosphere is significant and other sources of information are needed that can be used as a

proxy for the release of CO_2 from fossil fuel combustion alone.

Different chemical species connected with anthropogenic activities are used with various success as tracers for anthropogenic CO_2 emissions to the atmosphere (Miller et al., 2012). Sulfur hexafluoride (SF_6), for example, is of entirely anthropogenic origin and easy to measure. However, its emissions are only co-allocated with certain fossil fuel CO_2 sources (power network) and while effective on the large scale, on the regional scale this method is unreliable (Turnbull et al., 2006). Carbon monoxide (CO) has the advantage of being produced alongside CO_2 during combustion and is continuously observed at high temporal resolution. Its downsides lie in the variable emission rates between different sources, contributions of emissions from the natural biosphere, and its strongly varying life-time in the atmosphere (Gamnitzer et al., 2006; Djuricin et al., 2010). Other hydro- and halocarbon species can be used as direct or indirect tracers for fossil fuel emissions from particular anthropogenic sources, such as vehicular emissions or industrial processes (Turnbull et al., 2011a).

So far, the best direct tracer for anthropogenic CO_2 emissions is the radiocarbon (^{14}C) content of the atmospheric CO_2. Contrary to all the other significant sources, fossil fuel emissions contain no $^{14}CO_2$ and they leave unique footprint on the atmospheric $^{14}CO_2$ mixing ratios. I will discuss the different characteristics of ^{14}C and the atmospheric cycle of $^{14}CO_2$ next.

1.3 Radiocarbon

Radiocarbon (^{14}C) is the radioactive isotope of carbon, with half-life time of 5700±30 years (Roberts and Southon, 2007). ^{14}C in all materials decays through β-decay to ^{14}N. In nature, most carbon atoms are the stable isotopes ^{12}C and ^{13}C, which account for approximately 98.89% and 1.1% accordingly. In comparison, ^{14}C is found only in trace amounts and accounts for only $\sim 10^{-12}$ of the total carbon in the atmosphere. Due to its extensive use in the archaeological dating technique of the same name, large expertise is already available in the scientific community.

Because of the small quantities of ^{14}C in nature and consequent small absolute measurements with any of the counting methods we will describe later, observed values of $^{14}C/C$ (or corresponding activity) are usually reported as the deviation from the Modern Radiocarbon Standard (Stuiver and Polach, 1977). Exact notation differs between various scientific fields and for instance, atmospheric observations are usually reported as

$$\Delta^{14}C = \left[\underbrace{\frac{(^{14}C/C)_{sample}}{(^{14}C/C)_{standard}}}_{measurement} \; \underbrace{e^{-\lambda(t_s - t_0)}}_{decay\ corr.} \; \underbrace{\left(\frac{0.975}{1 + ^{13}\delta}\right)^2}_{fractionation\ corr.} -1 \right] \cdot 1000 \; [\permil]. \qquad (1.3)$$

In this notation the measured ^{14}C/C of the sample is corrected with two additional terms that account for normalization of radioactive decay and mass-dependent isotopic fractionation (Mook and van der Plicht, 1999). The decay term follows the convention in the field to report all measured activities normalized to a single year (1950). This allows to correctly compare the activity of samples taken at different times without recalculations, but requires newly measured samples to be corrected for the decay between 1950 (t_0) and the time of sampling (t_s) using the radiocarbon decay constant (λ, in y^{-1}). Isotopic fractionation occurs when a process has a preference for the molecules with a particular isotope, and results in a change in the isotopic ratios measured before and after the process. In mass-dependent fractionation, the process discriminates based on the mass of the isotope, usually favoring the lighter ^{12}C against the heavier ^{13}C and the heaviest ^{14}C. An example for such process is the plant photosynthesis, where the isotopic ratios of the carbon assimilated in the plant will be more abundant in the lighter isotopes than the atmospheric air originally was. In studies of ^{13}C, the fractionation occurring between reservoirs can be used to identify specific processes and the size of their fluxes. In studies of ^{14}C, additional measurements of ^{13}C ratios are used to correct for this effect and processes of transition from one carbon pool to another (e.g. CO_2 assimilation by plants or exchange of CO_2 between air and surface waters) do not change the $\Delta^{14}CO_2$ value associated with it.

Similar to Equation 1.2, we can construct a mass balance equation for $^{14}CO_2$, in which each radiocarbon term is described by its CO_2 content and the according $\Delta^{14}CO_2$ signature. Most commonly this approach is used to describe an air mass with initial characteristics (CO_{2bg}, Δ_{bg}), which is modified by various processes (each expressed by different CO_{2x}, Δ_x), until its final characteristics are observed in a sample ($CO_{2sample}$, Δ_{sample}). In a simplified case, adding fossil fuel CO_2 to an atmosphere with background characteristics (CO_{2bg}, Δ_{bg}), this method results in the following equations:

$$CO_{2sample} = CO_{2bg} + CO_{2ff} \tag{1.4}$$

$$\Delta_{sample}CO_{2sample} = \Delta_{bg}CO_{2bg} + \Delta_{ff}CO_{2ff} \tag{1.5}$$

A more complex and complete version of these equations is used in Chapters 4 and 5 of this thesis. The different processes that influence the atmospheric $\Delta^{14}CO_2$ are sometimes specific for the ^{14}C isotope of CO_2 and the $^{14}CO_2$ atmospheric cycle is described in more detail in the next section.
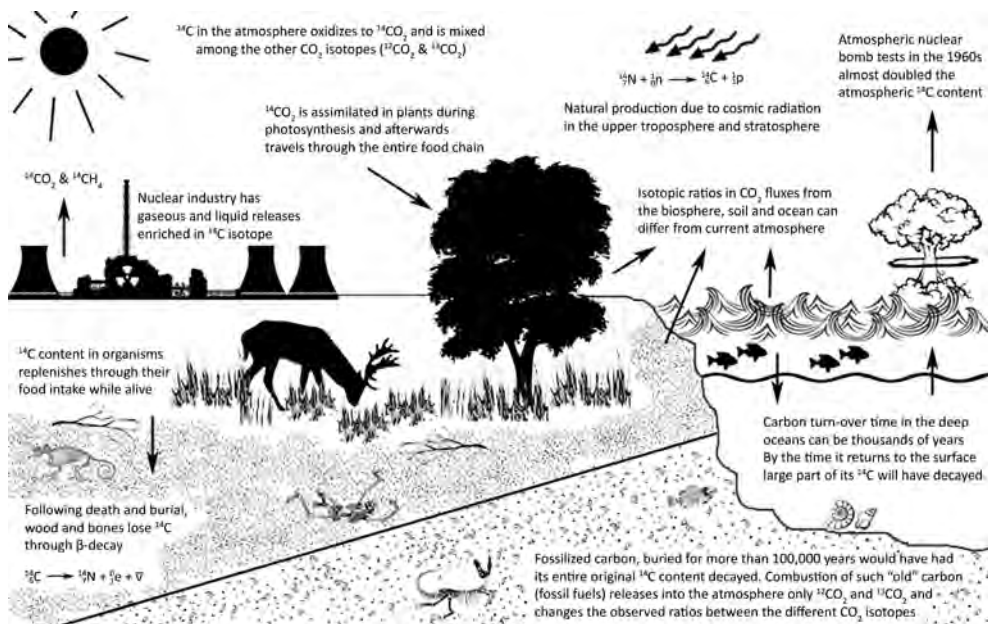
Figure 1.3: Simplified representation of the ^{14}C cycle. Figure by D. Bozhinova

1.4 The $^{14}CO_2$ cycle

In the natural carbon cycle, ^{14}C is created in the stratosphere and upper parts of the troposphere by a reaction between the cosmic radiation and abundant ^{14}N atoms (Libby, 1946; Anderson et al., 1947). The ^{14}C oxidizes first to form ^{14}CO, which later oxidizes to $^{14}CO_2$ and by the time it reaches the surface it is well-mixed with the other CO_2 molecules. CO_2 in all its forms is assimilated by photosynthesizing organisms and travels through the food chain until eventually the plants or animals die. Their carbon is then either released back into the atmosphere through decay and heterotrophic respiration, or it is transported to the slower carbon reservoirs through burial or transport to the deep oceans. In reservoirs that have turnover time significantly shorter than the ^{14}C half-life, the radioactive decay will hardly affect the relative $^{14}CO_2$ content. But given time, the ^{14}C atoms change back to ^{14}N through β^- decay and after long enough the entire ^{14}C content will be gone. This is the reason why anthropogenic CO_2 emissions are unique when looking at $^{14}CO_2$ in the carbon cycle.

Fossil fuels are millions of years old and their radiocarbon has entirely decayed ($\Delta_{ff} = -1000$ ‰). Their combustion releases only $^{12}CO_2$ and $^{13}CO_2$ to the atmosphere and as a result drastically lowers the atmospheric $\Delta^{14}CO_2$, which is known as the Suess effect (Suess, 1955). This relationship can be used to estimate the additional fossil fuel CO_2 content (CO_{2ff}) in a
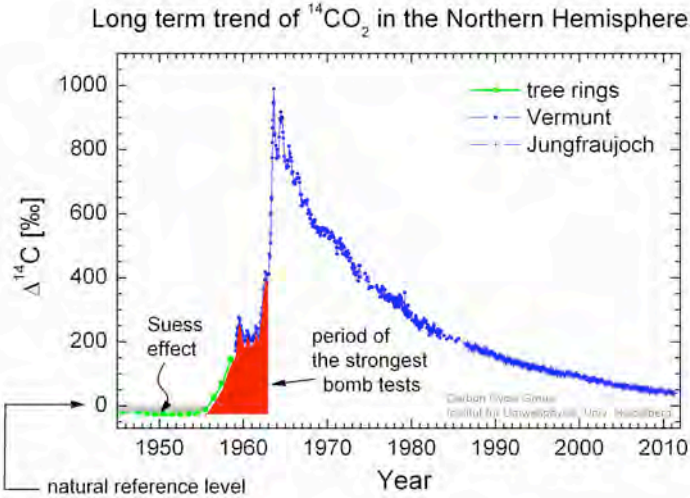
Figure 1.4: Development of the atmospheric $\Delta^{14}CO_2$ in the northern hemisphere. Data before 1959 have been derived from tree rings (Stuiver and Quay, 1981). From 1959 to 1986 measurements were performed at the Alpine site Vermunt subsequent data from 1986 onwards are from the Swiss High Alpine Research Station Jungfraujoch (Levin et al., 2010). Source: Institut für Umweltphysik, University of Heidelberg.

sample by comparing its $\Delta^{14}CO_2$ signature to that of clean background air, previously shown in Equations 1.4 and 1.5 (Levin et al., 2003).

$$CO_{2ff} = CO_{2sample} \frac{(\Delta_{sample} - \Delta_{bg})}{(\Delta_{ff} - \Delta_{bg})}. \tag{1.6}$$

In Equation 1.6 it is assumed that CO_{2ff} is the only source of CO_2 that has $\Delta^{14}CO_2$ signature different than that of the background air (Δ_{bg}). That might not always be true, as there are other anthropogenic activities that influence the $^{14}CO_2$ cycle.

Atmospheric nuclear bomb tests in the 1950s and 1960s produced large quantities of ^{14}C and nearly doubled the amount of $^{14}CO_2$ in the atmosphere (Figure 1.4). The rapid decline in the years following the "bomb peak" in the atmospheric $\Delta^{14}CO_2$ observations is not consistent with radioactive decay, but a result of the large exchange fluxes and relative $\Delta^{14}CO_2$ gradients between the atmosphere, biosphere and surface ocean (Levin and Hesshaimer, 2000). The excess radiocarbon was redistributed among the other carbon pools, however, the carbon in these reservoirs has longer residence time. This creates a disequilibrium, as the CO_2

17

returning from the biosphere and surface ocean is more enriched in ^{14}C than the current atmosphere. Furthermore, ^{14}CO$_2$ is being continuously produced by some methods of nuclear power production (McCartney et al., 1988a,b).

The presence of influences other than fossil fuel in a sample complicates the recalculation of CO$_{2ff}$ from Equation 1.6 and requires the introduction of a term for each other CO$_2$ addition and its respective Δ^{14}CO$_2$ signature (Turnbull et al., 2009b),

$$CO_{2ff} = \frac{CO_{2sample}(\Delta_{sample} - \Delta_{bg})}{(\Delta_{ff} - \Delta_{bg})} - \frac{CO_{2other}(\Delta_{other} - \Delta_{bg})}{(\Delta_{ff} - \Delta_{bg})} \tag{1.7}$$

The atmospheric enrichment from disequilibrium fluxes and nuclear ^{14}CO$_2$ production will thus act as an offset to the Δ^{14}CO$_2$ decline caused by fossil fuel emissions. How large these effects are for the territory of western Europe will be evaluated and discussed further in Chapters 4 and 5. I will now introduce the different methods used for atmospheric Δ^{14}CO$_2$ observations and how plant samples complement them.

1.5 Δ^{14}CO$_2$ observations

The three principal radiocarbon measurement methods are the Gas-Proportional counting (GPC), Liquid Scintillation counting (LSC) and Accelerator Mass Spectrometry (AMS). In the GPC technique, the carbon sample is combusted to CO$_2$ gas and in the counter every decayed β-particle is counted to measure the activity of the sample. In the LSC technique, the carbon sample is in a liquid form and a scintillator is added, that produces a flash of light when it interacts with a β-particle and the counter marks the number of such events. AMS is the most modern method, in which rather than counting β-particles, the number of carbon atoms in the sample is measured, alongside the proportion of each of the three carbon isotopes (^{12}C, ^{13}C and ^{14}C). This way the ^{14}C content is directly measured relative to all the carbon atoms in the sample.

Atmospheric Δ^{14}CO$_2$ observations are usually obtained through various methods, each with very different characteristics. Historically, the different sampling techniques developed to tackle the challenge of obtaining air sample that contains ^{14}CO$_2$ in sufficient quantity to be measured. However, with the development of the AMS measurement method, which requires a sample of only few mg of carbon, most of the original limitations are close to obsolete and conversely the largest difference in the various sampling methods lies in the sampling duration period, within which the atmospheric sample is obtained.

Measurements with the highest time resolution are obtained using a method, in which air is flushed in a large glass flask and stored for later CO$_2$ extraction and ^{14}C analysis. Flask observations represent an almost instantaneous look at the atmospheric Δ^{14}CO$_2$, as
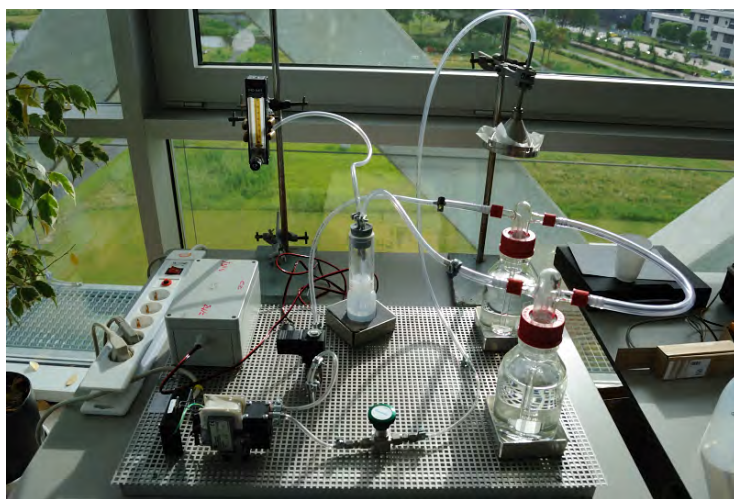
Figure 1.5: Example of NaOH absorption setup.

they collect air within few minutes (Graven et al., 2012b). Since this technique is used in many atmospheric observational sites to obtain and store air samples for analysis of other chemical species (CO_2, CO, SF_6 and many others), such archived samples can be used to investigate even the long-past atmospheric $\Delta^{14}CO_2$ record (Graven et al., 2012a).

On the other extreme of the time spectrum are the "integrated" $\Delta^{14}CO_2$ observations. In this so-called "bubbler" method (Figure 1.5), atmospheric air is pumped through one or several bottles filled with an alkaline solution. The air bubbles formed through various glass filters allow for the optimal absorption of the atmospheric CO_2 into the solution:

$$CO_2 + 2OH^- \rightarrow CO_3^{2-} + H_2O \tag{1.8}$$
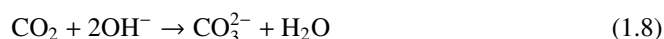
The length of the period, for which atmospheric carbon is recorded in this way, is limited only by the amount of alkaline solution available and most commonly such setup is used to obtain samples on a weekly to monthly basis. Since all the CO_2 from the air is absorbed, these samples provide an integrated observation of the atmospheric $\Delta^{14}CO_2$ during their sampling period (Levin et al., 1980; Meijer et al., 1995).

Additionally, an intermediate technique of integrated flask sampling (Turnbull et al., 2012) has been developed, which obtains atmospheric samples integrated over roughly an hour. The further development of new air sampling techniques is fueled by the desire to have a network of regular observations. However, the cost of single sample ^{14}C analysis (e.g. €350, but varies depending on laboratory and type of samples) forces researchers to look for a compromise between the methods that provide observations with high temporal

Figure 1.6: Typical maize field right after flowering (on the left) and leaf-sample preparation (on the right)

density and the integrated samples, which average over longer periods. Recent methods combine integrated $\Delta^{14}CO_2$ samples with continuous CO measurements and hold a great promise estimating CO_{2ff} (Levin and Karstens, 2007; van der Laan et al., 2010; Vogel et al., 2010; Turnbull et al., 2011b) on the finer temporal scale. However, despite the excellent qualities of all of these techniques, their largest disadvantage at present is that they require an elaborate infrastructure and a considerable investment to set up and maintain the observational equipment.

Another major motivation behind the search for alternative sampling strategies is that the current $\Delta^{14}CO_2$ measurement network is still extremely scarce. There are only about a dozen of sites in Europe that make semi-continuous integrated $\Delta^{14}CO_2$ observations and most of them are located in rural areas, targeting measurements of the background air. As such, their usefulness in the evaluation of the fossil fuel CO_2 on a finer spatial scale is limited and another method is needed to gather observations on the regional scale in a cost-efficient manner. Using plants to sample CO_2 and subsequent ^{14}C analysis could be that alternative.

Annual plants (maize, grasses) have been shown to identify qualitatively well the regional and continental gradients in atmospheric $\Delta^{14}CO_2$ in North America (Hsueh et al., 2007; Riley et al., 2008). Furthermore, even analyses of the atmospheric $\Delta^{14}CO_2$ of previous years might be possible by using for example wine-ethanol (Palstra et al., 2008) or rice grains (Shibata et al., 2005). Plants assimilate atmospheric CO_2 during photosynthesis and incorporate atmospheric carbon in their biomass during growth. Thus, the plant itself represents an integrated record of the atmospheric isotopic ratios of CO_2 during its growing period. However, this

method requires further analysis as a plant sample is not equivalent to an integrated air sample. While the integrated sampling devices absorb air continuously at a constant rate during their entire sampling period, a plant assimilates CO_2 only during daytime and its assimilation rate will vary considerably during the growing season.

Various environmental or internal factors modify the CO_2 uptake and in order to be able to interpret such a sample, one must first accurately model the way in which plants sample CO_2 from the atmosphere. This is my first research objective and I address it employing the Simple Universal CROp Simulator (SUCROS), which is described in more detail in Chapter 2. In Chapter 3 I present the results of a numerical experiment that evaluates the importance of the plant growth on the final accumulated $\Delta^{14}CO_2$.

Plant samples can be obtained with considerable ease compared to the atmospheric samples, as in most parts of the world crops are grown for agricultural purposes or are available as natural vegetation. Following the example set by Hsueh et al. (2007), we executed regional sampling campaigns and obtained samples of maize leaves across the Netherlands in three consecutive years (Figure 1.6). The samples underwent laboratory treatment (Figure 1.7) before their ^{14}C analysis at the Centre for Isotope Research (University of Groningen, the Netherlands) AMS facility. The analysis of the results from these samples is described in Chapter 5, including a complementary interpretation by our modeling framework. Our strategy for modeling the atmospheric $\Delta^{14}CO_2$ budget is described next.

1.6 Modeling the regional carbon cycle

In Section 1.1 of this Introduction, we presented the carbon cycle with a simplified overview of the fluxes between the different carbon reservoirs at the global and annual scales. When the carbon cycle is studied at the regional scale, however, the picture becomes more complex as the processes involved operate on very different time scales and furthermore, sources and sinks of carbon can be spatially separated from each other. For example, most anthropogenic CO_2 emissions are released at surfaces near urbanized areas. The air-sea gas exchange, on the other hand, occurs over the ocean surface and its rate depends mostly on the local wind and temperature conditions, and the gradient of CO_2 concentrations between the air masses and surface waters. The spatial separation of some of the sinks and sources means that the CO_2-enriched atmospheric masses will have to travel the distance between them before some of the excess CO_2 is removed from the atmosphere.

On the mesoscale, numerical weather prediction models are powerful tools to evaluate the atmospheric transport of pollutants using the up-to-date understanding of the physical processes that drive the atmosphere. This is a very important point, as the observed tracer quantities are not only a result of the emission fluxes to the atmosphere, but also a function
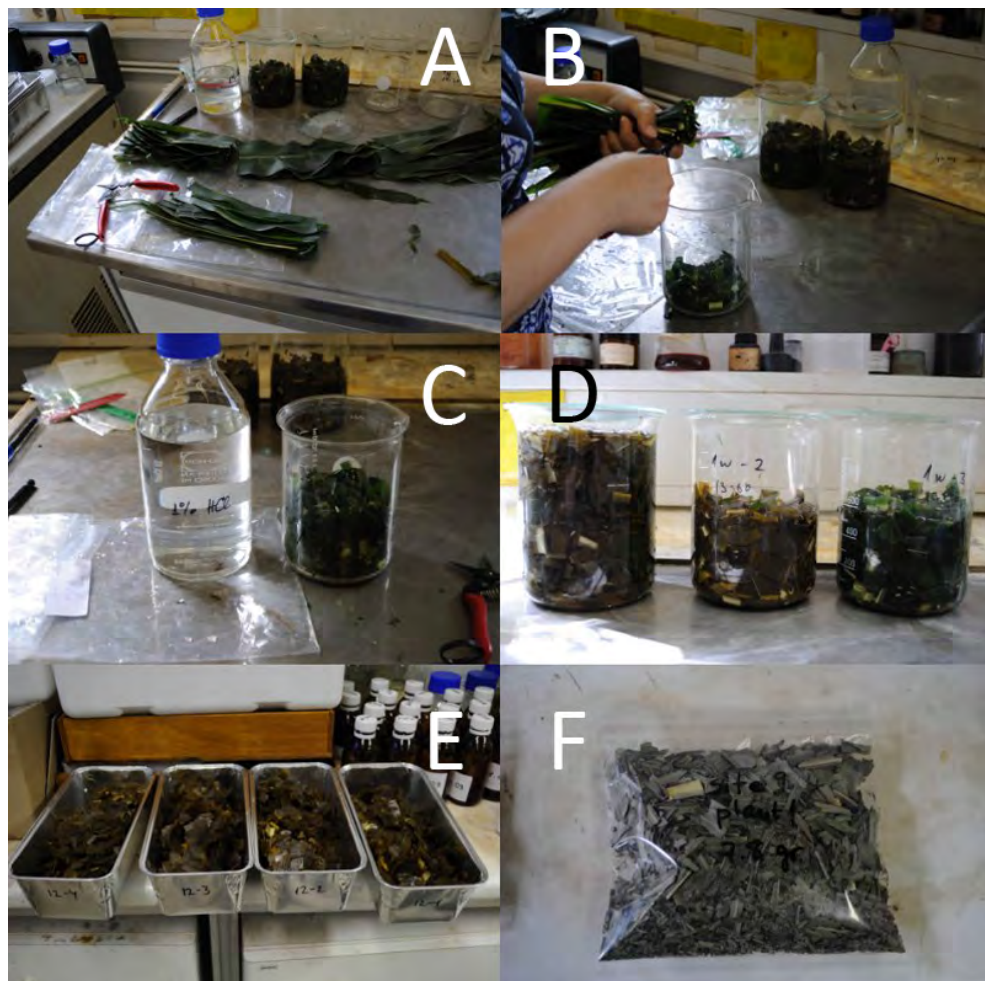
Figure 1.7: Photos of different stages of our leaf-sample preparation during our 2010 sampling campaign, as follow: the maize leaves are cleaned from dust and soil (A) and cut into small pieces (B), soaked into 1% HCl solution for about an hour (C), then rinsed thoroughly and soaked with demineralized water (D), dried in oven for at least 24 hours at 70° C (E) and finally crushed into small pieces and sealed in air-tight bags (F). In later years the crushed pieces were instead ground through grinding machine and samples were stored in plastic bottles.

of how these gases are mixed and transported from the sources to the point of observation. For example, higher CO_2 concentrations measured at an observational site do not necessary mean higher local emissions. Maybe there was a change in the dominant wind direction and a plume from more polluted area was advected to the location. Or maybe there was less opportunity for the emitted trace gases to travel because the vertical mixing was suppressed.

While these considerations would be valid concerns for the evaluation of any tracer transport, a proper prediction of the atmospheric state is even more important when investigating the carbon cycle. In the interactions between the land-surface and the atmosphere, the biosphere is the cross-point of the energy, water and carbon cycles (Combe et al., 2015). Changes in the weather conditions drive the biospheric surface CO_2 fluxes and this process is essential for the correct representation of the CO_2 budget on the diurnal time scale. On the seasonal scale, biospheric CO_2 fluxes are also controlled by the plant development and growth, which will differ between various vegetation types. On the regional scale, where the land cover is rarely homogeneous, it might be important to represent these differences in order to capture the resulting gradients in the surface CO_2 fluxes.

We have addressed these issues by employing the Weather Research and Forecast (WRF) model. This model will be used to simulate the dispersion of fossil fuels and the associated impact on $^{14}CO_2$. Together with the crop growth model, we can thus predict the $\Delta^{14}CO_2$ signatures that will be accumulated in the plant, with more details on the implementation and method of calculation following in Chapter 2. My second research objective is to identify the detail required to successfully model the atmospheric $^{14}CO_2$ budget on a regional scale.

In Chapter 4 I will present evaluation of our modeling framework against atmospheric observations of , with further improvements discussed and implemented for the version used in Chapter 5.

1.7 Scope of this thesis and research questions

In this thesis, I evaluate the challenges connected with using plant samples of ^{14}C from annual crops to measure the atmospheric radiocarbon content on the regional scale. I employ both modeling and experimental techniques and while this study focuses on western Europe and the Netherlands, the methods described here could be applied to other geographic regions.

In Chapter 2 I present the final version of the modeling framework that was assembled and verified within this thesis. The different numerical models used are discussed in detail, emphasizing on the settings relevant for our research interests. Additionally, I present the complete list of atmospheric CO_2 and $^{14}CO_2$ tracers that we have included in our modeling system and the method I use to calculate the $\Delta^{14}CO_2$ signature of the atmosphere.

In Chapter 3 I will address our first research question:

Question 1 How accurate can we model the $\Delta^{14}CO_2$ signature of an annual crop?

Plants assimilate CO_2 with a variable rate, which changes under the influence of both meteorological or phenological factors. The first step in the interpretation of such samples is to evaluate the magnitude of the plant growth and development effects on the final $\Delta^{14}CO_2$ signature. To address this question, in Chapter 3 we design a study that compares the resulting signatures when the accumulated $\Delta^{14}CO_2$ is estimated through several simpler proxies of plant growth and a more complex crop growth model. We discuss the sensitivity of these results to errors in the supplied weather data and the importance of the phenological information to lower the uncertainties in the results for samples from different plant parts. Finally, we present a numerical experiment, in which we model plant growth for two different crop species (wheat and maize) over the territory of the Netherlands, and use spatially uniform atmospheric $\Delta^{14}CO_2$ time series to evaluate only the effect of the variable plant growth for the resulting plant-sampled $\Delta^{14}CO_2$ at the regional scale.

Question 2 What modeling framework is required to simulate the regional $^{14}CO_2$ budget?

Aside from the exact models required to simulate the atmospheric and plant $\Delta^{14}CO_2$ signatures, many terms in the $^{14}CO_2$ budget equations shown previously in Section 1.4 will vary in magnitude in different regions of the world. If a term is of low importance in the region of study, its exclusion could simplify the $\Delta^{14}CO_2$ calculation without risking significant bias in the modeled results. In Chapter 4, we present our first order simulation of the $^{14}CO_2$ budget in Western Europe. We list the budget terms we choose to neglect based on their magnitude in the available scientific literature, and proceed to model the rest of the budget terms with individual tracers for a period of 6 months (April–October 2008). We evaluate the influence of both fossil fuel CO_2 and nuclear $^{14}CO_2$ anthropogenic tracers and discuss regions where the presence could mask the signal of the other due to their opposite effect on the atmospheric $\Delta^{14}CO_2$ signature. We further show the difference between the average atmospheric sample and modeled plant-sampled $\Delta^{14}CO_2$ in this setup, which allows to evaluate the covariance between the variable weather and plant growth and the atmospheric transport of CO_2 and $^{14}CO_2$ tracers at each location.

The final research question that I will address in this thesis is:

Question 3 Are plant samples a feasible source of new information for the anthropogenic CO_2 emissions on the regional scale?

Within Question 3 is locked our ultimate goal of weighting the advantages of using plant samples as additional source of atmospheric $\Delta^{14}CO_2$ observations against the uncertainties connected with their interpretation and the practical limits of their use. When we are aware of the limitations of this method, its application will become easier and the sampling strategies

where its use is beneficial to other observational techniques will be more clearly defined. In Chapter 5 we use both experimental and numerical methods to address this question. We describe an experimental study during which samples of maize leaves were obtained from the Netherlands, Germany and France in the summers of 2010 – 2012. We show the $\Delta^{14}CO_2$ results from these samples and we interpret them within our modeling framework. We use the model results to evaluate the anthropogenic signals found in the samples and the different emission sources they are associated with. We discuss the uncertainty connected with various aspects of the full modeling framework and provide advice for the use of plant samples in future combined experimental and modeling studies.

Finally, in Chapter 6 we summarize the main findings of this thesis and discuss our work in a broader perspective, outlining several still unanswered questions and future research opportunities.

2
Modeling framework

To address the research questions posed in the previous chapter we use throughout this thesis several numerical models in a modeling framework. This framework consists of two parts: a numerical weather prediction model to simulate the atmospheric transport of tracers (WRF-Chem, henceforth only WRF) and a plant growth model (SUCROS 2, henceforth only SUCROS) to simulate the CO_2 assimilation in crops. Their relationship and the various data required as input is depicted in Figure 2.1.

The weather simulated by WRF is used as input weather data for SUCROS and the plant model simulates the growth of a single crop field. Simultaneously with the weather, WRF also models the transport and atmospheric masses of the different CO_2 and $^{14}CO_2$ tracers, which allows us to calculate the $\Delta^{14}CO_2$ signature of the atmosphere. Finally, the daily plant growth increments from SUCROS and the daytime averaged atmospheric $\Delta^{14}CO_2$ are used to calculate the $\Delta^{14}CO_2$ signature of the plant.

In this chapter we will present each of these models with their basic capabilities and our general implementation, which includes the treatment of the input data products. In later chapters the focus will be on study-specific modifications and details.

2.1 Numerical Weather Prediction model

The numerical weather prediction model used in this thesis is version 3.2.1 of the Weather Research and Forecast model (Skamarock et al., 2008). This is a mesoscale model designed
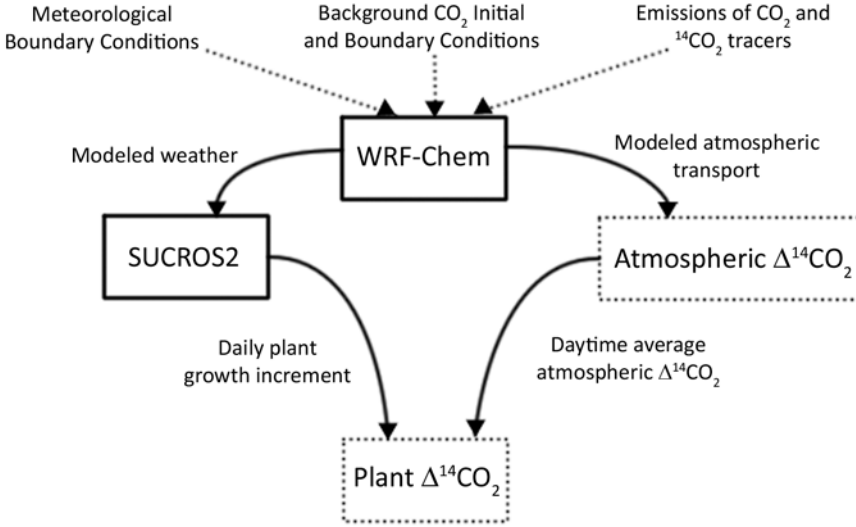
Figure 2.1: Schematic representation of our modeling framework. Solid boxes show the numerical models used, dashed boxes show the resulting products, while arrows indicate data input/output relationships.

for both operational forecast and atmospheric research, with a non-hydrostatic fully compressible atmosphere. Its extensive suite of numerical schemes allows for the representation of various physical processes in the atmosphere and is a result of the large scientific community that uses and develops the model. Our specific setup utilizes the Advanced Research WRF (ARW) dynamic solver and the fully coupled online module WRF-Chem to simulate the regional-scale weather and tracer transport.

2.1.1   Regional weather with WRF

For our study, WRF simulated a limited area, one "mother" domain covering Europe, with several domains nested within it with higher temporal and spatial resolutions. Meteorological data from the Final (FNL) Operational Global Analyses from National Centers for Environmental Prediction (NCEP, U.S.), at $1° \times 1°$ horizontal resolution is used to initialize the model over the simulated domains, and later on to provide information on the lateral boundaries of the mother domain every 6 hours. Boundary conditions for the nested domains are calculated internally, from the respective parent grids. In WRF the relationship between parent and nested domain can be either through one-way or two-way nesting. In both cases the changes

in the atmospheric state of the parent grid will be communicated to the nested domain, but in the two-way nesting changes in the state of the nested domain will also feedback to the parent. We use both of these options within the chapters of this thesis, usually stated explicitly in the description of the particular model setup for each study.

This model uses an eta-coordinate system for its vertical structure, meaning that the layers of the atmosphere will follow the terrain height near the surface, and gradually smoothen the vertical layers towards a constant pressure level of 50 hPa as the model top. The choice of the vertical structure reflects our interest in the near-surface atmospheric conditions, as our primary goal is to simulate growth conditions for plants. Furthermore, most of the observations we had available to compare with our model results are obtained within 0–200m height above surface. For our vertical structure we use 27 vertical layers, 18 of which are located in the lower 2 km of the atmosphere.

Our model simulates three types of domains with horizontal grid sizes of 36 km, 12 km and 4 km respectively (see Figure 4.1 on page 70 and Figure 5.2 on page 96). The horizontal scale defines processes that are explicitly resolved by the model and different parameterizations are used to describe the processes that occur at sub-grid scale. Often there is more than one way to represent physical processes within a numerical model and as a consequence there are sometimes multiple parameterization schemes that could describe the same process. There are multiple studies that investigate the effect different scheme choices would have on the forecasted weather (e.g. Sterk et al., 2013; Kleczek et al., 2014) or the transport of atmospheric pollutants (e.g. Hu et al., 2013; Wang et al., 2014; Hariprasad et al., 2014). In our settings, we try to use only one combination of schemes in all the chapters of this thesis, with the exception of the planetary boundary layer and surface layer settings in Chapter 3.

The planetary boundary layer (PBL) scheme used in our WRF weather-only simulation in Chapter 3 is the Yonsei University (YSU, Hong et al. (2006)) scheme, while later in our complete WRF-Chem framework it is the Mellor-Yamada Nakanishi and Niino (MYNN2.5) (Nakanishi and Niino, 2004). The boundary layer parameterization aims to describe the behaviour of turbulent mixing and the vertical transport of momentum, moisture, heat, and, in our case, tracers in the atmosphere. MYNN2.5 is a boundary layer scheme that is an improved version of the Mellor-Yamada-Janjic (MYJ, Janjić (1994)) local-closure scheme. In a local scheme the turbulent mixing occurs only between directly neighboring layers in the atmosphere. This contrasts non-local schemes, where larger turbulent eddies allow more distant vertical levels to interact, as for example in the YSU PBL scheme. Local (MYJ) and non-local (YSU) schemes have been extensively compared and the former usually underpredicts the daytime PBL height resulting in shallower and more moist boundary layers, while the latter overpredicts the mixing in stable and nocturnal conditions, resulting in deeper and drier PBLs (Hu et al., 2010).

One of the improvements in the MYNN scheme that separates it from MYJ is the more

elaborate mixing-length formulation included, that allows to change its behaviour across the stability spectrum. The original verifications of this boundary layer scheme were performed for cases of fog (Nakanishi and Niino, 2004, 2006), but a later study by Coniglio et al. (2013) found that the MYNN2.5 scheme performs significantly better than others also in predicting convection. The flexibility of the PBL scheme is important to our study as we consider the atmosphere over the period between April and October in all of our modeled years. The long time frame for the simulation ensures that we would observe the whole spectrum of atmospheric stability situations and every choice of schemes would have periods of advantage and disadvantage. Shortly after our first (weather-only) simulations, we learned of a technical problem in the YSU implementation in WRF (this bug was fixed in the later version 3.4.1, Hu et al. (2013)), and we therefore selected for the WRF-Chem tracer simulations the more reliable MYNN2.5 scheme. In Chapter 4 our comparison between modeled and observed boundary layer heights at Cabauw will show that even though this scheme underpredicts the boundary layer height during the night, in daytime the simulations fit the observations relatively well.

The MYNN2.5 boundary layer scheme uses the MYNN surface-layer scheme in WRF. Over land, the surface-layer scheme provides intermediate parameters required to calculate the heat and moisture fluxes in the land-surface model (LSM) and the surface stress in the respective boundary layer scheme. Over water, the scheme calculates the surface heat and moisture fluxes, as boundary conditions for the PBL scheme (Skamarock et al., 2008).

The land-surface model in our WRF setup is the unified Noah LSM (Chen and Dudhia, 2001; Ek et al., 2003), which is jointly developed by the National Center for Atmospheric Research and the National Centers for Environmental Prediction (USA). Its use provides an advantage when using the meteorological analysis datasets from these sources (NCEP/NCAR), as the time-dependent soil fields will stay consistent between the two. The model uses 4 layers of soil temperature and moisture distributed in the top 2 meters of the soil, and predicts the canopy moisture and snow cover. Its mechanics include the effects of the different vegetation types and soil texture on various processes, such as for example evapotranspiration and water run-off. Since our simulations extend over six months at a time, we used the WRF option to update the fields of sea-surface temperature, vegetation fraction, albedo and sea ice during the run.

Further schemes we used are mentioned in the description of the model setup for each particular study. These are the schemes that describe the radiative forcing due to long- and short-wave radiation, microphysics and cumulus parameterization. More details of the used parameterization schemes and their implementation can be found in Skamarock et al. (2008) and literature referenced therein.

Table 2.1: *List of all tracers used within our framework, with according data sources and descriptions. We include here reference to their use within this thesis and other research studies.*

Type	Nr.	Code	Description	Data Source	Used In
Background	1	CO_{2bg}	Total CO_2 at start of the simulation and changes due to the transport from outside the mother domain. Has only initial and boundary conditions, no emissions.	CarbonTracker Europe, (Peters et al., 2010)	Ch. 4, Ch. 5, V.N.
Disequilibrium	2	$^{14}CO_{2dis}^{bio}$	Biospheric tracer, scales with heterotrophic respiration. EAS.	(Miller et al., 2012)	Ch. 5
	3	$^{14}CO_{2dis}^{oce}$	$^{14}CO_2$ disequilibrium flux from the ocean. EAS.		
Cosmogenic Production	4	$^{14}CO_{2c}^{strat}$	Production in the upper troposphere and stratosphere, near or above the model top. ECAH.	(Miller et al., 2012)	Ch. 5
	5	$^{14}CO_{2c}^{alth}$	Production distributed linearly throughout the entire troposphere. ECAH.		
Biospheric	6	CO_{2p}^{ags}	CO_2 fluxes due to photosynthesis and respiration, calculated by A-gs model in WRF. EAS.	(Jacobs et al., 1996; Ronda et al., 2001)	*
	7	CO_{2r}^{ags}			
	8	CO_{2p}	Monthly CO_2 fluxes from GPP and TER, scaled with operational shortwave radiation (GPP) and with Q10 of the operational temperature (TER). EAS.	(Schaefer et al., 2008), (Olsen and Randerson, 2004)	Ch. 4, Ch. 5, V.N.
	9	CO_{2r}			
Nuclear	10	$^{14}CO_{2nuc}^{0}$	Total $^{14}CO_2$ emissions from the nuclear industry. EAS.		Ch. 4, Ch. 5**
	11	$^{14}CO_{2nuc}^{h}$	Total $^{14}CO_2$ emissions from the nuclear industry. ECAH.		
	12	$^{14}CO_{2nuc}^{SFR}$	Spent-fuel reprocessing plants. ECAH.	IAEA – PRIS, https://www.iaea.org/pris/, AREVA, http://www.areva.com/, (Graven and Gruber, 2011)	Ch. 5
	13	$^{14}CO_{2nuc}^{PWR}$	Pressurized water reactors. ECAH.		
	14	$^{14}CO_{2nuc}^{BWR}$	Boiling water reactors. ECAH.		
	15	$^{14}CO_{2nuc}^{AGR}$	Advanced gas-cooled reactors. ECAH.		
	16	$^{14}CO_{2nuc}^{MAG}$	Magnox advanced gas-cooled reactors. ECAH.		
	17	$^{14}CO_{2nuc}^{LWG}$	Light-water-cooled graphite-moderated reactors. ECAH.		
	18	$^{14}CO_{2nuc}^{rest}$	Heavy water reactors and Fast-breeder reactors. ECAH.		
	19	$^{14}CO_{2nuc}^{AGR_{temp}}$	2012 AGR tracer, with temporary shutdowns. ECAH.	EDF Energy reports, http://www.edfenergy.com/	Ch. 5**
	20	$^{14}CO_{2nuc}^{SFR_{day}}$	2012 SFRP tracer, only 4h-at-noon emissions. ECAH.		
	21	$^{14}CO_{2nuc}^{SFR_{night}}$	2012 SFRP tracer, only 4h-at-midnight emissions. ECAH.		
Fossil fuel (IER-based)	22	CO_{2ff}^{0}	Total IER-based fossil fuel CO_2 from all sectors. EAS.		Ch. 4, Ch. 5**
	23	CO_{2ff}^{h}	Total IER-based fossil fuel CO_2 from all sectors. ECAH.		
	24	$CO_{2ff}^{SNAP1_0}$	Energy production. EAS.	IER, University Stuttgart, (Vogel et al., 2013b), UNFCCC, http://unfccc.int	Ch. 5
	25	$CO_{2ff}^{SNAP1_h}$	Energy production. ECAH.		
	26	$CO_{2ff}^{SNAP2_0}$	Non-industrial combustion. EAS.		
	27	$CO_{2ff}^{SNAP3_0}$	Industrial combustion. EAS.		
	28	$CO_{2ff}^{SNAP3_h}$	Industrial combustion. ECAH.		
	29	$CO_{2ff}^{SNAP4_0}$	Production processes. EAS.		
	30	$CO_{2ff}^{SNAP4_h}$	Production processes. ECAH.		
	31	$CO_{2ff}^{SNAP7_0}$	Road transport. EAS.		
	32	$CO_{2ff}^{SNAPrest_0}$	Other sectors. EAS.		
	33	$CO_{2ff}^{SNAPrest_h}$	Other sectors. ECAH.		

Table 2.1: (continued)

Type	Nr.	Code	Description	Data Source	Used In
Fossil fuel (EDGAR-based)	34	$CO_{2ff}^{EDGAR_h}$	2010 only tracer, total fossil fuel CO_2 from all sectors. EAS.	European Commission, Joint Research Centre (JRC), Netherlands Environmental Assessment Agency (PBL), Emission Database for Global Atmospheric Research (EDGAR), version 4.2, FT2010, http://edgar.jrc.ec.europe.eu	*
	35	$CO_{2ff}^{EDGAR_0^1}$	2010 only tracer, Energy production. EAS.		
	36	$CO_{2ff}^{EDGAR_0^2}$	2010 only tracer, Non-industrial combustion. EAS.		
	37	$CO_{2ff}^{EDGAR_0^3}$	2010 only tracer, Industrial combustion. EAS.		
	38	$CO_{2ff}^{EDGAR_0^4}$	2010 only tracer, Production processes. EAS.		
	39	$CO_{2ff}^{EDGAR_0^7}$	2010 only tracer, Road transport. EAS.		
	40	$CO_{2ff}^{EDGAR_0^{rest}}$	2010 only tracer, Other sectors. EAS.		
Radon	41	Rn_{Ma}^{222}	Radon-222 tracer, Manohar emission maps. EAS.	(Manohar et al., 2013)	*
	42	Rn_{Sz}^{222}	Radon-222 tracer, Szegvary emission maps. EAS.	(Szegvary et al., 2009)	

* These tracers have been implemented in the framework, but not used within this thesis
** These tracers are used for some of the checks, but no explicit results are shown
V.N. Naipal V., Segers A.J, Peters W.: Simulation of CO_2 in The Netherlands, using the chemistry transport model LOTOS-EUROS, TNO report, MACC II project, July 2012
EAS Emitted at the surface, only in the first vertical model layer.
ECAH Emitted continuously at height, using several or all of the vertical model layers.

2.1.2   Atmospheric CO_2 and $^{14}CO_2$ with WRF-Chem

To simulate the atmospheric transport of the CO_2 and $^{14}CO_2$ in our framework, we select to use WRF coupled with chemistry version of the model (WRF-Chem, Grell et al. (2005)). WRF-Chem simulates the emission, transport, mixing, and chemical transformation of trace gases and aerosols simultaneously with the meteorology.

We have modified the WRF-Chem registry to include 42 different tracers (Table 2.1), most of which are used in the later chapters of this thesis. While some represent entirely different sources, as for example biospheric respiration of CO_2 and the $^{14}CO_2$ emitted from nuclear industry, others represent different vertical distribution of the emissions of the same source. Tracer emissions are supplied to WRF-Chem by the user on an hourly basis. In Chapter 4, the emissions are introduced only in the lowest model level, while in our other studies tracer emissions are introduced in the lowest 10 layers of the model (up to 400 m above surface) depending on the estimated or reported emission height. In Chapter 5 we use all of our 27 vertical atmospheric layers to simulate cosmogenic $^{14}CO_2$ production.

All tracers accumulate mass over the full duration of our simulations, starting from zero mass, and do not include any advection of mass from outside the domain, i.e., we prescribe zero lateral boundary conditions at the mother domain. The only exception is the background CO_2 tracer (CO_{2bg}), which represents all CO_2 (anthropogenic or not) imported from outside the domain, which implicitly also accounts for re-entry of mass that was transported outside the borders of our mother domain. Since WRF-Chem cannot accommodate the transport of negative tracer quantities, both sources and sinks are defined positive in our system and their exact nature is reflected by either adding (for sources) or subtracting (for sinks) the

tracer abundances in our calculations for the total atmospheric CO_2 and its respective $\Delta^{14}CO_2$ signature (explained later in Section 2.3 of this chapter). Table 2.1 shows in more details the different tracers we used and the source information for their input, with specific details:

1) The background CO_2 (CO_{2bg}, #1 in Table 2.1) tracer uses CO_2 mole fractions provided by the CarbonTracker Europe data-assimilation system (Peters et al., 2010). This tracer represents the effects of natural CO_2 fluxes between the atmosphere, biosphere and oceans, but also anthropogenic effects due to land-use change and fossil fuel combustion or emissions from natural fires that occur outside our mother domain. Its emissions inside our WRF domains are zero since these are represented by our dedicated WRF tracers. The 3D mole-fraction output from the larger CT Europe grid was interpolated, horizontally and vertically, to the higher resolution of our WRF domains. These fields supply the initial and lateral boundary conditions for our simulation at 6 hourly intervals.

2) The biospheric SiBCASA CO_2 (CO_{2p} & CO_{2r}, #8 and #9 in Table 2.1) tracers are supplied by monthly mean offline calculations using the SiBCASA terrestrial biosphere model (Schaefer et al., 2008). We performed multiple SiBCASA simulations at $1° \times 1°$ where the entire land was covered homogeneously by a single biome, and then cycled through each of the 10 biomes representative for the land-use map of Europe. The resulting coarse monthly Gross Primary Production (GPP) and Terrestrial Ecosystem Respiration (TER) are scaled-down to the finer horizontal resolution of the WRF domains by picking the appropriate SIBCASA biome simulation for each high resolution grid box of the WRF run. The biomes in SiB-CASA were compared to the WRF land-use categories (U.S. Geographical Survey land cover map) using the relationships shown in Table 2.2. To go to hourly time-resolution from these monthly mean fields, we used the method of Olsen and Randerson (2004), where a shortwave radiation (for GPP) and temperature (for TER) dependent time-variation is introduced that integrates to the SiBCASA monthly averaged fluxes. We use the WRF operational short-wave radiation and temperature at every time step, resulting in a higher temporal resolution biospheric fluxes than the original SIBCASA data.

3) The anthropogenic IER CO_2 (#22 – #33 in Table 2.1) tracers use the emissions from the Institute for Energy Economics and the Rational Use of Energy (IER, University Stuttgart), which provides different categories of anthropogenic emissions. The original data is at 5 geographical minutes horizontal resolution over most of Europe (Figure 1.2 on page 13). Table 2.1 provides descriptions using the Selected Nomenclature for Air Pollution (SNAP, EEA, 2001) categories to describe the different emission sources. The IER data also provides average emission heights for every category and grid point, which is used in Chapter 5 to vertically distribute the emissions in the model. IER provides annual emissions representative for the year 2005, and emission factors on a national level (Figure 2.2) allow the user to include temporal variability, as was done in this thesis. While in Chapter 4 our simulation of 2008 has used the 2005 annual totals reported in the original IER emission data, in our

Table 2.2: *Relationship between WRF (USGS) land cover categories and SiBCASA biome types, as used in this thesis to allocate biospheric CO_2 surface fluxes. Only categories found within our WRF domain are listed.*

	WRF USGS land-use	SiBCASA
#	Description	Fraction $\times$ Biome Code
2, 3	Dry and Irrigated Cropland and Pasture	$1.0 \times$ Cro[1]
5	Cropland/Grassland Mosaic	$0.5 \times$ GrC[2]$+0.5 \times$ Cro
6	Cropland/Woodland Mosaic	$0.5 \times$ MiF[3]$+0.5 \times$ Cro
7, 10	Grassland, Savanna	$1.0 \times$ GrC
8	Shrubland	$1.0 \times$ Shr[4]
9	Mixed Shrubland/Grassland	$0.5 \times$ GrC$+0.5 \times$ Shr
11	Deciduous Broadleaf Forest	$1.0 \times$ DBF[5]
12	Deciduous Needleleaf Forest	$1.0 \times$ DNF[6]
14	Evergreen Needleleaf	$1.0 \times$ NlF[7]
15	Mixed Forest	$1.0 \times$ MiF
19, 24	Barren or Sparsely Vegetated, Snow or Ice	$1.0 \times$ Des[8]
20–23	Herbaceous/Wooded/Mixed/Bare Ground Tundra	$1.0 \times$ Tun[9]

[1] Cro - Agriculture; [2] GrC - Grassland; [3] MiF - Mixed forest; [4] Shr - Shrubland; [5] DBF - Deciduous Broadleaf Forest; [6] DNF - Deciduous Needleleaf Forest; [7] NlF - Needleleaf Forest; [8] Des - No vegetation; [9] Tun - Tundra;

later study in Chapter 5 we have used the greenhouse gas emissions reported to the United Nations Framework Convention on Climate Change inventory (UNFCCC, http://unfccc.int) to correct for the changes in total annual emissions on a national level between the years 2005 and 2010–2012.

4) The anthropogenic $^{14}CO_2$ (#10 – #21 in Table 2.1) tracers use the method described in Graven and Gruber (2011) to estimate $^{14}CO_2$ emissions from nuclear power plants based on the reactor type and produced energy. The International Atomic Energy Agency (IAEA) Power Reactor Information System (PRIS, https://www.iaea.org/pris/) has been used to estimate the annual emissions from nuclear reactors for the years simulated in this thesis. Additional information about the annual gaseous releases of $^{14}CO_2$ from the only operational spent-fuel reprocessing plant in our area of interest (La Hague, France) was available from the environmental monitoring program of the operating company (AREVA, http://www.areva.com/). These annual emissions are assumed to be continuous and provided hourly to the model, but several of the tracers (#19 – #21) also test alternative temporal emission patterns.

5) The pure $^{14}CO_2$ (#2 – #5 in Table 2.1) tracers describe the effect of the disequilibrium fluxes and cosmogenic production (previously introduced in Section 1.4) using spatial monthly data provided to us by J.B. Miller, and were also used in Miller et al. (2012). Since the biospheric disequilibrium $^{14}CO_2$ flux is introduced to the atmosphere during biospheric respiration, we have used the same spatio-temporal downscaling on $^{14}CO_{2dis}^{bio}$ as we described earlier for CO_{2r}.

6) Some tracers are listed in Table 2.1, but not explicitly used in the chapters of this thesis.
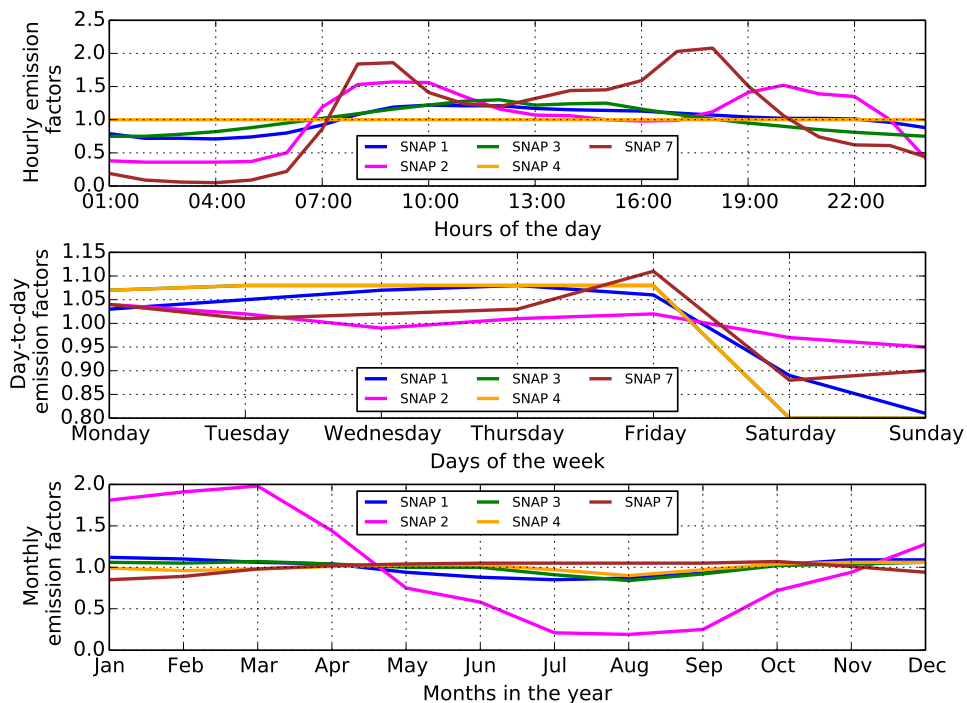
Figure 2.2: Example of the IER time profiles for the Netherlands. The selected emission categories shown in this figure (SNAP 1 - Energy production; SNAP 2 - Non-industrial combustion; SNAP 3 - Combustion in manufacturing; SNAP 4 - Production processes and SNAP 7 - Road transport) constitute up to 98% of the total anthropogenic CO_2 emissions for Europe.

These alternative biospheric or fossil fuel tracers were used to compare methods or emission datasets. Furthermore, we included two radon (^{222}Rn) tracers in our system to enable in the future the evaluation of the simulated vertical mixing.

2.2 Crop growth modeling with SUCROS

We use the Simple Universal CROp growth Simulator (SUCROS, Goudriaan and van Laar, 1994; van Laar et al., 1997) to model plant growth in our framework. The SUCROS model comes in two versions: SUCROS1, which simulates the crop potential growth without any water- or nutrient-limitations in a disease-, weed- and pest-free environment; and SUCROS2, which builds on the first version by modeling production in water-limited conditions. We have used SUCROS2 in this thesis and will refer to it simply as SUCROS.
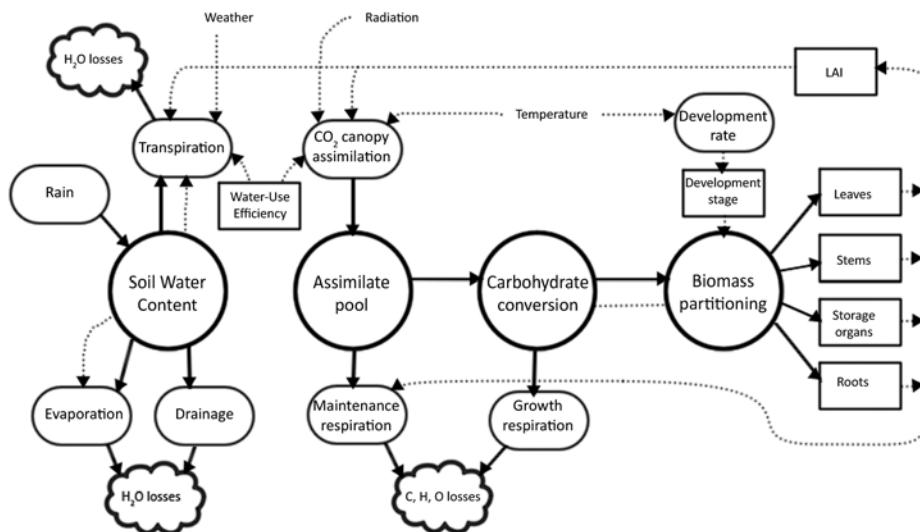
Figure 2.3: SUCROS diagram: Boxes are state variables, ellipsoids are rate variables, circles are intermediate variables. Solid lines represent flows of material, while dotted lines are flows of information. This figure is adapted from (van Laar et al., 1997).

SUCROS is a mechanistic model that simulates the dry mass accumulation (growth) in a crop through CO_2 assimilation and autotrophic respiration. It simulates not only plant growth, but also plant development (phenology) and the partitioning of carbohydrates to different parts of the plant such as leaves, and the resulting plant properties such as leaf area index (LAI). A diagram with the processes and variables involved is shown in Figure 2.3. This model runs on a daily time step and requires as input crop-specific physiological properties and weather conditions. These inputs are explained in more detail at the end of this Section.

2.2.1 Plant development

Plant development in annual crops can often be described with two successive growth phases: the vegetative period, when roots, stems and leaves are produced; and the reproductive period, when the production switches to include reproductive and storage organs, such as flowers, pollen and seeds. The vegetative phase starts when the plant emerges above the soil (emergence) and ends when the plant start to produce pollen (flowering). The reproductive phase starts with the flowering of the plant and ends when the fruits or seeds are ripe (maturity).

This development is implemented in SUCROS with a dimensionless variable to represent the current development stage of the plant, which has a value of 0 at the stage of emergence,

1 at flowering and 2 at maturity. The development stage results from the integral of the development rate, which in turn depends on the daily temperature. The two development phases require different amounts of accumulated temperature (Goudriaan and van Laar, 1994) to reach the next stage (measured usually in degree-days) and SUCROS has a different development rate before and after flowering.

The development stage affects the partitioning of CO_2 assimilates into biomass of the plant organs. For example in maize crops assimilated carbon produces new leaves, roots or stems before flowering, but after flowering leaves will no longer accumulate new biomass as the assimilates will be partitioned towards storage organs instead. Furthermore, after flowering a fraction of the biomass in stems, which represents the carbohydrate reserves (starch), is converted back to sugars to boost the growth of storage organs (Penning de Vries et al., 1989).

2.2.2 Plant growth

SUCROS calculates the instantaneous CO_2 assimilation rates from the intercepted photosynthetically active radiation (PAR) and from the individual leaf CO_2 assimilation-light response curve. The former is calculated using the LAI and the light extinction coefficient in the canopy (k), accounting for diffuse and direct radiation (Spitters, 1986; Spitters et al., 1986), and the impact of LAI on the light transmission in the canopy. The individual leaf CO_2 assimilation-light response depends on crop-specific characteristics, on the development stage, and on temperature.

The CO_2 assimilation of individual leaves and the PAR absorbed by the entire canopy determine the daily gross CO_2 assimilation in SUCROS. As a first step, the instantaneous assimilation rates at three levels of the canopy are calculated, and then integrated over the whole canopy depth. This procedure is then repeated at three different times of the day. The resulting canopy assimilation rates are integrated over the entire day to produce the daily gross CO_2 assimilation (Goudriaan, 1986). This stepwise approach is needed because the CO_2 assimilation response to light intensity is non-linear, and using averaged daily values of the inputs would result in large overestimation of the total canopy CO_2 assimilation.

The daily gross CO_2 assimilation provides the plant with a pool of CO_2 assimilates which are transformed to carbohydrates (represented as units of CH_2O with a molar mass of 30) through photosynthesis. A conversion factor is used such that for each gram of CO_2 assimilates, 30/44 grams of CH_2O are formed (van Ittersum et al., 2003; van Laar et al., 1997). Part of these carbohydrates are respired back in order to provide energy to sustain the existing biostructures (maintenance respiration). In SUCROS, the maintenance requirements are different between plant organs and in addition, a temperature dependence is included that represents the accelerated turnover rates in plant tissue and resulting increased costs of

Table 2.3: Relationship between WRF output and SUCROS input weather variables, as used in this thesis.

SUCROS input daily variable [Units]	WRF output hourly variable [Units]
Solar Radiation [kJ m^{-2} d^{-1}]	Shortwave downward radiation [W m^{-2}]
Minimum Temperature [°C]	Temperature at 2 m [K]
Maximum Temperature [°C]	Temperature at 2 m [K]
Water vapor pressure [kPa]	Water mixing ratio at 2 m [kg kg^{-1}] and surface pressure [Pa]
Mean wind speed [m s^{-1}]	U and V component of the wind at 10 m [m s^{-1}]
Precipitation [mm d^{-1}]	Convective and large-scale precipitation [mm]

maintenance at higher temperatures (Penning de Vries and van Laar, 1982).

The carbohydrates pool left after the maintenance respiration is entirely available to be converted into plant biomass. As mentioned, partitioning over the various plant parts is a function of the development stage, but in general, dry matter is first partitioned between roots and shoots, and then the shoot fraction is redistributed among leaves, stems and storage organs. Conversion from carbohydrate to gram of dry mass is executed through different factors for the different plant organs, which reflect their typical chemical composition (van Laar et al., 1997). The loss of carbon mass during this conversion represents the growth respiration in the model. The growth and maintenance respiration terms combined represent the crop autotrophic respiration of CO_2. Heterotrophic respiration is not accounted for in SUCROS.

SUCROS calculates its own LAI, taking into account the very different rate of the leaf area expansion during the development stages. In the early stages of growth during the vegetative phase, leaf area increases approximately exponentially over time with temperature being the driving factor of the appearance of new leaves. Later during the vegetative phase, the leaf area expansion becomes restricted by the supply of carbohydrates and the model starts to calculate the increase in the leaf area using the dry mass increment in the leaves compartment. SUCROS also has a senescence rate of LAI, which combines the effects of aging and self-shading, and partitions the leaves pool between dead and green leaves. This information is subsequently used in the calculation of the daily gross CO_2 assimilation.

2.2.3 Water stress

The SUCROS water balance is modeled in a simplified, parametric manner that nonetheless accounts for the major processes involved in the transport of water in and out of the plant-soil system (van Laar et al., 1997). The loss of water from the soil (evaporation) and the plant (transpiration) is calculated based on the Penman-Montheith equation for potential evapo-

transpiration (Monteith, 1965). The potential values for both evaporation and transpiration derived from this formulation reflect conditions with ample supply of moisture. In SUCROS these are used as reference values to the actual plant or soil water losses, as explained later.

In the model, when rain falls, part of the water is intercepted by the plant canopy and the rest reaches the soil surface. Runoff at the surface occurs when the rain is strong or the water content of the top soil layer is high. All water left after the interception by canopy and runoff, infiltrates the soil. Redistribution of the water content between the 4 soil layers in SUCROS is implemented through "tipping bucket" approach and every day half of the excess above the field capacity of the layer is transported to the lower soil layer. When the lowest layer has more water than it can retain at field capacity, part of it is lost through external drainage. Drainage is limited by soil characteristics and the excess water left in the layer will start to fill up until saturation level is reached. This triggers the waterlogging process, when water from the saturated soil layer will start to overflow to upper layers, and if the whole soil profile is saturated, it will flow over the surface.

Evaporation is an important variable when the canopy is not well developed, but is otherwise much lower than the transpiration. SUCROS accounts for soil dryness based on the days since last rainfall. In days without rain, the actual evaporation is less than the potential, and decreases further as the top soil layer starts drying. The model imitates the redistribution of water due to gradients in the water content by evaporating, although with different weights, from all soil layers.

The connection between soil and plant in SUCROS is realized through simulation of the root system for the plant. The root length determines the maximum depth from which the crop effectively extracts water. Elongation of the roots depends partly on the soil and species characteristics, accumulation of roots dry mass and temperature. Still, the root extension ceases when the root tip reaches a soil compartment with enough water content. Water uptake from the roots determines the moisture available to the plant in water-limited conditions.

Transpiration is the process in the water cycle of the plant that also affects its CO_2 assimilation. In the model, when there is water limitation, the actual transpiration becomes smaller than the potential and the plant begins experiencing water stress. Its transpiration becomes constrained by its water uptake from the soil. To reduce the loss of water the plant closes its stomata and thus limits the CO_2 assimilation (Goudriaan and van Laar, 1978). The amount of water stress in SUCROS is implemented through the ratio between the actual and potential transpiration of the plant. This value is used as direct multiplication factor for the CO_2 assimilation in the plant. As an additional effect, when the plant experiences severe water stress and this factor is <0.5 the partitioning of newly assimilated dry mass is changed in a way that suppresses the growth in shoots and promotes the root growth (Brouwer, 1963).

2.2.4 Weather variables and crop parameters

The default SUCROS model implementation is for spring wheat crop, and used in Chapter 3. Alternative settings for maize crops are used throughout this thesis and the values for the species-specific variables are provided through Boons-Prins et al. (1993). The user provides the emergence date of the crop, and weather information for the entire growing season. Daily weather variables are calculated from our hourly WRF variables shown in Table 2.3. These settings were previously used to model spring wheat in a study by Combe (2010).

2.3 Atmospheric and plant $\Delta^{14}CO_2$

There are several ways of modeling and calculating the $\Delta^{14}CO_2$ of a sample. The most direct approach is to transport the absolute quantities of all carbon isotopes (^{12}C, ^{13}C, ^{14}C) and use Equation 1.3 (page 14) to calculate the $\Delta^{14}CO_2$ of the air in the same way it would calculate the signature of a measured sample (Hesshaimer, 1997; Naegler and Levin, 2006; Turnbull et al., 2009b). This method would require one to take into account the mass-dependent isotopic fractionation when CO_2 is transported between the different carbon pools. The implementation of this process is challenging, considering that the magnitude of this natural discrimination against the heavier isotopes in the biosphere is not constant and will change during periods of droughts or increased water stress (van der Velde et al., 2014a).

In this thesis we use an alternative approach of modeling carbon dioxide by using tracers of pure radiocarbon ($^{14}CO_2$ only) and tracers that contains all carbon isotopes (CO_2). Each of the "general" CO_2 tracers has the $\Delta^{14}CO_2$ signature associated with its source, that gives the relative ^{14}C content but also already accounts for isotopic fractionation. This setup uses the $^{14}CO_2$ mass balance equations (Eq. 1.4–1.5, page 15) to calculate offline the $\Delta^{14}CO_2$ of the atmosphere (Δ_{air}). In a simplified version, each type of the tracers shown in Table 2.1 is presented by a single term and the resulting mass balance equation is:

$$\Delta_{air}CO_{2air} = \underbrace{\Delta_{bg}(CO_{2bg} + CO_{2r} - CO_{2p})}_{keep\ the\ current\ ^{14}C/C} + \underbrace{\Delta_{ff}(CO_{2ff})}_{lowers\ ^{14}C/C} + \underbrace{\Delta_n(^{14}CO_{2nuc} + ^{14}CO_{2dis} + ^{14}CO_{2c})}_{increase\ ^{14}C/C},$$

$$(2.1)$$

where CO_{2air} is the total CO_2 concentration in that atmospheric layer and Δ_n is the signature of a pure ^{14}C sample (the exact calculation is provided in Equations 4.5 and 4.6 on page 69).

It is important to note that while in this equation all CO_2 concentrations are provided by the model and Δ_{ff} and Δ_n can be calculated analytically, the $\Delta^{14}CO_2$ signature of the background air (Δ_{bg}) must be provided externally. In this thesis we most often use time-series from monthly integrated observations from the high-alpine observatory in Jungfraujoch, Switzerland (data courtesy to I. Levin and S. Hammer, University of Heidelberg, previously shown in

Figure 1.4 on page 17), however this choice is arbitrary and will be discussed in our following studies.

We calculate the $\Delta^{14}CO_2$ of the plant (Δ_{plant}) by combining the results from the two parts of our modeling framework offline. Firstly, we calculate the atmospheric $\Delta^{14}CO_2$ for every grid box in our domains from the WRF-Chem transported tracers. These hourly results are weighted within every separate day by the photosynthetic uptake (CO_{2p} tracer surface flux) calculated by WRF-Chem to produce (1) the daily daytime value of the atmospheric $\Delta^{14}CO_2$ signature (Δ_{air}). Secondly, we use the WRF-simulated weather for every grid box in our domains to simulate crop growth with SUCROS. In Chapter 3 and Chapter 4 we prescribe a uniform day of emergence for our entire domain, while in Chapter 5 we use emergence dates from local farmers to drive SUCROS for individual locations. We use the SUCROS-generated daily dry mass for each plant part to calculate (2) the daily dry weight increment (DWI). Finally, we use DWI as a weighting function (averaging kernel) on Δ_{air} to calculate the $\Delta^{14}CO_2$ signature that has accumulated in the plant biomass:

$$\Delta_{\text{plant}} = \sum_t \Delta_{\text{air}}^t \frac{DWI_t}{\sum\limits_t DWI_t}, \tag{2.2}$$

where DWI_t is the dry weight increment of a particular plant part, as provided by SUCROS, at time (day) t, for which the daily daytime atmospheric $\Delta^{14}CO_2$ signature has been Δ_{air}^t.

The construction of the averaging kernel and its significance for the calculation of plant-sampled $\Delta^{14}CO_2$ is explained in more detail in the following Chapter 3.

3

The importance of crop growth modeling to interpret the $\Delta^{14}CO_2$ signature of annual plants

The $^{14}C/C$ abundance in CO_2 ($\Delta^{14}CO_2$) promises to provide useful constraints on regional fossil fuel emissions and atmospheric transport through the large gradients introduced by anthropogenic activity. The currently sparse atmospheric $\Delta^{14}CO_2$ monitoring network can potentially be augmented by using plant biomass as an integrated sample of the atmospheric $\Delta^{14}CO_2$. But the interpretation of such an integrated sample requires knowledge about the day-to-day CO_2 uptake of the sampled plants. We investigate here the required detail in daily plant growth variations needed to accurately interpret regional fossil fuel emissions from annual plant samples.

We use a crop growth model driven by daily meteorology to reproduce daily fixation of $\Delta^{14}CO_2$ in maize and wheat plants in the Netherlands in 2008. When comparing the integrated $\Delta^{14}CO_2$ simulated with this detailed model to the values obtained when using simpler proxies for daily plant growth (such as radiation and temperature), we find differences that can exceed the reported measurement precision of $\Delta^{14}CO_2$ ($\sim$2‰). Furthermore, we show that even in the absence of any spatial differences in fossil fuel emissions, differences in regional weather can induce plant growth variations that result in spatial gradients of up to 3.5‰ in plant samples. These gradients are even larger when interpreting separate plant organs (leaves, stems, roots, or fruits), as they each develop during different time periods. Not accounting for these growth-induced differences in $\Delta^{14}CO_2$ in

plant samples would introduce a substantial bias (1.5-2 ppm) when estimating the fraction of atmospheric CO_2 variatons resulting from nearby fossil fuel emissions.

3.1   Introduction

Although observations of CO_2 have been very important for our current understanding of the carbon cycle (Keeling, 1978; Tans et al., 1990; Keeling et al., 1995; LeQuere et al., 2007; Stephens et al., 2007) it has proven difficult to extract process specific information from CO_2 alone. The observations are therefore usually complemented by observations of various trace gases connected with fossil fuel combustion, biosphere and ocean exchange (CO, $^{13}CO_2$, $^{14}CO_2$, SF_6, ^{222}Rn, O_2/N_2 and many others). Among the different alternatives, the radioactive isotope of carbon (^{14}C) is a tracer which is strongly influenced by anthropogenic CO_2 emissions. Its half-life time of 5730±40 years (Godwin, 1962) ensures that fossil fuel combustion releases only $^{12,13}CO_2$ into the atmosphere. This process effectively dilutes the atmospheric mixing ratios of $^{14}CO_2$ and is known as the Suess effect (Suess, 1955). The magnitude of the dilution can thus be used to quantify regional fossil fuel CO_2 addition to the atmosphere in regions where this addition is of relatively large importance for $\Delta^{14}CO_2$.

Usually the method to calculate the recently added fossil fuel CO_2 (denoted from hereon as CO_{2ff}) is based entirely (Meijer et al., 1996; Levin et al., 2003; Turnbull et al., 2006; Hsueh et al., 2007; Palstra et al., 2008; Turnbull et al., 2009b; Vay et al., 2009) or partly (Gamnitzer et al., 2006; Levin and Karstens, 2007) on observations of CO_2 and $^{14}CO_2$. Atmospheric observations of $^{14}CO_2$ are typically reported as $\Delta^{14}CO_2$ [‰], the normalized difference between the sample and a standard, corrected for various processes (Stuiver and Polach, 1977; Mook and van der Plicht, 1999). The total uncertainty in the calculation of CO_{2ff} mainly depends on the $\Delta^{14}CO_2$ measurement precision and can be less than 1 ppm per single observation for precision of ~2‰ (Turnbull et al., 2009b). Only few labs obtain such a precision, and in the more general case, where it is ~3-5‰ the uncertainty in the recalculation will be between 1 and 2 ppm. Still, comparing this to the typical summer daytime CO_{2ff} at the site of Cabauw in the Netherlands (2–8 ppm) (Tolk et al., 2009), or the CO_{2ff} in a polluted area like Heidelberg (10–12 ppm) (Levin and Rödenbeck, 2008) shows how $\Delta^{14}CO_2$ could provide useful information on regional fossil fuel emissions.

Globally, $\Delta^{14}CO_2$ observations are collected only at a limited number of sites, with interest mostly towards the atmospheric background levels and thus usually far from anthropogenic emission sources (Meijer et al., 1995; Levin et al., 2010; Graven et al., 2012b). To estimate the recently added fossil fuel CO_2 to the regional atmosphere, numerous flask samples or time-integrated samples should be taken from various sites (Levin et al., 2003). There are advantages and disadvantages to both sampling approaches, and besides the challenges in the measurement of ^{14}C itself, a major concern is the cost of long-term observations and

sample analysis. A possible solution for the lack of observational sites is to use annual plant samples, as these have been shown to adequately represent in a qualitative manner the fossil fuel emissions on a continental (Hsueh et al., 2007) and regional scale (Riley et al., 2008). Different types of annual plants are grown for agricultural and industrial use (for example wine or rice production), often close to anthropogenic sources, thus offering an opportunity to obtain samples without significant financial investment. Additionally, because of the variable use of crops in industry, there is even the possibility to access information from previous years by sampling, for instance, wine records or rice grains (Burchuladze et al., 1989; Shibata et al., 2005; Palstra et al., 2008).

Integrated $\Delta^{14}CO_2$ samples obtained at most observational sites (among others - Levin et al. (1980); Meijer et al. (1995)), differ substantially from plant samples. In the traditional method, atmospheric air is pumped for several weeks with constant flow rate through an alkaline solution (usually NaOH) that absorbs the CO_2 for later isotopic analysis. The absorbed CO_2 is thus proportional to the instantaneous CO_2 concentrations, and as the stable boundary layer traps the CO_2 emissions near surface overnight, this method usually weights nighttime periods more heavily (Hsueh et al., 2007). Even so, the interpretation of an integrated NaOH sample is relatively straightforward as its sampling period is fixed and its rate of sampling is constant. This differs considerably from plant samples, where the recorded signal is obtained only during daytime and both the growing/sampling period and assimilation rate vary substantially.

Plant samples are usually obtained by picking leaves or storage organs (e.g. seeds and fruits) from annual, perennial plants or even from trees. In the study of Hsueh et al. (2007), the plant samples analyzed consisted mostly of corn leaves, but in some regions, also corn husks and annual forb were used. Their findings showed that the biomass of the annual plants represents a time-integrated measure of daytime atmospheric $\Delta^{14}CO_2$ during the period of growth, weighted by the rate of carbon fixation. In a further study, Riley et al. (2008) sampled winter annual grasses in California and compared the observed signatures with predicted ones. In this case, the modeled atmospheric $\Delta^{14}CO_2$ and modeled gross primary production (GPP) for C_3 grasses over the simulated area were used to estimate the $\Delta^{14}CO_2$ signature of the biomass, by creating a GPP-weighted sum of the daytime atmospheric signature. In the study of Palstra et al. (2008), grapes, and more specifically wine, were used as samplers. They discuss the difficulties arising from the unknown sampling period, and the variable carbon uptake flow and their modeling approach takes into account that grapes will form in only few months while the growing period of the grapevine is much longer. All these studies followed the idea that the atmospheric carbon isotope ratios are recorded as part of the daily photosynthesis and fixed in the plant structure when the assimilated carbon is allocated. Additionally, they agree that the period for which the atmospheric isotopic ratios are represented in the plant is related to the period and rate of growth of the plant. Thus, to quantitatively interpret

a plant sample in the context of the atmospheric carbon isotope ratios, we must construct a function (averaging kernel) that weights the daily contribution of the atmospheric $\Delta^{14}CO_2$ signature to the signature of the entire integrated plant sample, or to the specific organ that was picked.

It is clear that the averaging kernel has to be a function of the plant CO_2 assimilation rate, but the level of complexity in this kernel required for a reasonable representation of the signature is still unknown. The instantaneous rate of CO_2 assimilation depends on multiple factors, some of which are external to the plant (the abundance or absence of photosynthetically active radiation, the surface temperature and humidity, nitrogen application or disturbances), and some of which are internal (such as the plant species, phenological changes during the plant life-time, and its drought sensitivity). In order to include plant observations to our suite of $\Delta^{14}CO_2$ sampling methods, we would like to reproduce the way plants sample atmospheric CO_2 and the resulting integrated $\Delta^{14}CO_2$ signature with sufficient accuracy. The latter is our objective in this paper.

To isolate the effect of plant growth variations on the integrated $\Delta^{14}CO_2$ signature, we exclude in this study the other main source of variability that will be recorded: the fossil fuel emissions in the vicinity of growing plants. But our ultimate goal is to estimate exactly this fossil fuel component through the recorded $\Delta^{14}CO_2$ in plant samples. The plant growth averaging kernels described here thus form a barrier to this intended interpretation, and we show in this work how it can be overcome by using a suitable crop model to account for temporal and spatial plant growth variations over a growing season. To make the recorded atmospheric $\Delta^{14}CO_2$ in our simulated plants over a growing season as realistic as possible, but without any local fossil fuel influences, we have constructed one time series with realistic day-to-day $\Delta^{14}CO_2$ changes over a growing season to supply to all our calculations of plant sampled $\Delta^{14}CO_2$ over the domain we study, as described in Section 2.1. The effects that we quantify here based on plant averaging kernel variations alone will be compared to expected fossil fuel (and other) signals from other published studies. We are working towards a full description of these variations for a follow-up study on the one presented here.

Specific questions that we address in this work are: (1) Which external data do we need to accurately construct an averaging kernel for plant samples? (2) Are there sampling or interpretation-related strategies that minimize the sensitivity of the resulting $\Delta^{14}CO_2$ signature to the averaging kernel? (3) Can a simple proxy for plant growth reasonably replace the more complex modeling of the crop growth pattern over time? And finally, (4) can the use of detailed plant growth models overcome the possibly limited interpretability of plant samples for fossil fuel monitoring?

3.2 Methodology

3.2.1 The modeled atmospheric $\Delta^{14}CO_2$ signature

To investigate the sample signatures resulting from the use of different averaging kernels, we construct one time series with realistic variations of the atmospheric $\Delta^{14}CO_2$ evolution on an hourly scale. This time series we prescribe to all the locations and kernels we use in this study to simulate integrated samples. We constructed this time series based on the regional budget of the atmospheric $\Delta^{14}CO_2$, and the estimation of recently added fossil fuel CO_2 as also used in Levin et al. (2003); Turnbull et al. (2006); Hsueh et al. (2007); Riley et al. (2008); Palstra et al. (2008); Graven and Gruber (2011) and thoroughly described in Turnbull et al. (2009b). The simplified form of the calculation is shown in Eq. 3.1 .

$$\Delta_{\text{sample}} = \frac{\Delta_{\text{bg}}(CO_{2\text{sample}} - CO_{2\text{ff}}) + \Delta_{\text{ff}}CO_{2\text{ff}}}{CO_{2\text{sample}}} \qquad (3.1)$$

Here the observed atmospheric $\Delta^{14}CO_2$ signature (Δ_{sample}) is described through a relation between the total observed CO_2 concentrations ($CO_{2sample}$), the background CO_2 concentrations (CO_{2bg}, consisting of biospheric, oceanic, fire derived, and non-recent fossil CO_2 emissions) and the recent fossil fuel addition (CO_{2ff}), with their respective $\Delta^{14}CO_2$ signatures (Δ_{bg},Δ_{ff}). Thus calculated, our atmospheric $\Delta^{14}CO_2$ series excludes the influence of the nuclear power plant production, ocean disequilibrium and biosphere disequilibrium fluxes, and of ^{14}C-enriched high tropospheric and stratospheric air (all to the extent they are not represented in the background terms). While these processes should be accounted for when actually interpreting observed $\Delta^{14}CO_2$ samples, in our current work, they are of less importance as the fossil fuel addition has much greater influence on the day-to-day variability.

Time series of CO_{2ff}, CO_{2bg}, and $CO_{2sample}$ (where $CO_{2sample}$= CO_{2bg}+CO_{2ff}) with 1.5 h temporal resolution were simulated for the Lutjewad sampling station (Centre for Isotope Research, Groningen University, the Netherlands; latitude 53°24'N, longitude 6°21'E, altitude 1m above sea level (asl); henceforth Lutjewad), based on CarbonTracker Europe modeling results (Peters et al., 2010). The fossil fuel emissions use the annual global and country totals from the Carbon Dioxide Information and Analysis Center (Marland et al., 2008), spatial distribution on national level according to the patterns of Emission Database for Global Atmospheric Research (Olivier and Berdowski, 2001) v4.0 and the seasonality per grid box is dependent on the inventory of the Institute of Economics and the Rational Use of Energy (Pregger et al., 2007), University of Stuttgart - more details are available on http://www.carbontracker.eu . The choice of location is somewhat arbitrary, since we will apply the same time series uniformly for our entire spatial domain, but we decided on this

location as it provides observational data from integrated monthly $\Delta^{14}CO_2$ samples. We estimate monthly averaged Δ_{bg} from observed time series for the Jungfraujoch site (Levin et al., 2010). Fossil fuels are totally devoid of $^{14}CO_2$ and as such their signature is $\Delta_{ff} = -1000$ ‰. Together with equation 3.1, these simulated and observed values allowed us to construct a realistic diurnal $\Delta^{14}CO_2$ time series.

The atmospheric $\Delta^{14}CO_2$ signature seen by the plants is always the signature of the sunlit part of the day, when the boundary layer is developed and usually well mixed. For the actual application of the atmospheric time series, we created daytime averages from the available daily data for the hours between 0600 and 2000 local time (LT) every day starting from 1 April and ending with 30 September 2008. The constructed time series for daytime daily $\Delta^{14}CO_2$ is shown in Figure 3.1(A) along with the observed Δ_{bg} from Jungfraujoch (as applied in our calculations) and a smooth curve fit (Thoning and Tans, 1989) to our full time series. The figure shows that day-to-day variations in $\Delta^{14}CO_2$ are large compared to month-to-month variations visible in the smoothed curve.

3.2.2 SUCROS model description

We use the Simple Universal CROp growth Simulator 2 (SUCROS 2) to model plant growth and associated CO_2 uptake (Goudriaan and van Laar, 1994; van Laar et al., 1997) . SUCROS 2 is a mechanistic model that includes the main processes of carbon assimilation, such as photosynthesis and autotrophic (growth and maintenance) respiration. It simulates the crop dry matter accumulation in water-limited conditions, but does not account for nutrient limitation, pests, diseases, and weed effects on growth. SUCROS 2 has the advantage of simulating plant phenology and as a result has a development-dependent carbohydrate partitioning and leaf area index. The model has been applied to several crops (wheat (van Laar et al., 1997), maize (Xevi et al., 1996; Arora and Gajri, 2000), sugar beet (Guérif and Duke, 1998), sugar cane (Singels et al., 2010), and cotton (Zhang et al., 2008)) and has evolved as the platform on which more complex and specialized models are built (van Ittersum et al., 2003).

SUCROS 2 simulates the growth of a field of specific plant species, and in this research we have modeled the growth of two common crops - maize (*Zea mays*) and spring wheat (*Triticum aestivum*). We chose these two species for their large use in agriculture and because they are widely grown not only in the Netherlands but most parts of the world. As they are of great interest for the food industry, there is an abundance of research and field data available to validate models for these crops, including SUCROS 2. Additionally, these two crops grow in similar conditions and consecutive periods in the year, opening the possibility for sampling scenarios that use multi-species samples to provide observations for longer period of time.

Besides the species specific physiological and phenological characteristics, the model requires limited information about the initial conditions of the crop growth and general daily
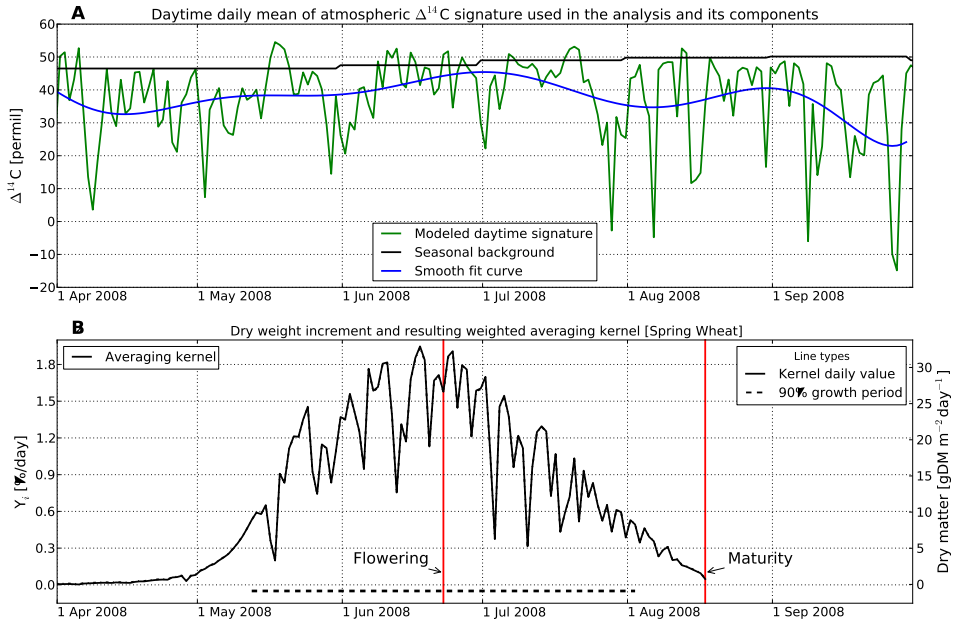
Figure 3.1: (A) Simulated daily averaged daytime-only atmospheric $\Delta^{14}CO_2$ signature over the Netherlands (in green). The series are estimated using observed 2008 hemispheric background $\Delta^{14}CO_2$ values from Jungfraujoch (Levin et al., 2010) (in black) and local fossil fuel addition modeled using CarbonTracker results for the location of Lutjewad (Netherlands) (in green). The smooth curve was created using NOAA ESRLs ccgcrv routine (Thoning and Tans, 1989) (in blue). (B) Total plant dry weight increment and resulting averaging kernel for spring wheat, modeled with SUCROS 2 and weather data from Wageningen (Netherlands). The averaging kernel is complemented by estimation of the 90% growing period (dashed horizontal line at bottom of the figure).

weather information for the location in question. For the species that we chose to investigate, water stress is rarely of importance before the flowering stage. The input weather data is described in more detail in Section 3.2.3.

In SUCROS 2, the different plant organs are represented as separate pools of dry mass for leaves, roots, stems, and storage organs. In this study, we investigate the dry weight increment for each of these organs, and for the entire plant, to use as kernels to express the CO_2 assimilation by the plant. The biggest change in growth dynamics of the chosen plant species occurs at flowering. This stage marks the end of the vegetative growth of the plant, and the beginning of the reproductive phase, when the development and growth of storage organs takes priority over all other plant part compartments. In cereals, the plant

will translocate biomass from stems and leaves to the storage organs, usually starting after the flowering stage. This process is captured by SUCROS 2, but is difficult to account for when modeling the recording of the $\Delta^{14}CO_2$ signature over time. We will further comment on the development driven differences that occur during the lifetime of the plant, as they are important for the $\Delta^{14}C$ signature of the plant and its organs.

3.2.3   Weather data

Observed and simulated weather for the year 2008 over the Netherlands was used as input for the SUCROS 2 crop growth model. Observational data was taken from the Haarweg meteorological station (Meteorology and Air Quality group, Wageningen University, Netherlands; latitude 51°58'N, longitude 5°38'W, altitude 7m asl; www.maq.wur.nl) and used to investigate the plant growth characteristics at a single location (Sections 3.3.1, 3.3.2). To get spatially explicit weather data for the growing season between April 1 and October 1 2008, we used the Weather Research and Forecast (WRF) model. A detailed description of WRF is available in Skamarock et al. (2008). The WRF-generated weather data is used in Section 3.3.3. To prevent confusion, we explicitly state that the WRF model was not used for any atmospheric transport of tracers, or CO_2, or its isotopes, but only to generate meteorological variables to drive plant growth.

The WRF model was initialized using boundary conditions from 6-hourly global reanalysis fields from the National Centers for Environmental Prediction - National Center for Atmospheric Research (Kalnay et al., 1996), for three two-way nested domains with the number of total grid points of 60x60/52x52/88x88 and corresponding horizontal resolution of 36/12/4 km. The vertical resolution was 28 levels, with 15 levels in the lower 2 km and 6 levels in the first 200 m of the atmosphere. The model setup included the Monin-Obukhov surface layer physics scheme, the Unified NOAH land-surface model (Ek et al., 2003) and the Yonsei University planetary boundary layer scheme (Hong et al., 2006). The resulting output that was used in this study has an hourly temporal resolution over the nested domain with spatial resolution of 4x4 km (88x88 grid points).

The WRF results were compared to observational data from 35 meteorological stations in the Netherlands [Royal Netherlands Meteorological Institute (KNMI), http://www.knmi.nl] to estimate the quality of the simulated weather conditions during the growing season. The daily weather input for the SUCROS 2 model, constructed from station observed data and the WRF simulation, was evaluated on a statistical basis through comparison between observed and predicted mean values, standard deviations, root mean square error (RMSE), and Pearson's correlation coefficient (r) – methods described in Willmott (1982). A selection of these results is shown in Table 3.1. Overall, our comparison shows that the WRF-simulated weather is close to the one observed in the local meteorological stations. The two variables

Table 3.1: Statistical comparison between observational data from 35 stations in the Netherlands [Royal Netherlands Meteorological Institute (KNMI), http://www.knmi.nl] and WRF-simulated weather for each station location[a].

Daily Weather Variable [Units]	$\overline{O-P}$	$\overline{O-P/O}$ x100%	σ_{O-P}	RMSE	r
Solar Radiation [W m^{-2}]	-45.27	-24.3	61.9	76.86	0.65
Minimum Temperature [°C]	0.04	0.4	2.7	2.84	0.81
Maximum Temperature [°C]	-2.11	-10.9	2.1	2.94	0.90
Water vapor pressure [kPa]	0.1	7.5	0.2	0.19	0.90
Mean wind speed [m s^{-1}]	-0.94	-22.0	1.22	1.72	0.75
Precipitation [mm d^{-1}]	0.3	14.4	5.0	5.02	0.37

[a] Shown are the results for the root mean square error (RMSE), correlation coefficient (r) and the absolute ($\overline{O-P}$) and relative ($\overline{O-P/O}$ x100%) differences between observed and predicted means and the standard deviation of the difference between observed and predicted (σ_{O-P}). Negative differences in the mean values occur when the model is predicting higher values than observed. The relative difference is expressed in [%], the correlation coefficient is unitless and all other measures refer to the units described in the first column.

in which we see largest differences during the 6 months of simulated weather are the daily radiation sum and daily precipitation sum. In both cases, the reason for the difference is the general difficulty, found also in other mesoscale models, to model the cloud formation and rain events at a particular location. On average, for the 6 months of weather simulation, this results in overprediction in the amount of daily radiation and underprediction in the daily precipitation. We assess that the difference in the radiation would add a slight bias in our total simulated plant growth, which, however, does not affect the day-to-day variations. The underprediction of both precipitation and mean wind speed could result in limiting plant growth conditions. Nevertheless, for the plant species we investigate, water stress occurs mostly after the flowering date, which is a growth period we do not analyze in depth, as discussed in Section 3.4.

3.2.4 The averaging kernels

To translate the atmospheric $\Delta^{14}C$ signal into the integrated $^{14}CO_2$ signal in plants, we construct an averaging kernel (Y) of a time series (X) by normalizing the value of each element towards the sum of all the elements of a chosen period. Thus, the daily value of the kernel (Y_i) is expressed as:

$$Y_i = \frac{X_i}{\sum\limits_{t} X_i} \tag{3.2}$$

After the application of the averaging kernel to the atmospheric $\Delta^{14}CO_2$ series ($\Delta^{14}C_{sample}$ or Δ_{sample}) the resulting integrated signature ($\Delta^{14}C_{res}$ or Δ_{res}) will be:

$$\Delta^{14}C_{res} = \sum_t \Delta^{14}C_{sample\,i}Y_i \qquad (3.3)$$

The kernel constructed from SUCROS 2-simulated daily dry weight increment is treated in this study as the "true kernel" as it represents the most complete simulation of all factors affecting plant growth simultaneously. In addition, we also constructed a flat kernel (representing an equal weighted mean of the atmospheric $\Delta^{14}CO_2$ signature), and kernels from daily incoming solar radiation and 2 m temperature as these are known to strongly influence plant growth.

We constructed separate averaging kernels for the plant organs (leaves, stems, roots and storage organs) from the daily dry weight increment of the respective compartments. We calculated the signatures resulting from these kernels for the period that ends when the plant reaches the flowering stage, and at the end of the growing period, when the plant reaches maturity. We define the peak period of an averaging kernel as the period, in which 90% of the growth of the plant is occurring, by removing the periods of lower relative weight. Hereafter, we refer to this period as the peak period, or the 90% period. The true kernel for the total plant simulation of spring wheat and the according 90% period can be seen in Figure 3.1(B).

3.3 Results

In the following sections we will address three main research questions of this study.

3.3.1 Can a plant growth proxy replace a plant growth model?

Daily plant growth is closely connected to the weather variables chosen as proxies (daily radiation sum and mean daily temperature), but the resulting averaging kernels have fundamentally different distributions (Figure 3.2). The weather-based proxies lack the bell-shape of the "true" (SUCROS 2-produced) kernel based on dry matter increment. This difference already suggests that plant samples represent the atmospheric signature for a period smaller than the entire growing season of the plant. During the peak growing season, the correlation with incoming solar radiation is highest (Pearson's coefficient $r = 0.60$ with 1 day lag) as we would expect from basic plant physiology. This correlation increases to $r = 0.90$ if we only analyze the period between mid-June to mid-July. Temperature does not correlate well with dry matter increment ($r = -0.09$ for peak period, $r = 0.12$ for June – July). This means that the variance of daily dry matter increment is generally not captured well by the weather proxies over the growing season.
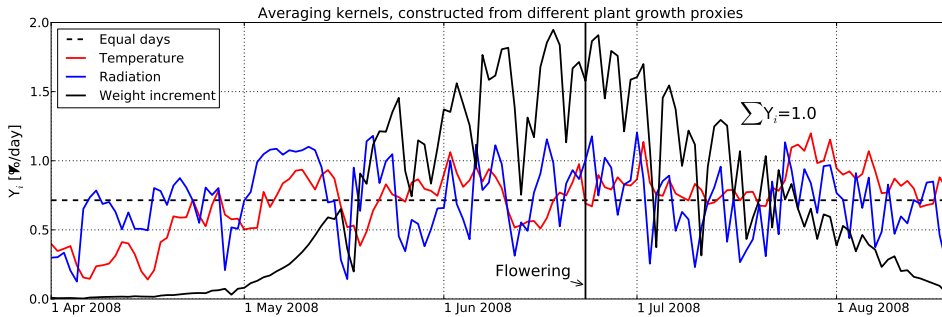
Figure 3.2: Examples of possible averaging kernels constructed for a given growing season for the location of Haarweg (Netherlands). Each solid line represents a different proxy for plant growth, as opposed to a kernel of equally weighted days (dashed). Both temperature and radiation are taken from station observations and are also used as input to the SUCROS 2 crop growth model that returns the daily dry weight increment (here shown for spring wheat) to which the other kernels are compared in the text.

When these kernels are combined with our simulated $^{14}CO_2$ time series, the resulting difference in the integrated $\Delta^{14}CO_2$ signature can be as small as 0.6‰ and as large as 3.1‰. Table 3.2 shows the full results. For example, signatures at the flowering stage range from 38.6‰ to 41.0‰ for spring wheat samples, and from 39.6‰ to 42.6‰ for maize, depending on the kernel applied. This range becomes larger when extending the sampling period to maturity.

3.3.2 Can we interpret samples from different plant organs?

An additional advantage of using a plant growth model like SUCROS 2 to construct the averaging kernel instead of a simpler growth proxy is the opportunity to account for plant phenology. An example is the partitioning of carbohydrates between different plant parts. Even in a model with very simple phenology such as SUCROS different plant organs grow in different periods during the growing season (Figure 3.3). The organs thus integrate the signal of the atmospheric $\Delta^{14}CO_2$ from different temporal windows, and this may result in internal signature gradients in the plant.

We simulate internal gradients as large as 3.5‰ if we include storage organs in our analysis. Typical values of 2-3‰ are found if we limit our analysis to the organs growing before the flowering stage (leaves, roots, and stems). The largest absolute gradients before flowering are found between the stems and the roots/leaves (see Table 3.2). This is true for both species, and results simply from the later development (the 90% period) of the stems by about 1 month. Leaves and roots both have their peak development at the same time and gradients

Table 3.2: *Final signatures at flowering and at the end of the growing period (maturity) -* $\Delta^{14}C_{res}$ *[‰][a].*

$\Delta^{14}C_{res}$[‰]	Spring wheat		Maize	
	flowering	maturity	flowering	maturity
Leaves	39.0	39.0	39.6	39.6
Roots	38.6	38.8	39.6	39.5
Stems	41.0	41.3	42.6	41.7
St. organs	-	40.6	-	38.1
Total plant	40.5	40.8	41.4	39.5
Flat-kernel	37.8	38.3	38.4	38.9
Radiation	37.6	38.0	38.4	38.4
Temperature	37.6	37.8	38.3	38.5

[a] We compare here averaging kernels for different plant parts and plant growth proxies, for spring wheat and maize. The kernels for the proxies are constructed using the same period in which the plant growth occurs.

therefore typically remain small (<0.5‰). We note, however, that the sampling of roots in the field is a very impractical approach. Leaves thereby remain the only practical organ to sample and interpret, though we note that for this example of growing season in our study, their signature is up to 1.8‰ different from the one accumulated in the whole plant, and also close to 1‰ different from the equal atmospheric average.

Finally, we calculated the sensitivity of these internal gradients towards the simulated atmospheric $\Delta^{14}C$ series by shifting the original time series 30 times by increasing intervals from 2 to 60 days. This resulted in the calculated uncertainty (1-σ) in Table 3.3. Although the absolute plant signature (not shown) depends on the temporal evolution of the atmospheric $\Delta^{14}C$ series used, the internal gradients were persistent and on average of measurable size for most compartments.

3.3.3 How does the averaging kernel affect gradients on the regional scale?

Local weather can be consistently different on a regional scale, creating variable crop growing patterns and timing. We investigated the effect of these differences on the $\Delta^{14}CO_2$ signature for plants across the Netherlands. For this purpose, we combined WRF-generated weather for each point on the model 4 km grid with the plant growth of the SUCROS 2 model, and applied the resulting dry matter increment averaging kernels to the simulated atmospheric $\Delta^{14}C$ for Lutjewad (Section 3.2.1). This simulation of the plant $\Delta^{14}C$ signature thus *excludes* any gradients of fossil fuel emissions within the domain. Instead, it shows the spatial gradients in the plant signature that result solely from the different plant growth rates, which in turn are driven by the spatial differences in the weather conditions. We show the results (Figure 3.4
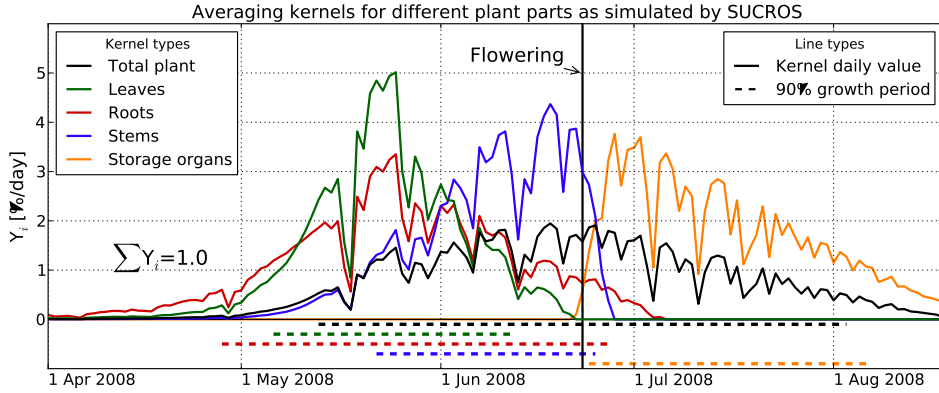
Figure 3.3: Averaging kernels constructed for different plant organs in comparison to the total plant kernel, all modeled with SUCROS 2 for spring wheat for the location of Haarweg. Plant part kernels are based on the daily dry weight increment and complemented with estimation of the according 90% growth periods (dashed lines).

and Figure 3.5) as a difference between the signature at flowering at each grid point and the location of Lutjewad, rather than as an absolute value.

Differences in plant growth rates resulted in spatial $\Delta^{14}C$ gradients of over 2.5‰ for a total plant sample, and from 1.7‰ to over 4‰ for separate plant organs for spring wheat (Figure 3.4). For maize, we simulated more than 3.5‰ spatial gradients in the total plant samples, and up to 4.0‰ for the separate plant organs (Figure 3.5). The difference in gradients when considering different organs depends on species-specific crop development rates and the atmospheric $\Delta^{14}CO_2$ evolution. As an example, predicted flowering dates within the Netherlands vary by more than ±6 days for spring wheat and more than ±8 days for maize, even with explicitly forced emergence (start of growing period) at the same date over the entire domain. Even with a unified $\Delta^{14}CO_2$ time series to record, the plants thus accumulate gradients that can exceed the usual measurement precision, and this gradient will likely be even larger if we also allow realistic (±30 days) differences in the sowing date of crops across the country.

We additionally evaluated the differences between the plant and atmospheric mean $\Delta^{14}C$ signature using Δ_{bg} only, the full daytime series and its smooth curve fit and residual components (all shown earlier in Figure 3.1). This allows us to quantify the contribution of each component of the $\Delta^{14}C$ time series to the total plant-atmosphere difference. Our calculations show that whether one applies a plant or a flat kernel to the seasonal background has very little impact on the signature (<0.4‰). Much larger differences arise from applying the kernels to the smooth curve (monthly variations) and to the residuals (daily variations). We calculate

Gradients in the simulated signature in spring wheat
Δ^{14}C [permil] as compared to Lutjewad location (the Netherlands 2008)
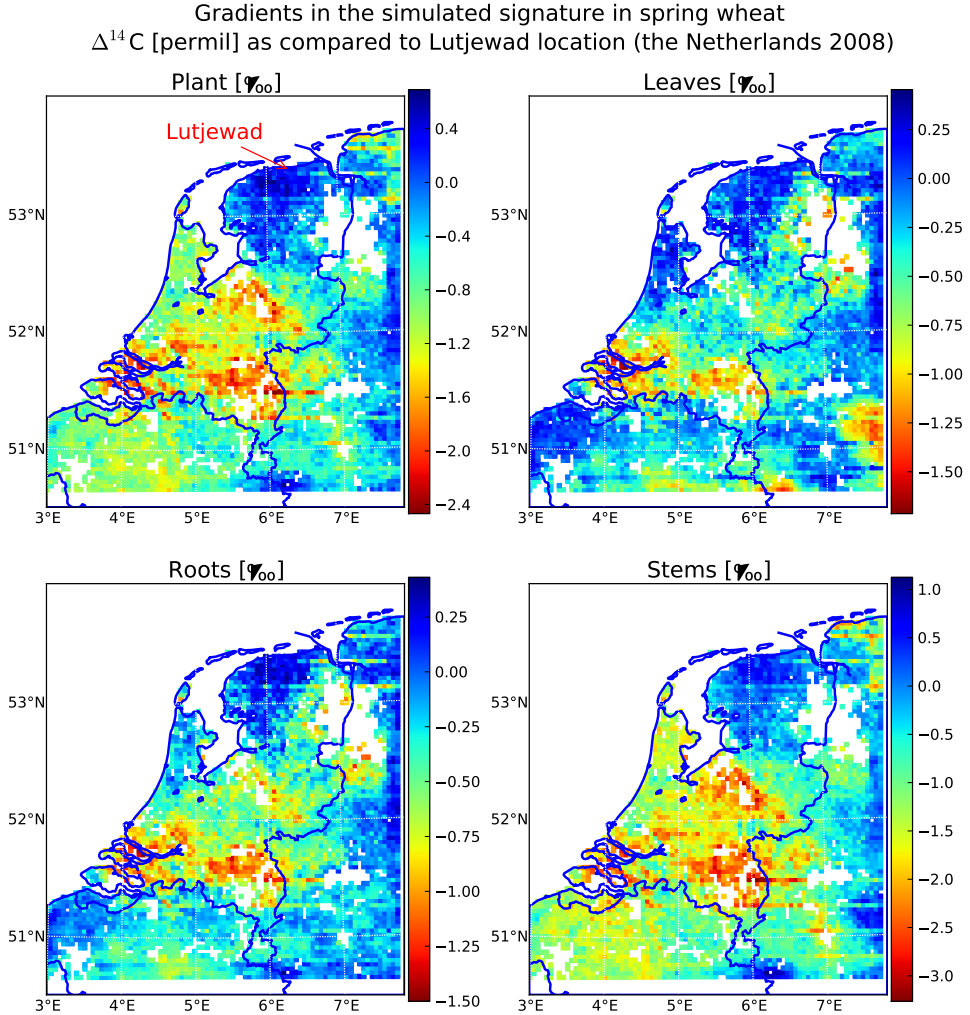
Figure 3.4: Spatial gradients of the simulated $\Delta^{14}C$ signature in spring wheat at flowering, constructed by subtracting the signature at each location from the one simulated at Lutjewad (red arrow). The gradients result only from different growth patterns induced by regional weather differences, as the temporal evolution of the atmospheric $\Delta^{14}C$ signature is unified over the entire domain. These gradients will superimpose on gradients from local fossil fuel emissions, resulting in biases when the fossil fuel addition is calculated back from observed plant samples if the plant growth differences are ignored. Each panel shows a different plant part sampled.

Gradients in the simulated signature of maize samples
in Δ^{14}C [‰] (as compared to Lutjewad location)
and growing period differences in the Netherlands 2008

Figure 3.5: Upper two panels are respective to Figure 3.4, but modeled for Maize. The lower panels additionally show differences in the flowering date occurrence and length of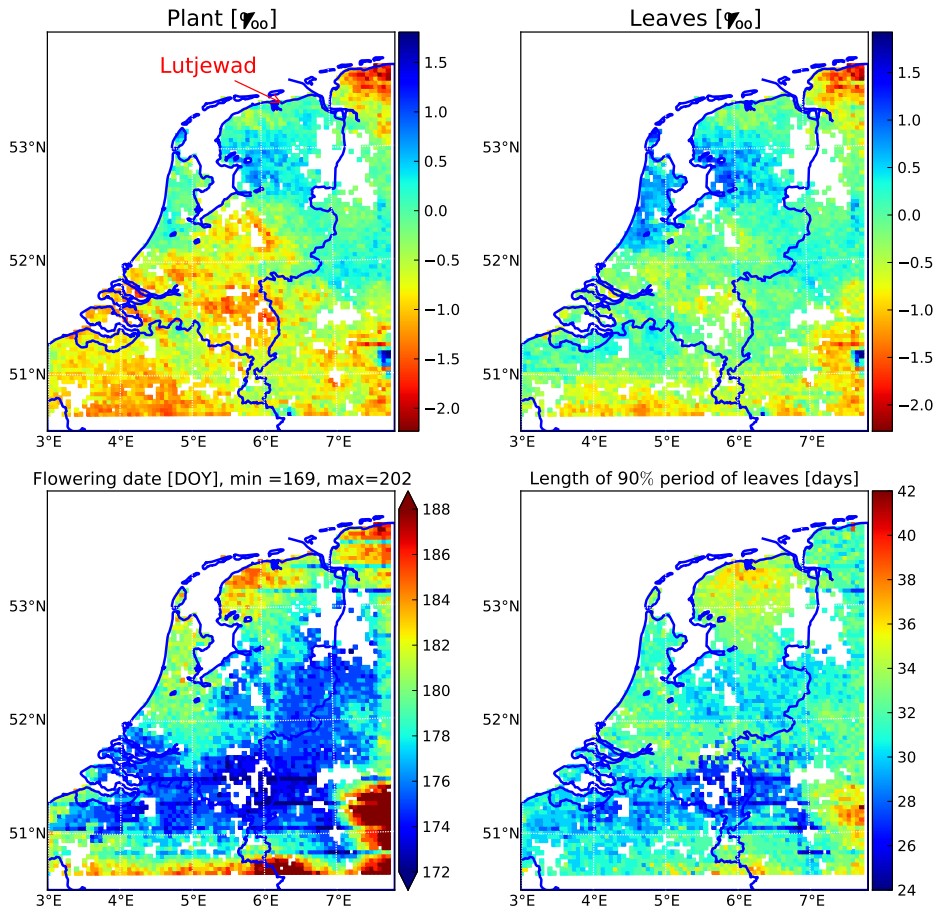 the period with 90% growth of leaves. Growing season differences are caused by differences in the regional weather patterns, that affect the crop development and growing pattern.

Table 3.3: Mean and standard deviation (σ) of the difference in $\Delta^{14}C$ signature in different plant compartments at flowering (upper half) and maturity (lower half) using 30 permutations of the 2008 atmospheric $\Delta^{14}C$ signature at Lutjewad[a].

Absolute difference in $\Delta^{14}C_{res}$ [‰]	Spring wheat		Maize	
	mean	σ	mean	σ
Leaves – Stems	3.0	1.5	2.1	1.2
Leaves – Roots	0.8	0.4	0.2	0.2
Roots – Stems	2.5	1.0	2.0	1.2
Leaves – St. organs	4.8	2.5	5.7	2.3
Roots – St. organs	3.9	2.1	5.7	2.4
Stems – St. organs	3.4	2.7	4.8	2.4

[a] The signature of storage organs is calculated by analogy to other plant organs, thus ignoring the effects of translocated stem dry mass.

that the monthly time scales dominate and typically lead to a signature that is ~2–3‰ higher in the plant samples than in the atmosphere. This strong effect is partly countered by the residual daily variations (mostly negative) which are more strongly expressed in plants than in the atmosphere. Together, this leads to a difference of about 1.7±0.5‰ when applying each kernel to the total time series. This suggests that both components of variation must be accounted for when interpreting plant sampled $\Delta^{14}CO_2$.

3.4 Discussion

We investigated the requirements on simulating averaging kernels to properly interpret a plant sampled $\Delta^{14}CO_2$ signature. We compared the very complex kernel (modeled plant growth using SUCROS 2) with very simple ones (observed weather variables) and a temporally flat kernel. Results for these kernels (Section 3.3.1) are generally comparable, but 1-2‰ different from the simulation of the signature of leaves with the complex growth model. Leaves are the plant parts previously used for analysis (Hsueh et al., 2007). Quantitatively, our study suggests that using a plant growth proxy that does not account for the day-to-day variations in plant growth comes at a price which varies from a possibly acceptable bias in $\Delta^{14}C$ (~0.5‰) to an absolutely unacceptable one (>3.0‰). We note that as the measurement precision of $\Delta^{14}CO_2$ increases, even the smaller bias might become unacceptable.

An alternative kernel that is between the simple and complex extremes mentioned above, is one constructed from the leaf area index (LAI). LAI is a result of plant growth and additionally has the attractive advantage of being available over large areas from remote sensing. A step further towards complexity stands gross primary production (GPP) modeled from LAI observations. For some plant species, this approach has proven to give reasonable results, for

instance in the case of annual grasses (Riley et al., 2008). We tried to investigate these prox-ies using monthly LAI data at $1°\text{x}1°$ spatial resolution (constructed from Global Inventory Modeling and Monitoring Study normalized difference vegetation index with 8 km/15 days resolution, source: K. Schaefer), MODerate resolution Imaging Spectroradiometer observed LAI with 1 km/8 days resolution (MOD15A2) and high-resolution (250m/1day) spatial maps of GPP for the Netherlands (Kooistra et al., 2009). However, satellite observations depend on the lack of cloud cover, which results in periods where data is not available or is aver-aged over time, and we found it nearly impossible to construct data-based proxies for a full growing season for more than a few locations. Additionally, the data obtained is spatially averaged over the area covered by a pixel and would average signals from different plants species and from plants at different development stages. This is a significant drawback be-cause neighboring crop fields can have up to a month difference in the sowing date even if they are from the same species. In the end, we did not include these mostly failed attempts with remotely sensed GPP and LAI in the paper. We did, however, construct one simulated LAI time series from the plant growth model to use but found it to perform poorly compared to the full growth model, with differences in the simulated total plant signature varying from 0.3‰ for wheat to 0.8–1.6 ‰ for maize.

One of the questions arising for the general application of the growth averaging kernel is if it can be replaced by fitted curve that resembles the parabolic shape of the kernel and avoids the complication of using a crop growth model. As visible from Fig 3.3, the kernels for different plant parts differ substantially in their amplitude, skewness, the timing of the maximum, even in the case shown where the shape of the kernel is not seriously modified by limited growth periods. To construct a curve for a kernel, we would need to know at least the period of the intensive growth, the time when the maximum occurs and the peak amplitude. These parameters would differ per plant species and growing conditions in different time periods or locations. We are unaware of a method that can obtain this information while avoiding the use of a crop growth model itself.

We evaluated the uncertainty in our plant $\Delta^{14}C$ signature results ($\Delta^{14}C_{res}$) introduced by the uncertainty in the model forcing (weather and initial conditions) data. Random errors of up to 25% in the weather variables did not produce significant change in our resulting signature. The biggest sensitivity found in our results (~1.0‰) was due to changes in the sequences of weather that follow each other over the entire growing season (synoptic vari-ability). Consequently, we advise to interpret plant samples using appropriate growing season weather and avoid using an average climate year.

Interestingly, differences in weather from location-to-location as presented in Section 3.3.3 have a much larger effect on $\Delta^{14}CO_2$ than the changes in local weather from day-to-day, mentioned above. The resulting "growth-gradients" in the $\Delta^{14}CO_2$ signature of plant samples will superimpose on the atmospheric gradients by regional fossil fuel emissions that

we are ultimately planning to interpret from the plants. Using again Eq. 3.1, the gradients in $\Delta^{14}CO_2$ will be equivalent to CO_{2ff} gradients of close to 1.5 ppm. This bias is of considerable size when compared to, for instance, the average fossil fuel CO_2 fraction during daytime at the site of Cabauw (2–8 ppm) in the Netherlands (Tolk et al., 2009) or Heidelberg (10–12 ppm) in Germany (Levin and Rödenbeck, 2008) and is likely to be even larger when differences in sowing date (now excluded) are incorporated. Thus, the influence of local plant development rates as modified by local weather conditions during the growing season cannot be ignored when interpreting integrated samples.

The next most used tracer for fossil fuel emissions after $^{14}CO_2$ is carbon monoxide (CO). Gamnitzer et al. (2006) estimates the uncertainty when using this tracer to be within ±20-35% of the recalculated fossil fuel CO_2. For the summertime period when plant samples are most easily available though, the uncertainties in the CO method are even higher, as the photochemical production, biomass burning, and OH consumption of CO, are most significant in summer (Turnbull et al., 2006). This suggests that plant $\Delta^{14}CO_2$ samples can be a useful addition to other tracer samples obtained to constrain regional fossil fuel CO_2 emission estimates.

Various studies used plant-sampled $\Delta^{14}C$ from different plant parts and different species of grasses, cereal crops, forbs, or grapevines (Burchuladze et al., 1989; Shibata et al., 2005; Hsueh et al., 2007; Palstra et al., 2008; Riley et al., 2008). There are difficulties comparing the data between different studies, when the period and rate of carbon uptake is unknown or not taken into account. The use of a crop growth model allows for comparison when interpreting $\Delta^{14}C$ results from samples from different locations, sampling approaches, and materials or different time periods. In studies that use various types of samples, crop modeling should be a requirement to separate the effects of the atmospheric $\Delta^{14}CO_2$ signal and the different crop development and growing period.

In our work, we focused on results obtained from plant samples at flowering and not as much for samples of storage organs at maturity. In cereal crops, such as spring wheat and maize, the storage organs (seeds) are different from the other organs in three important ways: (1) they grow exclusively after flowering, when (in cereal species) the other organs stop growing, (2) they grow partly from biomass that is reallocated from the other organs, rather than purely from newly assimilated carbon, and (3) the period after flowering shows much larger influence of weather variations (water limitations) on plant growth. Together, this makes $\Delta^{14}CO_2$ in storage organs difficult to relate to atmospheric $\Delta^{14}CO_2$. For instance, reallocation of biomass from stems to storage organs in our study accounted on average for 15% of the final biomass in that organ pool, introducing a $\Delta^{14}CO_2$ signature from an earlier growing stage. Our calculation of the resulting signature (Eq. 3.3) does not account for this influence, and the uncertainty of our results for $\Delta^{14}C_{res}$ of storage organs is much higher than for other plant organs. In other plant species, the biomass dynamics could be quite different.

For example, in grapevines, the reallocation of biomass happens before flowering, and the fruits grow almost exclusively from freshly assimilated CO_2. Such differences should be carefully considered when choosing the plant species and material that will be sampled.

As a result of our work, we advise different plant parts to be obtained and analyzed separately, rather than a mixed sample. This is advantageous when their growth pattern is modeled, and it allows to correctly interpret samples from different plant parts, rather than assuming that they have the same signature as the total plant, as has been done up to now. Local farmers choose their sowing dates depending on local weather and other practical reasons. This results in up to a month differences in the development in neighboring fields of same species with different owners. This further implies that in order to be able to interpret plant observations, we should model the plant growth at the sampling location with the specific initial conditions.

The next step in our research is to combine our crop growth model with simulations of the regional fossil fuel emissions and atmospheric transport. Once the regional weather is simulated, we can model the crop growth for locations where samples were previously obtained, and compare the predicted signature and gradients with observed ones. Our method might be advantageous for deciding which samples we want to analyze, as we will be able to predict the magnitude of expected gradients between plant samples.

3.5 Conclusions

In our study, we constructed averaging kernels that allow us to calculate the $\Delta^{14}CO_2$ signature of a plant by making a weighted average of the daily contribution from the atmospheric $^{14}CO_2$ mixing ratios. This kernel needs to be known with sufficient accuracy in order to interpret the local fossil fuel signals recorded in plants growing over a full season. By explicitly excluding these local fossil fuel influences in our simulations, we were able to isolate the effect of using different averaging kernels constructed from proxies of plant growth and from simulated crop growth. Our main conclusions are the following:

1. The influence of the day-to-day plant growth on recorded $\Delta^{14}CO_2$ signals is not negligible and should be taken into account when interpreting plant sampled $\Delta^{14}CO_2$ values.

2. In addition to a reliable crop growth model, the construction of an averaging kernel requires the local weather information for the correct growing season and in case of crops, information about the timing of particular phenology events, such as the sowing, emergence and flowering.

3. For some plant species, in our case for maize and wheat samples at flowering, sampling after a particular phenology stage can be beneficial as it clearly defines the end of the

growing period for the organs we wish to sample. The interpretation of storage organs (fruits, seeds) in cereal plants holds much higher uncertainty than of other plant parts as they are very sensitive to water limitations and grow using reallocated carbon. As growth dynamics may differ substantially between plant species, it is important that the choice of which plant part to sample from a particular species should be made early in the planning stage of plant sampling campaigns.

4. The use of plant growth proxies that do not account for the plant development, like temperature or radiation, introduces an uncertainty that can result in measurable (2‰) bias between predicted and observed plant $\Delta^{14}CO_2$ signature.

5. The use of an appropriate plant growth averaging kernel helps to avoid regional plant growth variations being mistakenly interpreted as local fossil fuel emissions when using integrated plant samples to learn about fossil emissions. The biases in the calculation of the fossil fuel CO_2 fraction are up to 2 ppm of fossil fuel CO_2 signal ($\sim$10–20% of the total expected signal) when using samples from different plant parts and up to 1–1.5 ppm when not accounting for the effect of the regional weather differences on growth period and growth rate.

4

Simulating the integrated summertime $\Delta^{14}CO_2$ signature from anthropogenic emissions over Western Europe

Radiocarbon dioxide ($^{14}CO_2$, reported in $\Delta^{14}CO_2$) can be used to determine the fossil fuel CO_2 addition to the atmosphere, since fossil fuel CO_2 no longer contains any ^{14}C. After the release of CO_2 at the source, atmospheric transport causes dilution of strong local signals into the background and detectable gradients of $\Delta^{14}CO_2$ only remain in areas with high fossil fuel emissions. This fossil fuel signal can moreover be partially masked by the enriching effect that anthropogenic emissions of $^{14}CO_2$ from the nuclear industry have on the atmospheric $\Delta^{14}CO_2$ signature. In this paper, we investigate the regional gradients in $^{14}CO_2$ over the European continent and quantify the effect of the emissions from nuclear industry. We simulate the emissions and transport of fossil fuel CO_2 and nuclear $^{14}CO_2$ for Western Europe using the Weather Research and Forecast model (WRF-Chem) for a period covering 6 summer months in 2008. We evaluate the expected CO_2 gradients and the resulting $\Delta^{14}CO_2$ in simulated integrated air samples over this period, as well as in simulated plant samples.

We find that the average gradients of fossil fuel CO_2 in the lower 1200 m of the atmosphere are close to 15 ppm at a 12 km × 12 km horizontal resolution. The nuclear influence on $\Delta^{14}CO_2$ signatures varies considerably over the domain and for large areas in France and the UK it can range from 20 to more than 500 % of the influence of fossil fuel emissions. Our simulations suggest that the resulting gradients in $\Delta^{14}CO_2$ are well

captured in plant samples, but due to their time-varying uptake of CO_2, their signature can be different with over 3‰ from the atmospheric samples in some regions. We conclude that the framework presented will be well-suited for the interpretation of actual air and plant $^{14}CO_2$ samples.

4.1 Introduction

The magnitude of anthropogenic fossil fuel CO_2 emissions is relatively well known on the global scale (Raupach et al., 2007; Friedlingstein et al., 2010) as bottom-up inventories constrain the sum of all emissions to within 6–10 % uncertainty (Marland and Rotty, 1984; Turnbull et al., 2006; Marland, 2008). But it is widely acknowledged that confidence in the estimated magnitude of these emissions reduces quickly when we consider the regional and national scale (Olivier and Peters, 2002; Gurney et al., 2009; Francey et al., 2013). At length scales of 150 km and smaller, bottom-up emission maps can differ up to 50 % (Ciais et al., 2010). This is partly a disaggregation problem that arises when nationally reported data on economic activity, energy use, and fuel trade statistics must be attributed to smaller geographic areas and more diverse processes. At the same time, there is a challenge to aggregate available bottom-up information on the level of individual roads, or power plants, or industrial complexes to a larger scale consistently. In between these two lies an important opportunity for atmospheric monitoring, as it can independently verify the reported emission magnitudes at the intermediate scales, uniquely constrained by the integrating capacity of atmospheric transport.

Several atmospheric monitoring strategies for fossil fuel emissions have been applied in recent years. Most of these use spatio-temporal variations in CO_2 mole fractions (Koffi et al., 2012), often augmented with various other energy related gases such as CO (Levin and Karstens, 2007), NO_x (Lopez et al., 2013), or SF_6 (Turnbull et al., 2006). An advantage of these other gases is that they can be measured continuously and relatively cheaply with commercially available analyzers, of which many have already been deployed. However, one of the disadvantages lies in attribution, as each process induces its own typical ratio of these gases to the atmosphere. An example is the much higher CO/CO_2 ratio produced by traffic emissions than by power plants. Another disadvantage is that not all of these trace gases are direct proxies for fossil fuel CO_2 release as some have totally independent, but co-located sources with the sources of anthropogenic CO_2 emissions. This is in large contrast with the one tracer that is generally considered the "gold standard" for fossil fuel related CO_2 detection: radiocarbon dioxide or $^{14}CO_2$ (Kuc et al., 2003; Levin et al., 2003, 2008; Levin and Karstens, 2007; Levin and Rödenbeck, 2008; Turnbull et al., 2006; Djuricin et al., 2010; Miller et al., 2012), reported usually as $\Delta^{14}CO_2$ (Stuiver and Polach, 1977; Mook and van der Plicht, 1999).

Radiocarbon derives its strength for fossil fuel monitoring from the absence of any ^{14}C in carbon that is much older than the typical half-life time of the radiocarbon -5700 ± 30 years (Roberts and Southon, 2007). This typically applies only to carbon in fossil reservoirs, as other carbon reservoirs are continuously supplied with fresh ^{14}C from exchange with the atmosphere where ^{14}CO$_2$ is produced in the stratosphere and upper troposphere (Libby, 1946; Anderson et al., 1947). In the natural carbon balance this ^{14}C would cycle through the atmospheric, biospheric, and oceanic reservoir until it decays. But very large anthropogenic disturbances on this natural cycle come specifically from (a) large scale burning of very old and ^{14}C depleted carbon from fossil reservoirs, the "Suess effect" (Suess, 1955; Levin et al., 1980), and (b) production of highly enriched ^{14}C in CO$_2$ such as from nuclear bomb tests (Nydal, 1968), or some methods of nuclear power production (McCartney et al., 1988a,b). Samples of ^{14}CO$_2$ taken from the atmosphere, but also from the oceans and biosphere that exchange with it, consistently show their dominant influence on the ^{14}CO$_2$ budget of the past decades (e.g.: Levin et al., 1989, 2010; Meijer et al., 1996; Nydal and Gislefoss, 1996; Levin and Hesshaimer, 2000; Randerson et al., 2002; Naegler and Levin, 2006; Graven et al., 2012a,b).

Monitoring of atmospheric ^{14}CO$_2$ is done through several methods. One commonly applied approach is by absorption of gaseous CO$_2$ into a sodium hydroxide solution from which the carbon content is extracted for ^{14}C/C analysis either by radioactive decay counters, or converted into a graphite target for analysis by accelerator mass spectrometry. The air flowing into the solution typically integrates the absorbed CO$_2$ with sampling time of days, weeks, or even longer periods. While there is a new technique, which uses integrated flask sampling (Turnbull et al., 2012), the other method generally used is to collect an air sample in a flask, which is filled within less than a minute and thus representative of a much smaller atmospheric time-window. Compared to these, at the other end of the time spectrum is the use of plants to sample ^{14}C/C ratios in the atmosphere through their photosynthetic fixation of atmospheric CO$_2$. Depending on the species these integrate over sampling windows of a full growing season (annual crops, fruits – Shibata et al., 2005; Hsueh et al., 2007; Palstra et al., 2008; Riley et al., 2008; Wang et al., 2013) or longer (trees, tree-rings – Suess, 1955; Stuiver and Quay, 1981; Wang et al., 2012).

An effective monitoring strategy for fossil fuel emissions is likely to take advantage of all methods available to collect ^{14}C samples, and combine these with high resolution monitoring of related gases (e.g. CO, SF$_6$). Levin and Karstens (2007), van der Laan et al. (2010) and Vogel et al. (2010) already demonstrated the viability of a monitoring method in which observed CO/CO$_2$ ratios are periodically calibrated with ^{14}CO$_2$ to estimate fossil fuel emissions at high temporal resolutions. More recently, this strategy was also employed by Lopez et al. (2013), where additionally the CO$_2$/NO$_x$ ratios were used to estimate fossil fuel derived CO$_2$ from continuous CO and NO$_x$ observations in Paris. Turnbull et al. (2011a) showed for

the city of Sacramento, that using a combination of $\Delta^{14}CO_2$ and CO observations can reveal structural detail in CO_2 from fossil fuel and biospheric sources that cannot be obtained by CO_2 measurements alone. Van der Laan et al. (2010) and recently Vogel et al. (2013b) showed that the agreement between modeled fossil fuel CO_2 estimates and observations of ^{14}C-corrected CO can be further improved by including ^{222}Rn as a tracer for the vertical mixing. Finally, Hsueh et al. (2007) and Riley et al. (2008) used ^{14}C/C ratios in corn leaves and C3 grasses to reveal fossil fuel emission patterns on city, state, and national scales. Given so many different methods to use ^{14}C in monitoring strategies, its increasing accuracy, reduction in required sample size, and decreasing costs, it is likely that this tracer will play a more important role in the future of the carbon observing network.

The quantitative estimation of fossil fuel emissions from all of the ^{14}C-based monitoring strategies above requires different methods and emphasizes different terms in the $^{14}CO_2$ budget. For example, interpretation of ^{14}C in air samples from aircraft requires detailed dispersion modeling of surface emissions into a highly dynamic atmosphere, while interpretation of monthly integrated air samples from tall towers requires the inclusion of the re-emergence of old ^{14}C signals after longer turn-over in the oceans and biosphere. In a recent publication (Bozhinova et al., 2013), we showed that the interpretation of growing season integrated plant samples additionally requires simulation of location and weather dependent photosynthetic uptake and plant development patterns. A successful ^{14}C monitoring strategy will thus depend strongly on our ability to capture these diverse processes on diverse scales.

In this work, we present a newly-built framework designed to interpret $^{14}CO_2$ from different types of samples and from different monitoring strategies. The framework includes atmospheric transport of surface emissions of total CO_2 and $^{14}CO_2$ on hourly scales on a model grid of a few kilometers, but integrates signals up to seasonal time scales and even down into the leaves of growing crops (maize and wheat). Both regional transport and plant growth are based on meteorological drivers that are kept consistent with large-scale weather reanalyses. In addition to fossil fuel signals in the atmosphere and in plants, we simulate the spread of nuclear derived ^{14}C release from major reprocessing plants and from operational nuclear power production plants across Europe based on work of Graven and Gruber (2011). We applied our framework to the European domain for the summer of 2008. After explaining the components of the framework (Sect. 2) we will demonstrate its application (Sect. 3.1), assess the fossil and nuclear derived ^{14}C gradients across Europe (Sect. 3.2), and simulate the signal that will be recorded into annual crops growing across the domain (Sect. 3.3). We will evaluate its potential benefits compared to simpler but less realistic fossil fuel estimation methods from integrated samples alone (Sect. 3.4). We will conclude with a discussion (Sect. 4) of the application of this framework to actual measurements and recommendations for future studies.

4.2 Methods

4.2.1 The regional atmospheric CO_2 and $\Delta^{14}CO_2$ budget

The regional CO_2 mole fractions and $\Delta^{14}CO_2$ signature of the atmosphere observed at a particular location are described in Eqs. (4.1) and (4.2), following the methodology used by Levin et al. (2003), Turnbull et al. (2006), Hsueh et al. (2007), Palstra et al. (2008) and described thoroughly in Turnbull et al. (2009b). Here the Δ_x and CO_{2x} (or $^{14}CO_{2x}$) indicate the $\Delta^{14}CO_2$ signature of CO_2 (or $^{14}CO_2$) mole fractions of particular origin, expressed in the index as follows: obs – observed at location, bg – background, ff – fossil fuels, p – photosynthetic uptake, r – ecosystem respiration, o – ocean, n – nuclear and s – stratospheric.

$$CO_{2obs} = CO_{2bg} + CO_{2ff} + CO_{2p} + CO_{2r} + CO_{2o} + CO_{2s} \tag{4.1}$$

$$\Delta_{obs}CO_{2obs} = \Delta_{bg}CO_{2bg} + \Delta_{ff}CO_{2ff} + \Delta_{p}CO_{2p}$$
$$+ \Delta_{r}CO_{2r} + \Delta_{o}CO_{2o} + \Delta_{n}{}^{14}CO_{2n} + \Delta_{s}CO_{2s} \tag{4.2}$$

Several of the terms in both equations can be omitted or transformed in our study, as described next.

We set $\Delta_p = \Delta_{bg}$ similar to the approach in Turnbull et al. (2006) as the calculation of $\Delta^{14}CO_2$ accounts for changes in the signature of the photosynthesized CO_2 flux due to fractionation. The atmosphere-ocean exchange in the northern Atlantic makes the region generally a sink of carbon (Watson et al., 2009), but we assume that its transport to our domain is uniform and captured by the inflow of background air and thus also carries the signature Δ_{bg}. For the ecosystem respiration and ocean exchange the terms Δ_r and Δ_o can be also written as $\Delta_{bg} + \Delta_{bio}^{dis}$ and $\Delta_{bg} + \Delta_{ocean}^{dis}$, where the disequilibrium terms (Δ^{dis}) describe the difference between the signature of the carbon in the particular reservoir and the current atmospheric background. These differences arise from the past enrichment of the atmosphere with $^{14}CO_2$ from the atmospheric nuclear bomb tests since the 1960s. In the following decades this enrichment was incorporated into the different carbon reservoirs (Levin and Kromer, 1997; Levin and Hesshaimer, 2000) and currently these terms are of dominant importance only in particular regions of the globe. For our domain both terms are considered of much smaller influence than the dominant effect of the fossil fuels and are consequently omitted (Levin and Karstens, 2007; Hsueh et al., 2007; Palstra et al., 2008; Turnbull et al., 2009b; Naegler and Levin, 2009a,b; Levin et al., 2010). Because we currently do not correct for this, the omission of the biospheric disequilibrium in the region and period of our study will likely result in a small bias in our results, as our atmosphere will be less enriched during the period of peak biospheric activity. For the northern hemisphere Turnbull et al. (2006) estimates an

overestimation of fossil fuel CO_2 by 0.2–0.5 ppm or up to 1.3 ‰ enrichment in $\Delta^{14}CO_2$ due to this lack of disequilibrium influence, while Levin et al. (2008) evaluates this influence on the observational sites in Germany to be within 0.2 ppm or about 0.5 ‰ enrichment. The intrusion of $^{14}CO_2$-enriched stratospheric air can be of importance for observations in the upper troposphere or higher, however in our case this term can be considered as part of the background, as the stratospheric $^{14}CO_2$ is already well mixed by the time it reaches the lower troposphere.

Most studies ignore the effects of anthropogenic nuclear production of $^{14}CO_2$ on the atmospheric $\Delta^{14}CO_2$ since on the global scale this production averages to the smallest contribution, compared to the other terms (Turnbull et al., 2009a) and few try to quantify and correct for it in observations taken nearby nuclear power plants (Levin et al., 2003). However, Graven and Gruber (2011) showed that the regional influence of a dense nuclear power plant network cannot be ignored. They estimated the potential bias in the recalculation of fossil fuel CO_2 due to nuclear power plant production is on average between 0.5 and 1 ppm for Europe, but the horizontal resolution of their transport model ($1.8° \times 1.8°$) limits the analysis for the regions close to the sources. We note that two of the three existing worldwide spent fuel reprocessing plants are located in Western Europe (SFRP, in La Hague, France and Sellafield, United Kingdom), which generally have higher than average emissions of $^{14}CO_2$ (McCartney et al., 1988a). Particularly the site of La Hague is estimated to be the largest current point-source of $^{14}CO_2$ emissions in the world, in recent years accounting for more than 10 % of the global budget of nuclear produced $^{14}CO_2$ (Graven and Gruber, 2011). The magnitude of this source and its spatial location close to the major fossil fuel emitters in Europe pose a challenge in estimating the uncertainty with which the method of recalculating fossil fuel CO_2 can be applied in the region.

All these considerations allow us to simplify Eqs. (4.1) and (4.2) to Eqs. (4.3) and (4.4).

$$CO_{2obs} = CO_{2bg} + CO_{2ff} + CO_{2p} + CO_{2r} \qquad (4.3)$$

$$\Delta_{obs}CO_{2obs} = \Delta_{bg}(CO_{2bg} + CO_{2p} + CO_{2r}) + \Delta_{ff}CO_{2ff} + \Delta_n^{14}CO_{2n} \qquad (4.4)$$

The instantaneous $\Delta^{14}CO_2$ signature of the atmosphere is calculated using Eq. (4.4), using the specific signatures for various sources of CO_2 (various Δ terms) as listed below:

1. Fossil fuels are entirely devoid of $^{14}CO_2$ and their $\Delta_{ff} = -1000$ ‰.

2. The nuclear emissions are of pure $^{14}CO_2$ and in this formulation Δ_n is the $\Delta^{14}CO_2$ signature that a pure $^{14}CO_2$ sample would have. We calculate it using the activity of

pure $^{14}CO_2$ sample in the formulation of $\Delta^{14}CO_2$ as follows:

$$A_s = \lambda \cdot N_a / m_{^{14}C}, \tag{4.5}$$

where $N_a = 6.022 \times 10^{23}$ mol^{-1} is the Avogadro constant, $\lambda = 3.8534 \times 10^{-12}$ Bq is the decay rate of ^{14}C and $m_{^{14}C} = 14.0$ g mol^{-1} is the molar mass of the isotope. In a sample of a pure $^{14}CO_2$ there is no fractionation and the calculation of $\Delta^{14}CO_2$ (Stuiver and Polach, 1977; Mook and van der Plicht, 1999) can be simplified to the ratio between the activity of the sample and activity of the referenced standard $A_{ABS} = 0.226$ Bq g C^{-1} (Mook and van der Plicht, 1999):

$$\Delta_n = A_s / A_{ABS} \cdot 1000 \, [‰] \tag{4.6}$$

The resulting $\Delta_n \approx 0.7 \times 10^{15} \, [‰]$ is much higher than any of the other Δ signatures, but this is balanced by the concentrations of the $^{14}CO_2$, which are only a very small fraction ($\sim 10^{-12}$) of the observed CO_2 concentrations.

3. Finally, we use Δ_{bg} from monthly observed $\Delta^{14}CO_2$ at the high alpine station Jungfraujoch (3580 m a.s.l., Switzerland) (Levin et al., 2010), which is considered representative for European $\Delta^{14}CO_2$ background. These are shown in red on Fig. 4.3a.

We note that the choice of background can be crucial for the estimation of Δ_{obs} and consequently for the recalculation of CO_{2ff}. Local influences captured in the background might modify the seasonality of the derived Δ_{obs} and result in biases when applied to observations from other locations. These influences include local fossil fuel or nuclear signals, biospheric enrichment or modified vertical mixing during parts of the year (Turnbull et al., 2009b).

The transport and resulting spatiotemporal gradients in total CO_2 and $^{14}CO_2$ over Europe are simulated with WRF-CHEM model, described next.

4.2.2 WRF-CHEM

For our simulation with WRF-Chem (version 3.2.1) (Skamarock et al., 2008) we use meteorological fields from the National Centers for Environmental Prediction Final (FNL) Operational Global Analyses (NCEP) at $1° \times 1°$ for lateral meteorological boundary conditions, which are updated every 6 h. We model the atmospheric transport and weather for the period between April and September 2008 including. We use three domains with horizontal resolution of 36, 12 and 4 km and, respectively, 60×62, 109×100 and 91×109 grid points, centered over Western Europe and the Netherlands, as shown in Fig. 4.1. Our vertical resolution includes 27 pressure levels, 18 of which are in the lower 2 km of the troposphere, and the time step used is 180 s in the outer domain. Important physics schemes used are the
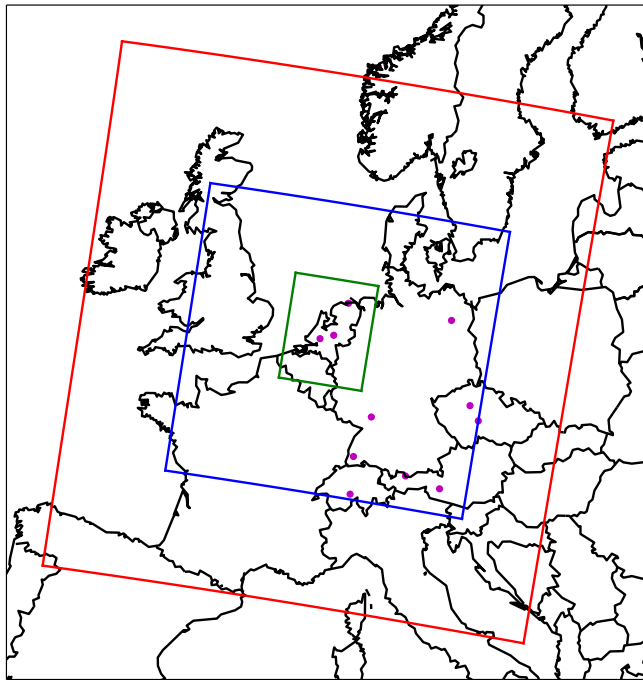
Figure 4.1: The location of modeled domains. The respective horizontal resolutions are according to the color of the domain boundaries: red – 36 km×36 km; blue – 12 km×12 km; green – 4 km × 4 km. The scatter markers indicate the locations of various observational sites used in this study.

Mellor-Yamada Nakanishi and Niino (MYNN2.5) boundary layer scheme (Nakanishi and Niino, 2006), the Rapid Radiation Transfer Model (RRTM) as our longwave radiation scheme (Mlawer et al., 1997), and the Dudhia shortwave radiation scheme (Dudhia, 1989). We use the Unified Noah Land-Surface Model (Ek et al., 2003) as our surface physics scheme and additionally use time-varying surface conditions, which we update every 6 h.

We use separate passive tracers for the different CO_2 terms in Eq. (4.4). We prescribe our initial and lateral boundary conditions for the background CO_2, while the biospheric uptake, respiration, fossil fuel CO_2 and nuclear $^{14}CO_2$ are implemented with surface fluxes only, which are prescribed and provided to the model every hour. Once CO_2 leaves our outer domain it will not re-enter it again. This setup reflects our interest in the recent influence of the biosphere and anthropogenic emissions. For this reason we will avoid using direct results from the outer domain, and instead use only the nested domains, where boundary conditions for all tracers are provided through their respective parent domain.

The background (CO_{2bg}) initial and boundary conditions are implemented using 3-D mole

fraction output from CarbonTracker (Peters et al., 2010) for 2008 at $1° \times 1°$ resolution and interpolated vertically from 34 to 27 levels using the pressure fields. The CO_2 lateral boundary conditions are added to the standard meteorological boundary conditions and also updated every 6 h.

Our biospheric fluxes (CO_{2r} and CO_{2p}) are generated using the SiBCASA model (Schaefer et al., 2008; van der Velde et al., 2014a), which used meteorological fields from the European Centre for Medium-Range Weather Forecasts (ECMWF). It provides us with monthly averaged gross photosynthetic production (GPP) and terrestrial ecosystem respiration (TER) at $1° \times 1°$ resolution. Due to the coarse resolution of the SiBCASA model, we find land-use categories in the higher resolution map of WRF that are not in the natural land-use map of SiBCASA. To address this issue, we ran 9 simulations with SiBCASA prescribing a single vegetation category, alternating through all the vegetation categories to produce biospheric fluxes for the different land-use categories within the resolution of WRF. For temporal interpolation of the monthly fluxes, we scale the GPP and TER with the instantaneous WRF meteorological variables (temperature at 2 m and shortwave solar radiation) following the method described in Olsen and Randerson (2004).

Anthropogenic (fossil fuel) CO_2 emissions (CO_{2ff}) are from the Institute for Energy Economics and the Rational Use of Energy (IER, Stuttgart, Pregger et al., 2007) at a horizontal resolution of 5 (geographical) minutes over Europe in the form of annual emissions at the location and temporal profiles to add variability during different months, weekdays and hours during the day. These are then aggregated to every WRF domain horizontal resolution and updated every hour for the duration of our simulation. The emissions are introduced only at the lowest (surface) level of the model.

Anthropogenic (nuclear) $^{14}CO_2$ emissions ($^{14}CO_{2n}$) are obtained by applying the method described in Graven and Gruber (2011) for the year of 2008. We used information from the International Atomic Energy Agency Power Reactor Information System (IAEA PRIS, available online at `http://www.iaea.org/pris`) for the energy production of the nuclear reactors in our domain and reported $^{14}CO_2$ discharges for the spent fuel reprocessing sites (van der Stricht and Janssens, 2010). The data is available only on annual scale and once converted from energy production to emissions of $^{14}CO_2$, these are scaled down to hourly emissions, assuming continuous and constant emission during the year. This is likely true when the nuclear reactors are operating, however, in reality regular maintenance and temporary shutdowns of individual reactors would result in periods of weeks and sometimes months of lower energy production and subsequently lower $^{14}CO_2$ discharge. We will further comment on these assumptions in our Discussion (Sect. 4).

4.2.3 Integrated $\Delta^{14}CO_2$ air and plant samples

Integrated $\Delta^{14}CO_2$ samples ($\Delta_{\text{absorption}}$), where the sampling rate is usually constant (e.g. in various CO_2 absorption setups), are represented with the concentration-weighed time-average $\Delta^{14}CO_2$ signature for the period and height of sampling, as seen in Eq. (4.7). When actual sampling is restricted to specific wind conditions or times-of-day, we include this in our model sampling scheme as well.

$$\Delta_{\text{absorption}} = \sum_t \Delta_{\text{obs}}^t \frac{CO_{2\text{obs}}^t}{\sum_t CO_{2\text{obs}}^t} \tag{4.7}$$
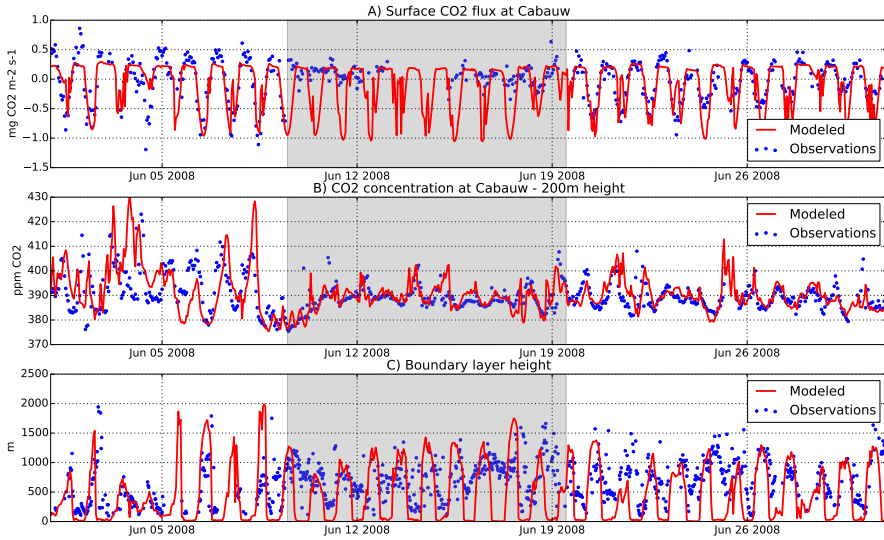
Figure 4.2: Comparison between modeled and observed CO_2 fluxes, concentrations and boundary layer height for the location of Cabauw for one month in the simulated season. Performance is usually better on clear days as compared to cloudy ones, as indicated in the graph with the gray background.

Plant samples (Δ_{plant}) integrate the atmospheric $\Delta^{14}CO_2$ signature with CO_2 assimilation rate which varies depending on various meteorological and phenological factors. Photosynthetic uptake and the allocation of the assimilated CO_2 in the different plant parts strongly depend on the weather conditions and plant development. To simulate such samples we use WRF meteorological fields in the crop growth model SUCROS2 (van Laar et al., 1997) and

use the modeled daily growth increment as a weighting function (averaging kernel) on the daytime atmospheric $\Delta^{14}CO_2$ signatures (Bozhinova et al., 2013). For each location we use the same sowing date and the model simulates the crop development until it reaches flowering, when we calculate Δ_{plant}. More explicitly these integrated sample signatures are calculated as follows:

$$\Delta_{plant} = \sum_t \Delta_{obs}^t \frac{X_t}{\sum_t X_t},$$

(4.8)

where X_t is the growth increment at time t, which in the case of SUCROS2 simulation is the dry matter weight increment at day t.

4.3 Results

4.3.1 Model evaluation – how realistic are our CO_2 and $\Delta^{14}CO_2$ simulations?

The meteorological conditions for 2008 that were simulated by WRF and used for the plant growth simulation in SUCROS2 were previously assessed in Bozhinova et al. (2013). Here we assess the model performance compared to observed CO_2 fluxes, CO_2 mole fractions, and boundary layer heights. Figure 4.2 shows this comparison at the observational tower of Cabauw, the Netherlands (data available at http://www.cesar-observatory.nl). The simulated net CO_2 flux (NEE) compares well to observations with a root-mean squared deviation (RMSD) of $0.26 \text{ mg} CO_2 \text{ m}^{-1} \text{ s}^{-1}$ and correlation coefficient (r) for the entire period of 0.70, which is even higher in clear days. Overestimates of NEE occur during cloudy conditions, which are notoriously difficult to represent in many mesoscale models. The CO_2 mole fractions compare well to observations (Vermeulen et al., 2011) and overall model performance is similar to other studies for the region (Tolk et al., 2009; Meesters et al., 2012). Similar to Steeneveld et al. (2008), Tolk et al. (2009), Ahmadov et al. (2009) the night-time stable boundary layer poses a challenge to the model. Note that the skill at modeling the boundary layer height can be of a particular importance for the correct simulation of the CO_2 budget, as it controls the diurnal evolution of the CO_2 mole fractions (Vilà-Guerau de Arellano et al., 2004; Pino et al., 2012). Thus, we have included this comparison in the last panel of Fig. 4.2. More detailed statistics for this and other stations and observations are listed in Table 4.1. We show the mean difference between the predicted and observed time series, with the according RMSD, and calculated correlation coefficient and coefficient of determination (Willmott, 1982) for each location. While in Table 4.1 we show the statistics for the daily time-series, we also evaluated their hourly and daytime-only counterparts and the differences

between each. Overall, our comparison shows that although the model overestimates the night-time CO_2 concentrations, it captures the observed daytime CO_2 mole fractions features and their variability on scales of hours to days satisfactorily over the full period simulated for Cabauw.
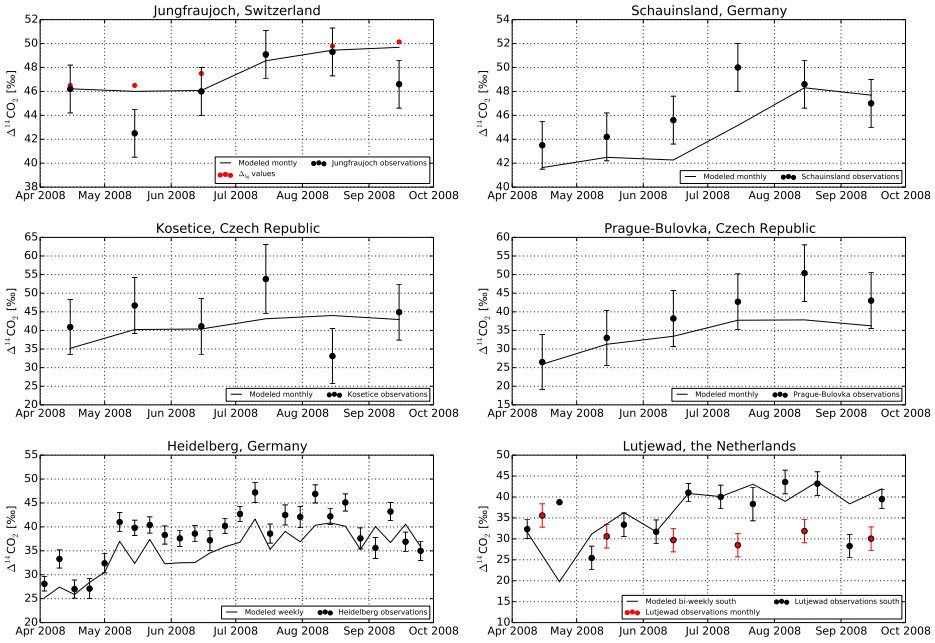
Figure 4.3: *Comparison between observed and modeled atmospheric $\Delta^{14}CO_2$ integrated samples for six observational sites. Red circles in the Jungfraujoch graph show the monthly fit used as the signature of the background CO_2 (Δ_{bg}) in our calculations. Observations are monthly continuously integrated samples at Jungfraujoch, Schauinsland, Kosetice, and Prague. At Heidelberg the weekly samples integrate only during the night-time. At Lutjewad the bi-weekly samples only integrate during periods of southerly winds, and the monthly integral over all sectors (discussed in the main text) is shown in red.*

We next analyze the results for the $\Delta^{14}CO_2$ signature corresponding to these CO_2 mole fractions to evaluate our skill at modeling the large scale $^{14}CO_2$ over Europe. Figure 4.3 shows the comparison between integrated (monthly, bi-weekly or weekly) samples and their modeled counterparts for six measurement sites – Jungfraujoch, Switzerland, Heidelberg and Schauinsland, Germany (Institut für Umweltphysik, University of Heidelberg, Germany, Levin et al., 2013), Prague-Bulovka and Kosetice, Czech Republic (Academy of Sciences of the Czech Republic, Svetlik et al., 2010) and Lutjewad, the Netherlands (Centre for Isotope Research, University of Groningen, The Netherlands, unpublished data for the monthly

Table 4.1: *The observational sites with data used in this study and statistics for the daily concentrations of CO_2 and CO_{2ff} estimated from CO observations, hourly flux CO_2 and monthly integrated $\Delta^{14}CO_2$ observations as compared with modeled results. Here $\overline{P_i - O_i}$ represents the mean model-data difference and $\sigma_{P_i-O_i}$ is the spread of this difference. Both expressions carry the units described in the header of each section. r and d are respectively the Pearson's coefficient of correlation and the coefficient of determination. n is the number of members used in the statistical analysis.*

Site	Latitude [°N]	Longitude [°E]	Elevation [m]	Altitude [m]	Owner	Provider	$\overline{P_i - O_i}$	$\sigma_{P_i-O_i}$	r	d	n
CO₂ concentration [ppm]											
Cabauw, NL	51.97	4.93	0.7	20	ECN, NL[a]	CarboEurope IP[b]	5.58	8.19	0.64	0.72	185
Cabauw, NL	51.97	4.93	0.7	60	ECN, NL	CarboEurope IP	3.69	6.37	0.65	0.74	185
Cabauw, NL	51.97	4.93	0.7	120	ECN, NL	CarboEurope IP	2.76	5.48	0.67	0.77	185
Cabauw, NL	51.97	4.93	0.7	200	ECN, NL	CarboEurope IP	1.40	4.50	0.74	0.84	185
Heidelberg, DE	49.42	8.67	116	30	IUP-UHEI, DE[c]	CarboEurope IP	4.29	7.31	0.69	0.77	185
Loobos, NL	52.17	5.74	25	24.5	Alterra-WUR, NL[d]	CarboEurope IP	3.82	6.90	0.59	0.71	185
Lutjewad, NL	53.40	6.36	3	60	CIO-RUG, NL[e]	CIO-RUG, NL	-0.60	7.43	0.53	0.73	167
Neuglobsow, DE	53.17	13.03	65	–	UBA, DE[f]	WDCGG[g]	-2.31	8.62	0.58	0.74	185
Schauinsland, DE – 5 min	47.92	7.92	1200	7	UBA, DE	WDCGG	0.20	4.13	0.81	0.89	153
Schauinsland, DE – conti	47.92	7.92	1200	7	UBA, DE	WDCGG	0.17	3.59	0.85	0.92	177
Sonnblick, AT	47.05	12.95	3106	–	EEA, AT[h]	WDCGG	1.57	2.74	0.86	0.88	185
Zugspitze, DE	47.42	10.98	2656	–	UBA, DE	WDCGG	0.79	3.07	0.82	0.88	161
Estimated fossil fuel CO₂ concentration [ppm]											
Lutjewad, NL – CO₂ff	53.40	6.36	3	60	CIO-RUG, NL	CIO-RUG, NL	-3.29	3.64	0.66	0.69	166
CO₂ surface flux [mg CO₂ m⁻² s⁻¹]											
Cabauw, NL	51.97	4.93	0.7	1	KNMI, NL[i]	CESAR[j]	-0.01	0.26	0.70	0.83	2662
Δ¹⁴CO₂ integrated sample [‰]											
Heidelberg, DE – weekly	49.42	8.67	116	30	IUP-UHEI, DE	IUP-UHEI, DE	-3.28	3.05	0.82	0.82	26
Jungfraujoch, CH	46.55	8.00	3450	5	IUP-UHEI, DE	IUP-UHEI, DE	1.05	1.61	0.71	0.74	6
Kosetice, CZ	49.58	15.08	534	3.5	NPI AS CR	NPI AS CR	-2.44	6.78	0.07	0.26	6
Lutjewad, NL	53.40	6.36	3	60	CIO-RUG, NL	CIO-RUG, NL	8.82	5.16	-0.87	0.12	6
Lutjewad, NL – south	53.40	6.36	3	60	CIO-RUG, NL	CIO-RUG, NL	0.16	6.79	0.39	0.63	12
Prague-Bulovka, CZ	50.12	14.45	266	8	NPI AS CR	NPI AS CR	-5.23	3.88	0.95	0.77	6
Schauinsland, DE	47.92	7.92	1200	7	IUP-UHEI, DE	IUP-UHEI, DE	-1.89	1.83	0.74	0.75	6

a ECN – Energy Research Center of the Netherlands, the Netherlands; contact person – Alex Vermeulen, a.vermeulen@ecn.nl

b CarboEuropeIP – CarboEurope Integrated Project; http://www.carboeurope.org

c IUP-UHEI – Institute of Environmental Physics, University of Heidelberg, Germany; contact person – Ingeborg Levin, Ingeborg.Levin@iup.uni-heidelberg.de

d Alterra-WUR – Alterra, Wageningen University, the Netherlands; contact person – Eddy Moors, eddy.moors@wur.nl

e CIO-RUG – Center for Isotope Research, University of Groningen, the Netherlands; contact person – Harro Meijer, H.A.J.Meijer@rug.nl

f UBA, DE – Federal Environmental Agency, Germany; contact person – Karin Uhse, karin.uhse@uba.de

g WDCGG – World Data Center for Greenhouse Gases; http://ds.data.jma.go.jp/gmd/wdcgg/

h EEA, AT – Environmental Agency Austria, Austria; contact person – Marina Fröhlich, marina.froehlich@umweltbundesamt.at

i KNMI – Royal Netherlands Meteorological Institute, the Netherlands; contact person – Fred Bosveld, Fred.Bosveld@knmi.nl

j NPI AS CR – Nuclear Physics Institute, Academy of Sciences of Czech Republic, Czech Republic; contact person – Ivo Svetlik, svetlik@ujf.cas.cz

integrated samples, south sector data was previously used in van der Laan et al., 2010). Complementary statistics are included in Table 4.1. For the high-altitude locations of Jungfraujoch and Schauinsland the model topography differed significantly from the altitude of the observational site. Similar to the procedure described in Turnbull et al. (2009b) we sampled a model layer in the free troposphere instead of at the modeled surface to better represent the observations. At all other sites we sample the pressure-weighted signature of the boundary layer, applying a minimum boundary layer height of 350 m during the night to avoid sampling too low surface signatures in a too stable nighttime boundary layer. The comparison shows we capture reasonably well the seasonal cycle for most sites, however the model generally underestimates the $\Delta^{14}CO_2$. This is partly caused by the omitted biospheric disequilibrium term, which accounts on average for up to 1.5 ‰ at these latitudes. Additional bias could be introduced through our choice of background site. In their study, Turnbull et al. (2009b) showed that the signature of free tropospheric air in the northern-hemispheric mid-latitudes can vary within 3 ‰ and additionally the signatures at mountain background sites (as Jungfraujoch) are slightly influenced by local fossil fuel emissions.

In the lowest left panel of Fig. 4.3 we show the comparison for Heidelberg, where observations are collected as weekly night-time (between 19:00 and 07:00 local time) integrated samples. On higher temporal resolution our model estimates reproduce the temporal variations of the observations well. Still, the already discussed underestimation in $\Delta^{14}CO_2$ is also present at this site, which is located near a large urban area with considerable fossil fuel emissions. During the period from May to August, this underestimation is on average 5 ‰ in the model (~ 1.8 ppm of fossil fuel CO_2). In the lowest right panel of Fig. 4.3 we show the comparison between the observed and modeled signatures at Lutjewad for the wind-specific measurements at this site in addition to the observed monthly samples that were continuously integrated. The monthly $\Delta^{14}CO_2$ observations for 2008 from this location show atypical seasonality with a lack of the expected summer maximum, and 10 to 20 ‰ lower $\Delta^{14}CO_2$ than the observations in Jungfraujoch and Schauinsland in that year. Although this suggests a large fossil fuel CO_2 signal for 2008, we could not find further evidence of this in the rest of the Lutjewad observational record (CO, CO_2), nor in the selected southerly wind sector data (van der Laan et al., 2010), which our model matches rather well. Since the measurements themselves seem valid, this feature in the continuous monthly Lutjewad $\Delta^{14}CO_2$ data remains unexplained. We will however take a closer look at the temporal variability of the different $\Delta^{14}CO_2$ components and the general model performance at Lutjewad for the more accurately simulated southerly wind sector.

Figure 4.4 shows the 6-month hourly comparison of simulated and observed CO_2 and fossil derived CO_2 for Lutjewad. The latter is derived from ^{14}C-corrected high-resolution CO observations (van der Laan et al., 2010). Statistics for the comparison are also shown in Table 4.1. The fossil fuel signal dominates over any variability in the background, clearly
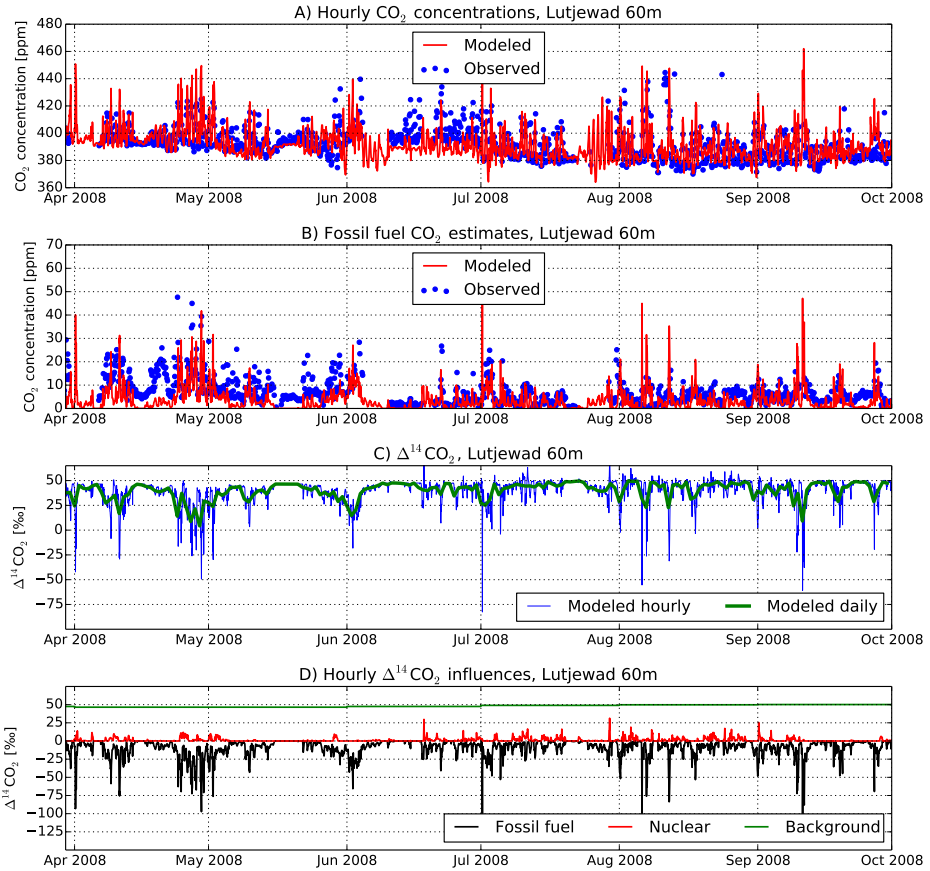
Figure 4.4: 6 months of hourly results for Lutjewad at 60 m height. Comparison between observed and modeled **(a)** CO_2 *concentrations,* **(b)** CO_{2ff} *concentrations* **(c)** *atmospheric* $\Delta^{14}CO_2$ *and* **(d)** *the contribution of different compounds for the resulting* $\Delta^{14}CO_2$. *The transport of air that is enriched in fossil fuel* CO_2 *is directly connected to the variations in the* $\Delta^{14}CO_2$ *signal at the location, but these are not captured by current observations due to their low temporal resolution.*

defining periods with enhanced transport of fossil fuel CO_2 to the location (late April, start of May, start of July, start of August) as compared to less polluted air transported from the North Sea (mid-May, mid-June). The larger mismatch in particular periods (second half of April, start of May) can be attributed to the specific way the CO observations are calibrated

using the 3-year fit of the ^{14}C-CO ratio at the site. While this would ensure that on an annual scale the actual ^{14}C-CO relation is reached, on the bi-weekly scale of the ^{14}C observations this sometimes results underestimation of the ^{14}C-CO ratio compared to the observed values and consequently overestimation of the estimated fossil fuel CO_2. For more information, see van der Laan et al. (2010).

In the last panels we see this influence on the resulting $\Delta^{14}CO_2$ signature and especially its high temporal variability that is not captured in the typically integrated monthly samples. Note that even though station Lutjewad is far away from nuclear emission sources, the signal from nuclear activity (shown in the last panel) can sometimes be of the same order of magnitude as the fossil fuel signal. This shows that it is important to evaluate the nuclear influence at every measurement site using a model like presented here, as it will contribute to the uncertainty in the recalculation of fossil fuel CO_2.

4.3.2   Fossil fuel vs. nuclear emissions influence on $\Delta^{14}CO_2$

The lowest $\Delta^{14}CO_2$ values in the domain are modeled in the regions with high fossil fuel emission in Germany (the Ruhrgebiet), and the highest $\Delta^{14}CO_2$ is near the large emitting sites in western France and UK. This pattern can be clearly seen in Fig. 4.5a–c where results averaged over the lower 1200 m of the atmosphere over the full 6 months are shown. Note that the nuclear enrichment reaches much higher amplitude than the opposite effect by the fossil CO_2, but its influence on the atmospheric $\Delta^{14}CO_2$ is usually restricted to the vicinity of the average nuclear power plant reactors. The influence is more pronounced in the western part of our domain, where it captures the influence from the spent fuel reprocessing plant in La Hague (France) and several newer generation nuclear reactors in the UK. Even then, the influence of the nuclear enrichment averaged over 6 months is typically about 1 to 6 ‰ in areas that are not in direct vicinity of the sources. As a comparison, the fossil fuel influence in our domain on the same temporal and spatial scale is mostly between -3 and -15 ‰ outside the very polluted area of the Ruhrgebiet, Germany.

As the nuclear enrichment will (partially) mask the effect of fossil fuel CO_2 on the atmospheric $\Delta^{14}CO_2$, we show in Fig. 4.5d the average 6-month ratio of the influences due to nuclear and fossil fuel sources in our domain. Again, in most of the eastern and central parts of our domain the nuclear influence is less than 10 % the fossil fuel influence. This differs from the western part of our domain, where the ratio varies between 3 times smaller to about the same magnitude as the fossil fuel contribution and even to a more than 5 times larger influence in the area around the nuclear sources. The area affected depends on the strength of the source, and in our case the influence of most water-cooled reactors rarely exceeds the grid cell of the source, while for the gas-cooled reactors the influence can be seen up to 50 km distance. These findings are consistent with Graven and Gruber (2011). The magnitude of the
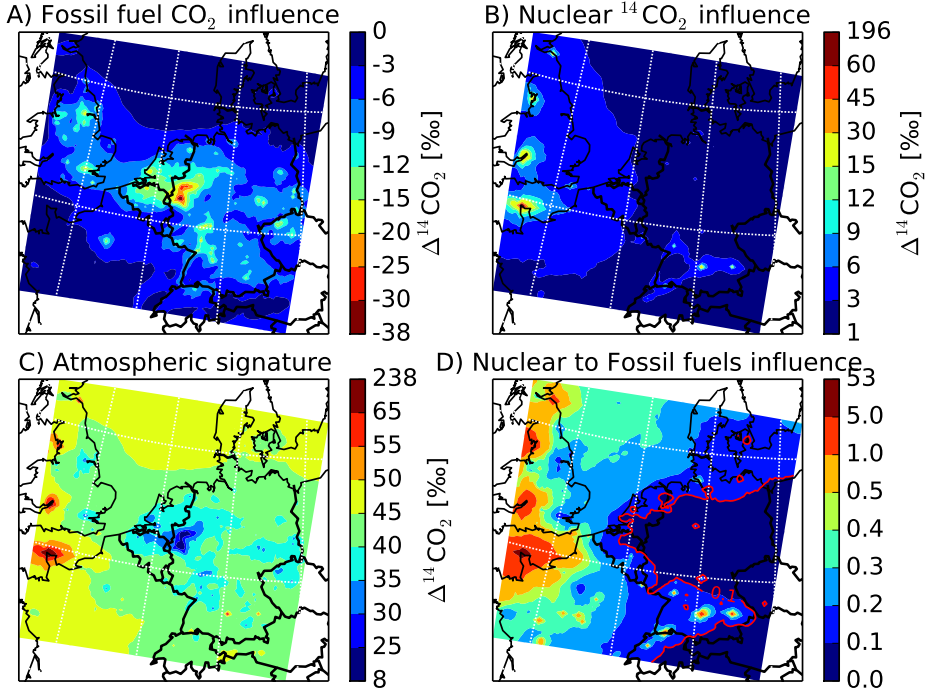
*Figure 4.5: Spatial distribution for the 6-month averaged **(a)** fossil fuel CO_2 emissions influence, **(b)** nuclear $^{14}CO_2$ emissions influence, **(c)** resulting $\Delta^{14}CO_2$ signature in the atmosphere and **(d)** the ratio between the nuclear and fossil fuel influences on the atmospheric signature, all averaged over the lower 1200 m of the atmosphere. While the largest influence over Europe is from fossil fuel CO_2, the effect of the nuclear emissions of $^{14}CO_2$ can be of comparable magnitude for large areas in France and UK.*

enrichment and size of the area influenced are both highly variable and strongly dependent on the atmospheric transport. As a result, in months with dominant easterly winds the nuclear enrichment has a minimum effect in our domain, as most of the nuclear emissions are transported towards the Atlantic ocean and out of our area of interest. However, in months with dominant westerly winds, which is the prevailing wind direction, the nuclear $^{14}CO_2$ spreads widely over the domain.

Graven and Gruber (2011) evaluated the uncertainty of the emission factors reported in previous literature and estimated mean values with associated 70 % confidence interval. While for our main results we used the estimated mean emission factors for a 2-month period we separately simulated the 70 % confidence interval of the emission factors ("low estimate" and "high estimate" runs). In Fig. 4.6 we show these results as the absolute difference when
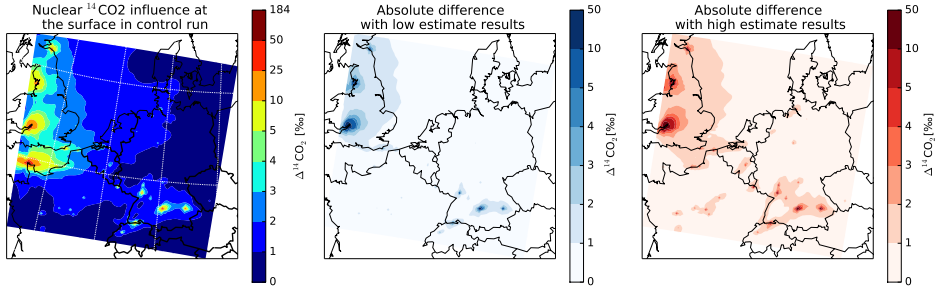
Figure 4.6: Spatial distribution for the uncertainty in the nuclear $^{14}CO_2$ influence simulated for August and September, due to the uncertainty in the emission factors associated with different reactor types. (Left) The nuclear influence modeled with the central estimate of the reactor emission factors; (middle) the absolute difference between the lower estimate and central estimate; (right) the absolute difference between the higher estimate and the central estimate. Low and high estimates refer to the 70% confidence interval for the emission factors.

compared to the mean run. While our largest source of nuclear emissions – located in La Hague, France, has directly reported emissions of $^{14}CO_2$ and is thus not subject to uncertainty in the emission factors, considerably higher or lower $^{14}CO_2$ signatures could be associated with the nuclear estimates in the United Kingdom, southern Germany and central France.

For sites located in northern and central France, southern Germany and the UK the nuclear enrichment means that corrections are needed that account for the nuclear influence in the observed $\Delta^{14}CO_2$ before estimating the fossil fuel influence. As an illustration, we show in Fig. 4.7 the influence of the different anthropogenic emissions for three locations with different characteristics in our domain: Cambridge (UK), Cabauw (the Netherlands) and Kosetice (Czech Republic). The locations were chosen to be in rural or agricultural areas, without large local CO_2 emissions. As seen in Fig. 4.7, the western part of our domain (represented by Cambridge) has an equal influence from fossil fuel and nuclear emissions; the center (represented by Cabauw) experiences some events with relatively high nuclear emissions influence, but is influenced mostly by the very high fossil fuel emissions in this region (on average about 3 times higher than in Cambridge). In the east (represented by Kosetice) there is no significant signal of influence of nuclear emissions, but the influence of fossil fuel emissions is also considerably lower.

4.3.3 $\Delta^{14}CO_2$ plant vs. atmospheric samples

In our previous work (Bozhinova et al., 2013) we described a method to model the $\Delta^{14}CO_2$ in plant samples as the first step in quantifying the differences between such samples and integrated atmospheric samples. Here we build on this work by calculating the plant signature resulting from uptake of spatially and temporally variable atmospheric $\Delta^{14}CO_2$. The results for modeled samples from maize leaves at flowering, are shown in Fig. 4.8. Clearly, spatial gradients in $\Delta^{14}CO_2$ in plants are sizable compared to the measurement precision of approximately 2 ‰. The regions with high influence from anthropogenic emissions from Fig. 4.5, namely the Ruhrgebiet in western Germany and the Benelux are also visible in the modeled plant signature, and so are some hot spots around larger european cities, like Frankfurt, Paris, London and others. It is important to point out that in addition to fossil fuel and nuclear gradients, plants develop at a different rate in different parts of the domain, and even the different parts of a plant (roots, stems, leaves, fruits) grow during different time periods.

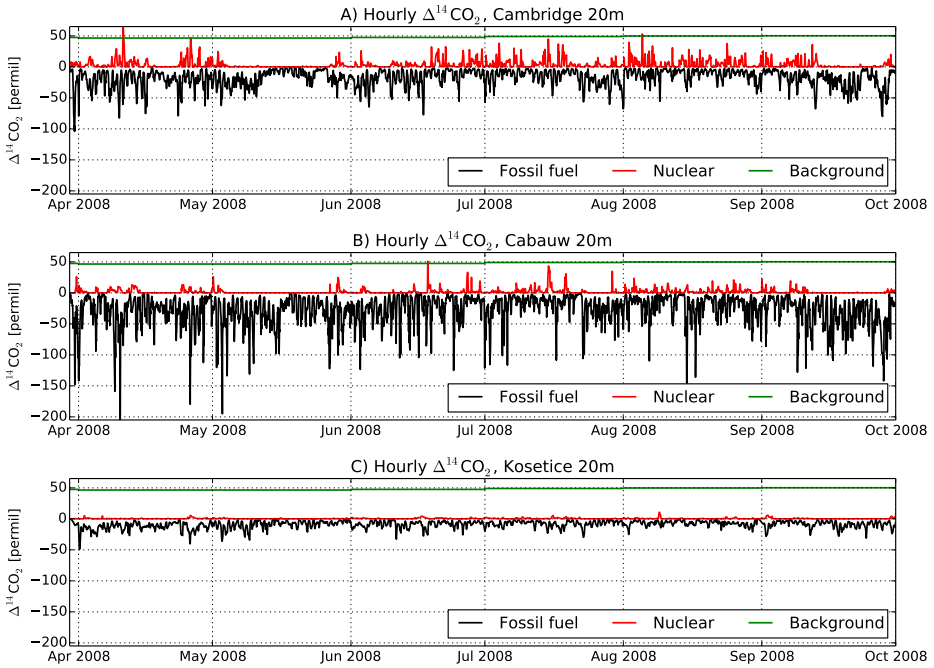*Figure 4.7: Time series for the relative importance of nuclear vs. fossil fuel influence on the resulting atmospheric $\Delta^{14}CO_2$ for three locations in our domain – near Cambridge (UK), Cabauw (the Netherlands) and Kosetice (Czech Republic).*

The plant-sampled $\Delta^{14}CO_2$ includes the effect of the covariance between the atmospheric $\Delta^{14}CO_2$ variability and the variability in the assimilation of CO_2 in the plant during growth, which is absent in traditional integrated samples where the absorption of CO_2 is based on constant flow rate through an alkaline solution and thus only varies with the CO_2 concentration present in the flow (Hsueh et al., 2007). In Fig. 4.9 (left) we show this effect of the plant growth on the resulting plant $\Delta^{14}CO_2$ signature when comparing the resulting plant signature with the daytime atmospheric average we provide to our crop model. We should stress, that this is the magnitude of the error one should expect if the plant-sampled $\Delta^{14}CO_2$ is assumed equal to the atmospheric mean $\Delta^{14}CO_2$ for the growing period of the plant. For many parts of Europe in our simulated period this error is approaching the measurement precision of the $\Delta^{14}CO_2$ analysis (of approximately $\pm 2 \text{‰}$). In the region located between the areas with high fossil fuel and large nuclear emitters, however, the magnitude of the error can be several times larger. This is likely due to the absorption of some very high signature values in periods when the wind direction is directly from the nuclear source. Actual plant samples, taken during different period than the one investigated here (namely 2010–2012), will be used to further investigate these signatures in a follow-up publication.
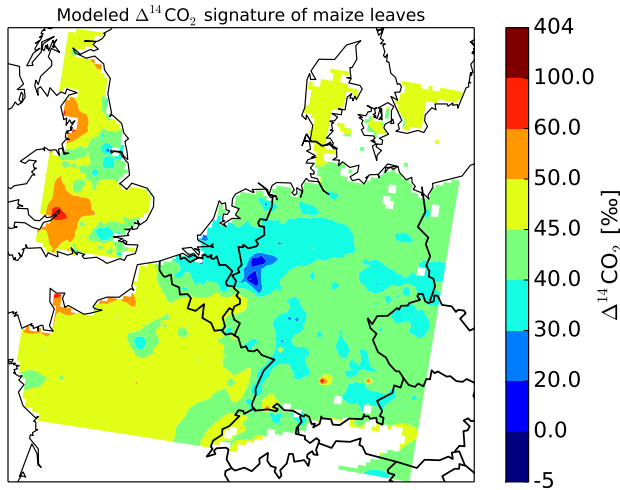
Figure 4.8: Modeled absolute $\Delta^{14}CO_2$ signature of maize leaves at flowering. Both the highly industrialized areas in Germany, where the atmospheric $\Delta^{14}CO_2$ is lower than the background, and the enriched areas near the big nuclear sources in France and UK are visible also in the plants. Even on this resolution we see in the plant signature the hot spots around Paris, London, Frankfurt, and many other big cities.

We also evaluated the bias that would be introduced if the nuclear influence is not included

in the modeling of the plant samples. We show this on Fig. 4.9 (right) as the difference between the plant signatures when the nuclear influence is included or excluded from the simulation. For the continental part of our domain this bias mostly stays within 0–4 ‰, while in the United Kingdom it ranges from 2–8 ‰ and higher. This suggests that also when interpreting plant samples, the ability to correctly account for nuclear influences such as through a modeling system could be important.

4.3.4 Direct estimation of the fossil fuel CO_2 emissions

While the entire emission map of Europe might be difficult to verify, most of the fossil fuel CO_2 emissions are produced at only a number of locations. For instance, 10 % of all emissions in our domain come from only 30 grid cells and more than half of these are located in densely populated cities or urban conglomerations. This might provide an opportunity for a better fossil fuel estimate of the highest emitting regions in Europe even when only selected locations are visited in a plant sampling campaign. One could for instance assume that the $\Delta^{14}CO_2$ signatures in plants in these high-emission areas directly reflect the local anthropogenic sources, and a straightforward determination of their $^{14}CO_2$ signature would suffice to estimate emissions using a simple box-model approach. We show in the following analysis that this simplification can lead to large errors though, and a more complete modeling framework like ours is needed for a proper interpretation of $\Delta^{14}CO_2$.

In our modeling framework, we know the exact emissions we prescribe in each grid box as well as the resulting atmospheric $\Delta^{14}CO_2$ signatures. If we take the anthropogenic emissions over a 60 km × 60 km area around 25 large European cities, mix them through a 500 m deep boundary layer (typical 24 h average for our domain), and assume the air to have a residence time of 3.3 h (corresponding to a typical wind speed of 5 ms^{-1} through a 60 km domain), we can make a simple estimate of the resulting $\Delta^{14}CO_2$ signature relative to the background from Jungfraujoch. This box-model estimate is shown in Fig. 4.10 as the continuous straight line, in which the downward slope with increasing emissions is controlled mostly by the assumed residence time and the prescribed boundary layer height.

If we compare this linear relationship with the simulated $\Delta^{14}CO_2$ signatures over these cities simulated with the full model developed in this paper (including its detailed horizontal advection, vertical mixing, and nuclear influence), one can see the large variability and substantial bias one would incur using the simple box-model approach. Up to 8 ‰ differences from this line would be found for Paris and Cologne, while the nuclear influence would lift Birmingham plant samples back toward the Jungfraujoch background $\Delta^{14}CO_2$ despite its emissions being similar to Berlin. Even if the full model-derived slope of approximately -4.85 ‰ per 10 000 mol km^{-2} h^{-1} could be reproduced with the box-model, the coefficient of determination (R^2) would be just over 0.7, meaning that close to 30 % of the spatial variance

in emissions across Western Europe will not be captured in the simple approach. We therefore caution strongly against a simplified quantitative interpretation of $\Delta^{14}CO_2$ signatures, both in plants and in the atmosphere.
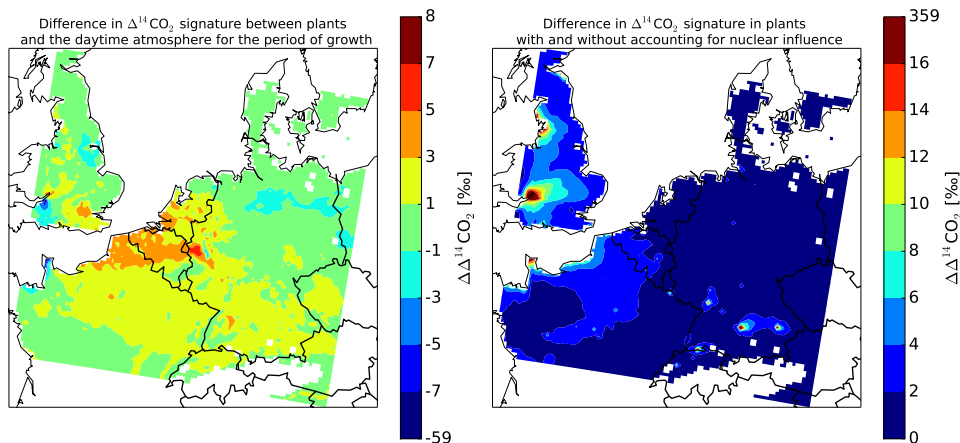

Figure 4.9: *Difference between $\Delta^{14}CO_2$ modeled in plants and the daytime atmospheric average (left) and between modeled plants with and without taking the nuclear influence into account (right). While the left figure shows the error that should be expected if the plant growth is not taken into account and the plant signature is assumed to be equal to the atmospheric average, the right one shows the error that will be introduced if nuclear emissions of $^{14}CO_2$ are not accounted for in the model simulation.*

With a typical $\Delta^{14}CO_2$ single measurement precision of about $\pm 2\,‰$ and the full model-derived slope given above, we can tentatively estimate that even a perfect modeling framework will have a remaining uncertainty of 4000 mol km^{-2} h^{-1} for area-average emissions in these top-25 emitters over Europe. This is quite substantial (20–50 %) for most of them, with the possible exception of the cities in the German Ruhr area (5–15 %). We therefore see an important role for a monitoring program of $\Delta^{14}CO_2$ signatures in which emissions from all major sources are captured in multiple samples from multiple locations to minimize dependence on single observations and single atmospheric transport conditions. A modeling framework that can capture the specific characteristics of the regional atmospheric transport, fossil fuel emissions, and nuclear contributions like the one presented here would bring added value to the interpretation of such data.

4.4 Discussion

Our modeling results show that over a significant part of our domain, the nuclear influence on the atmospheric $\Delta^{14}CO_2$ signature will be more than 10 % (ratio = 0.1 on Fig. 4.5d) of the estimated fossil fuel influence, introducing considerable uncertainty to the method of using $\Delta^{14}CO_2$ to calculate the fossil fuel CO_2 addition to the regional atmosphere. The strongest gradients of $\Delta^{14}CO_2$ in Western Europe are found in the relatively polluted region in western Germany and the Netherlands due to the high population density and large industry sector there, and hence high CO_2 emissions. As was shown for California by Riley et al. (2008), more detailed $^{14}CO_2$ observations in this region can possibly prove useful in lowering the uncertainty of the regional fossil fuel emission estimates. Furthermore, the high fossil-to-nuclear ratio ensures that uncertainties arising from nuclear emissions will be at their minimum.

This result relies partly on the underlying emission maps for the anthropogenic (fossil fuel) CO_2 and (nuclear) $^{14}CO_2$ emissions. We should consider various factors that are uncertain or unknown at this point for these emissions (Peylin et al., 2011; Graven and Gruber, 2011) – such as temporal characters, vertical resolution and even small irregularities in the spatial allocation of the emission sources. All our anthropogenic emissions are currently introduced in the lowest (surface) layer of our model, but according to the emission database used (IER, Stuttgart), most of the industrial emission stacks are located on average at 100 to 300 m height. Using this information in our model will likely result in the emitted CO_2 being transported away faster, and result in less local enrichment. This is also true for our nuclear emissions sources, but information on their vertical emission heights is more difficult to find.

For the fossil fuel CO_2 emissions we apply temporal profiles that disaggregate monthly, weekly and diurnal signals from the provided annual emissions. For the nuclear emissions such profiles are unknown and information on their temporal heterogeneity is not publicly available. In this study we consider these emissions as continuous and constant throughout the year. This is a relatively safe assumption for the emissions from nuclear power plants as their $^{14}CO_2$ is a by-product of the normal operation of the reactor. Temporary shutdowns for scheduled maintenance that covers periods of weeks and sometimes months would invalidate this assumed emission pattern. Continuous constant emissions are not likely for reprocessing sites, where the emissions will depend on the type and amount of fuel being reprocessed. Additionally, there is uncertainty if these emissions are released continuously or in a few large venting events, where the venting procedures are moreover likely to be reactor-type dependent. Currently, we lack the information to account for such complications.

When using flask samples for $^{14}CO_2$ measurement nuclear enrichment can relatively easily be recognized. However, in integrated air and plant samples this signal will be averaged
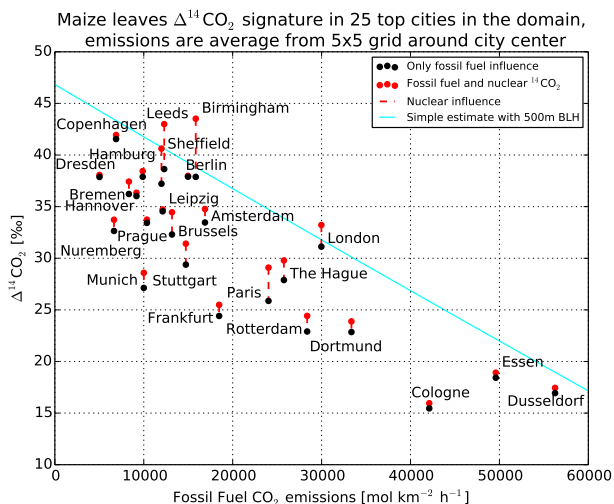
Figure 4.10: Comparison between the results of the simple box model (see main text) and the modeled maize leaves $\Delta^{14}CO_2$ signature at city center and fossil fuel CO_2 emissions averaged for 5×5 grid around the city center on 12 km horizontal resolution.

over the total sampling period. Depending on weather variability, local fossil fuel CO_2 addition and the proximity to the nuclear sources, the enrichment in $\Delta^{14}CO_2$ can often be within the measurement precision (of approximately $\pm 2\,‰$) as we have shown. Thus, integrated samples likely have too low time resolution and sensitivity to attribute nuclear emissions, and areas where this influence is high would profit from flask sampling of $\Delta^{14}CO_2$ in addition to integrated plant sampling. Because plant samples can be used only as complementary observations during particular seasons and depending on the species sampled a dual monitoring approach with flasks and integrated samples seems best. Based on our results, a better characterization of the temporal structure of the nuclear emissions is a prerequisite for any $^{14}CO_2$-based monitoring effort in Europe.

Our study is subject to known uncertainties in atmospheric transport of mesoscale models. An inaccurate simulation of wind speed and direction (Lin and Gerbig, 2005; Gerbig et al., 2008; Ahmadov et al., 2009) or boundary layer height development (Vilà-Guerau de Arellano et al., 2004; Steeneveld et al., 2008; Pino et al., 2012) will affect the transport of emission plumes and resulting mole fractions. Resolving more meso-scale circulations, and improved representation of topography can be particularly advantageous, as they can cause large gradients in CO_2 (de Wekker et al., 2005; van der Molen and Dolman, 2007). While WRF-Chem is used for a variety of atmospheric transport studies (among others: Tie et al., 2009; de Foy et al., 2011; Lee et al., 2011; Stuefer et al., 2013), more general air quality

studies have shown that an ensemble of models can forecast air pollution situations more accurately than a single model (Galmarini et al., 2004, 2013). While in our research we focused on the transport of CO_2 and $^{14}CO_2$, other chemically active tracers (e.g. CO, NO_x) that are regularly measured and connected with anthropogenic emissions could be used too. Including ^{222}Rn as an additional tracer can help lowering the uncertainty associated with the vertical mixing in the model and provide correction factors to be applied to the other passive tracers, as shown in van der Laan et al. (2010), Vogel et al. (2013b).

Considering future uses of $\Delta^{14}CO_2$ observations as additional constraint on the carbon cycle, we should note that atmospheric inversions currently typically use only afternoon observational data. In that case, plant-sampled $\Delta^{14}CO_2$ observations may provide a better representation of the afternoon atmospheric $\Delta^{14}CO_2$ signals than conventional integrated samples that also absorb CO_2 during the night. However, the use of plant samples is typically limited to the summertime, which is a period with lower anthropogenic CO_2 emissions, more vertical mixing and larger biospheric fluxes. This will correspond to larger uncertainty in the recalculation of the fossil fuel CO_2 emissions compared to wintertime.

We explored the possibility that a relatively simple box-model can be used to calculate the emissions directly from $\Delta^{14}CO_2$ observations, and showed its inability to capture the variability in $\Delta^{14}CO_2$ signals across 25 European cities. Using such a simple box model has high inherent uncertainty for the reconstructed emissions, a portion of which is a direct consequence of the $\Delta^{14}CO_2$ measurement precision.

Our results suggest that a combination of the available sampling methods should be used when planning a $^{14}CO_2$ observational network for fossil fuel emissions estimates. Integrated air and plant samples alone can provide a longer period observations at a lower cost, but are less useful for evaluation of large nuclear influences in shorter periods. Flask samples are much better suited for this, however their continuous analysis is too costly. A possible compromise could be to obtain flask samples for a limited period alongside integrated samples for new sampling locations. This would already provide information about the possible nuclear enrichment and the wind directions from which it usually occurs. Additionally, while integrated air samples are the current standard for quasi-continuous observations of $^{14}CO_2$, plant samples can be obtained at a much higher spatial resolution without additional infrastructure investment. Their use is however constrained to the sunlit part of the day and generally the summer season, and the exact time and locations where the chosen crop grows.

4.5 Conclusions

In this work, we demonstrated the ability of our modeling framework to simulate the atmospheric transport of CO_2 and consequently the atmospheric $\Delta^{14}CO_2$ signature in integrated

air and plant samples in Western Europe. Based on our results we reach the following conclusions.

1. Simulated spatial gradients of $\Delta^{14}CO_2$ are of measurable size and the 6-month average CO_{2ff} concentrations in the lower 1 km of the atmosphere across Western Europe are between 1 to 18 ppm.

2. Enrichment by $^{14}CO_2$ from nuclear sources can partly mask the Suess effect close to nuclear emissions, particularly in large parts of UK and northwestern France. This is consistent with previous studies (Graven and Gruber, 2011) and we show that in these regions the strength of the nuclear influence can exceed the influence from fossil fuel emissions.

3. The simulated plant $\Delta^{14}CO_2$ signatures show spatial gradients consistent with the simulated atmospheric gradients. Plant growth variability induces differences between the simulated plant and the daytime atmospheric mean for the period of growth, of a magnitude that is mostly within the measurement precision of ± 2 ‰, but can be up to ± 7 ‰ in some areas.

4. Integrated $\Delta^{14}CO_2$ samples from areas outside the immediate enrichment area of nuclear emission sources are not sensitive to occasional advection of enriched air due to their long absorption period. However, to properly account for the nuclear enrichment term on smaller time scales, improvements in temporal profiles of nuclear emissions are needed.

5. New $\Delta^{14}CO_2$ sampling strategies should take advantage of different sampling methods, as their combined use will provide a more comprehensive picture of the atmospheric $\Delta^{14}CO_2$ temporal and spatial distribution.

5

Three years of $\Delta^{14}CO_2$ observations from maize leaves in the Netherlands and Western Europe

$\Delta^{14}CO_2$ measurements are useful to investigate the regional signals of anthropogenic CO_2 emissions, despite the currently scarce $\Delta^{14}CO_2$ observational network. Plant samples are an easily attainable alternative, which have been shown to work well as a qualitative measure of the atmospheric $\Delta^{14}CO_2$ signals integrated over the growing period of the plant. Here, we present the ^{14}C analysis results for 79 samples from maize (Zea mays) leaves samples from the Netherlands gathered in the years 2010 to 2012, and from western Germany and France in 2012. In addition to our sampling strategy and results, we include a comparison to a modeling study of the plant-sampled atmospheric $\Delta^{14}CO_2$. Our model results agree with observed plant samples for the de-trended $\Delta^{14}CO_2$ signatures relative to the background with RMSD of 2.78‰(excluding 8 large outliers), which is comparable to the inherent measurement uncertainty. We found that both measurements and model capture the large-scale (>100 km) regional gradients, with significant correlations across all three countries. The modeled plant results reveal that the largest signals found in the Netherlands and Germany are associated with emissions from the energy production and road traffic, while in France the $^{14}CO_2$ enrichment from nuclear sources dominates in almost all samples. The interpretation of plant samples adds additional uncertainty to the already relatively large measurement uncertainty. In view of this, we advise that future large monitoring strategies prioritize more accurate sampling techniques and plant

sampling is used only in areas without atmospheric observational infrastructure.

5.1   Introduction

^{14}C is a promising tracer with an increasing importance in studies of the anthropogenic CO_2 emissions to the atmosphere (Ciais et al., 2010; Vogel et al., 2013b; Turnbull et al., 2014b). However, even with the rapidly increasing number of observational sites around the globe that measure atmospheric $^{14}CO_2$ (Graven et al., 2012b), the spatial resolution of the network limits the information that potentially can be used to infer regional scale CO_2 emissions. $\Delta^{14}CO_2$ measurement of annual plants can provide some additional information on a higher spatial scale and can be used in addition to semi-continuous measurements from the observational network to partially negate the coarse horizontal resolution of pure atmospheric samples. Plant samples have been shown previously (Hsueh et al., 2007; Riley et al., 2008) to represent qualitatively well the atmospheric fossil fuel CO_2 concentrations. Nevertheless, a more complete interpretation of the signals that they record is required before this method can be used to evaluate anthropogenic CO_2 emissions quantitatively.

Plants assimilate atmospheric CO_2 during their daily photosynthesis, so their $^{14}CO_2$ signature will be representative of only the daytime period. This period is usually characterized by well-mixed conditions and hence by smaller signals from anthropogenic CO_2 emissions. Additionally, growth limiting factors, such as available solar radiation, water and others, will modify the amount of assimilated CO_2. The plant sample will often differ from the atmospheric average due to the variable assimilation rate of the plant (Bozhinova et al., 2014), thus the growing conditions should be accounted for when interpreting such samples. Furthermore, species specific development differences also need to be considered, as samples are usually taken of a particular plant part (e.g. leaves), for which the assimilation period can differ depending on how favorable the growing conditions were in different seasons or locations (Bozhinova et al., 2013). In maize, for example, the leaves stop growing shortly after flowering, while the stems still accumulate carbohydrates for a bit longer, resulting in different period for which these two parts of the same plant are representative of the atmospheric $\Delta^{14}CO_2$.

We present here an intensive regional sampling study conducted in 2010, 2011 and 2012 for western Europe, during which samples of maize (*Zea Mays*) leaves were gathered from the Netherlands, Germany and France. We draw inspiration from the similar studies for maize and grasses in North America (Hsueh et al., 2007; Riley et al., 2008) and an European study, which utilized samples of wine-ethanol to explore $\Delta^{14}CO_2$ from past years (Palstra et al., 2008). Nevertheless, this is the first attempt to map the atmospheric $\Delta^{14}CO_2$ spatial gradients from annual plants across Europe on such high spatial resolution. Alongside the results from
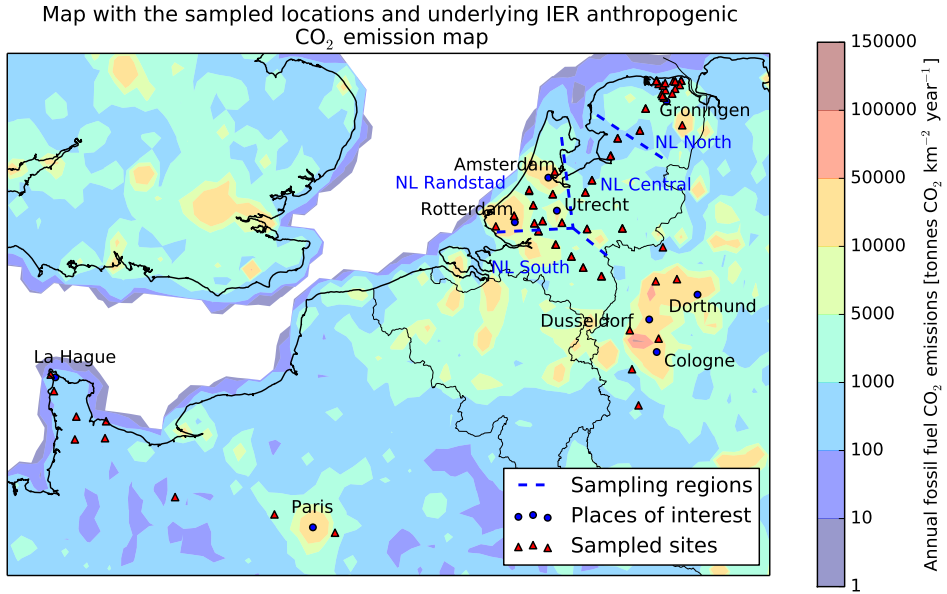
Figure 5.1: Overview of the sampled locations and the modeled underlying fossil fuel CO$_2$ emissions map (annual estimate for 2012 based on the 2005 emission map developed by Institute for Energy Economics and the Rational Use of Energy, University Stuttgart). Dashed lines signify the borders of sampling regions later used in the presentation of our results.

the ^{14}C analysis, we include our complete sampling strategy and protocols, which also include the additional plant development information that was obtained from the cooperating farmers. This information allows us to evaluate the uncertainty associated with the assimilation rate and development rate of the sampled plants.

In addition to our experimental results, we present here a modeling study that aims to reproduce the observed plant results, and to verify the $\Delta^{14}CO_2$ gradients captured in them. This numerical experiment uses the regional atmospheric and plant $\Delta^{14}CO_2$ modeling framework described previously in Bozhinova et al. (2014), with a few improvements that are explicitly described in our methods. We use the modeling results to compare with observed plant $\Delta^{14}CO_2$ signatures and evaluate the current limits to our ability to interpret them. Furthermore, we discuss the general use of plant samples for fossil fuel CO_2 emission verification and give recommendations for future sampling strategies.

5.2 Materials and Methods

5.2.1 Experimental

In the period 2010–2012 we collected and analyzed 63 samples of maize leaves (*Zea mays*) from 37 individual locations in the Netherlands, most of which were sampled in both 2011 and 2012. In the last year 16 samples were collected from seven sites in the Ruhrgebiet area in Germany and nine sites in Lower Normandy and Isle of France in France. These regions are strongly influences by fossil fuel CO_2 and nuclear $^{14}CO_2$ emissions, respectively. A complete map of the sampled locations is shown in Figure 5.1, with the underlying anthropogenic CO_2 emission map (Institute for Energy Economics and the Rational Use of Energy, University Stuttgart, henceforth referred to as IER) to highlight the relatively polluted regions. Additionally, on this figure we define four regions for the territory of the Netherlands, which we expect to show different characteristics. In order of expected fossil fuel pollution these are: Randstad, which is the densely populated industrialized region between Amsterdam, Rotterdam and Utrecht; south Netherlands, which is the zone between Randstad and the Ruhrgebiet, a highly industrialized region in western Germany; the central Netherlands, which covers the region between the Randstad and the north; and north of the Netherlands, which is relatively rural and receives clean air with maritime characteristics from northwesterly winds.

We focused on maize as it is a crop that is available throughout most of Europe and particularly in the Netherlands. Additionally, due to the agricultural importance there is already a large expertise available in the scientific community with regard to its growth and development - both in observational and modeling studies. Using that modeling experience, previously discussed in Bozhinova et al. (2013), we chose to sample the leaves of the crop and sampled all leaves from each chosen plant. Theoretically, this would provide us with information for the atmospheric signals for a longer period than a single leaf. This is one of the differences between our work and a similar study executed in North America in the summer of 2004 (Hsueh et al., 2007), where most of the samples represented a cross-section of the upper three leaves of each plant. Our sampling protocol also differed slightly and will be discussed in more details later in this section.

In 2010 the study was focused on an area located in the northern part of the Groningen province in the Netherlands. Samples were taken with approximately 4 km between sampling sites in a triangular pattern between the city of Groningen, Lutjewad observational station and Eemshaven, an industrial harbor area with several power plants. We used the modeling results for the average anthropogenic $^{14}CO_2$ and CO_2 concentrations for 2008 presented in Bozhinova et al. (2014), and modified accordingly our sampling routes in 2011 and 2012 to try and capture the large $\Delta^{14}CO_2$ gradients expected between regions with higher or lower anthropogenic CO_2 emissions (illustrated in Figure 5.1). Thus, in these years the horizontal

resolution between sampled locations of approximately 20 km and in some cases up to and exceeding 50 km. For the Netherlands the sampled trajectories cover the distance between the Randstad and three different end points - eastwards all the way towards the border with Germany, north towards the province of Groningen and southeast towards the industrialized Rurhgebiet region in western Germany. In 2012 additional samples covering the area in Germany towards and into the Rurhgebiet and samples covering a trajectory between La Hague and Paris in France were also taken.

In order to evaluate the role of the actual plant development in our interpretation of the gathered maize samples, additional information was obtained from the owners of each maize field. We asked for the dates when the field was sowed, when the emergence of the majority of the field was observed and the approximate date when the ear has appeared marking the flowering stage of the crop. We note that while the sowing was well known and the emergence was known to within a few days, the uncertainty associated with the flowering date is larger as this information was given as an approximate to within a week or two. The details about the dates obtained can be found in the supplementary material (Table S1 - General sample information).

In terms of our sampling protocol, we always sampled plants at least 20–50 m away from the borders of the field. We picked plants that visibly appeared average compared to their neighbors and avoided sick and severely damaged plants. We gathered leaves from three plants for each sampled location. Those were not neighboring plants, but rather chosen within the same part of the field. For this study, we analyzed all three plant samples separately from site 9 (2010), and otherwise analyzed only one plant sample per location and the rest of the material is archived for possible further investigation.

After sampling, the leaves were kept refrigerated until post-sampling treatment. That included cleaning the leaves from dirt with water, cutting them into pieces, treating them with 1% solution of hydrochloric acid for one hour and afterwards rinsing thoroughly with demineralized water until close to neutral pH value was reached. Afterwards the samples were dried at 70°C for at least 48 hours. In 2010 the leaves were afterwards crushed manually into relatively small pieces, while in the latter years the samples were ground into powder using laboratory grinder Peppink 200AN (particle size <1 mm). Special care was taken to clean the grinder after each sample to avoid cross-contamination. The prepared samples were then sent for analysis to the Centre for Isotope Research (CIO, University of Groningen, the Netherlands).

To analyze the maize samples for their ^{14}C content, these have first been combusted to CO_2. For the ^{14}C Accelerator Mass Spectrometer (AMS) analysis only a very small amount (<5 mg) of material is needed. We combusted 2 g of each sample in 2010 and extracted two subsamples to use for the further processing, while in 2011 and 2012 we combusted only 2×4.5 mg of each sample to obtain the two subsamples. This difference was a direct result of

the grinding procedure and the reduced particle size in the sample material in the latter two years, which allowed us to obtain a more representative carbon mixture in a smaller sample before combustion.

In 2010, the samples were combusted using a handmade combustion system at the CIO. This system contains ovens with oxygen supply to combust the material to CO_2 and to oxidize formed CO to CO_2, several water removing cryogenic traps, silver and copper containing ovens and MnO_4-solution to remove sulfur and nitrogen containing components. The samples of 2011 and 2012 have been combusted with an Elemental Analyzer to CO_2 (Aerts-Bijma et al., 2001). Part of the CO_2 has been analyzed for $\delta^{13}C$ with an Isotope Mass Ratio Spectrometer and of the rest, for each obtained CO_2 sample, the two subsamples were graphitized to pure graphite (Aerts-Bijma et al., 1997, 2001). This graphite has been pressed into a target, on which we measured the carbon isotopes ^{12}C, ^{13}C and ^{14}C using the ^{14}C-dedicated AMS at the CIO (van der Plicht et al., 2000). Both subsamples have been measured in the same AMS batch. Generally, an AMS batch has been measured twice, giving four ^{14}C measurement results for each maize sample. The AMS results were corrected for influences due to the preparation procedure using the results of AMS measurements of graphitized ^{14}C-free CO_2 (Rommenhöller gas) sample or combusted anthracite. We should note that this is a minor correction for modern samples such as the investigated in this study.

In Table A1 we show the averaged results for each location and individual sampled plant. We report the $^{14}CO_2$ content of the sample relative to the Modern Standard as $\Delta^{14}CO_2$ [‰] following the conventions in the field for atmospheric CO_2 samples (Stuiver and Polach, 1977; Mook and van der Plicht, 1999). The number of analyses used for the reported average $\Delta^{14}CO_2$ results might differ in case there was problem with the AMS measurement or additional analyses were performed. More detailed information can be found in the supplementary material (Table S2 - ^{14}C analysis information).

5.2.2 Modeling study

In our modeling study we use an atmospheric model to simulate the transport and mixing of CO_2 and $^{14}CO_2$ emissions and weather conditions for six-month periods spanning from April to September in 2010, 2011 and 2012 at an hourly time resolution. We use the daily weather information from the model and the sowing dates from the farmers as an input for a crop growth model, which provide us with the crop growth pattern for each location. We use the concentrations of the transported CO_2 and $^{14}CO_2$ to estimate the $\Delta^{14}CO_2$ of the atmosphere, while we use the modeled crop growth pattern to estimate the $\Delta^{14}CO_2$ signature that would have integrated in the different parts of the crop between the start of the growing period and the sampling date. For the simulation of weather conditions and atmospheric transport of tracers we use the Weather Research and Forecast model (WRF-Chem version 3.2.1). The

specific plant growth at each sampled location has been simulated using the Simple Universal CROp Simulator (SUCROS 2). The modeling framework used here has been introduced previously in Bozhinova et al. (2014). In this section we will elaborate in more detail on the innovations to the model and the additional data we use for this newly simulated time period.

In the general setup of the model, there are changes to the size of the model domains. Our outer domain (121x116 grid points at 36 km horizontal resolution) now covers Europe and the surroundings of the Black Sea, while our second domain (199x193 at 12 km) spans western and central Europe. In this study, however, we will show results only from the two domains with the highest horizontal resolution (4 km) that include the sampling sites covered in our campaigns in the Netherlands and western Germany and in 2012 also between Normandy and Paris (outlined with green and magenta in Figure 5.2).

The fossil fuel CO_2 emissions used in the model are based on the 2005 emission map provided at 5 (geographical) minutes horizontal resolution, developed by IER. A more elaborate description of the emissions sectoral, spatial and temporal disaggregation is provided in Vogel et al. (2013b). For the years simulated in this study we have scaled the emissions from 2005 to 2010, 2011 and 2012 using the national and sectoral annual emission totals reported in the United Nations Framework Convention on Climate Change (UNFCCC). The emissions are vertically disaggregated and prescribed to the corresponding vertical layer in our WRF framework based on the average emission height for each model grid and emission sector as provided by IER.

The $^{14}CO_2$ emissions originating from the nuclear power production are estimated from the International Atomic Energy Agency Power Reactor Information System (IAEA PRIS, available online at http://www.iaea.org/pris) by applying the method described in Graven and Gruber (2011) for the years of our study. The emissions for the one active Spent Fuel Reprocessing Plant in La Hague, France, are based on the values officially reported by the company operating the site for the monthly gaseous releases (AREVA, www.areva.com). All nuclear $^{14}CO_2$ emissions are also prescribed at the vertical level in WRF that corresponds to the height of the emission stacks, where such information was available. In the cases where the emissions occur at surface level, these are introduced in the model in the lowest vertical layer.

We have included several terms from the $^{14}CO_2$ budget in this study that we previously neglected: the biospheric and ocean disequilibrium and ^{14}C production by cosmic radiation. The disequilibrium fluxes result from older carbon dioxide that was taken up by the biosphere or ocean and re-enters the atmosphere through plant respiration or ocean-atmosphere exchange. The monthly $^{14}CO_2$ fluxes for 2010 were taken from the study of Miller et al. (2012), and were interpolated to our finer model grid. The peak of cosmogenic production is usually located in the upper troposphere and stratosphere. Since most of this production lies above the top of our model domain (50 hPa), we also included a secondary tracer to eval-
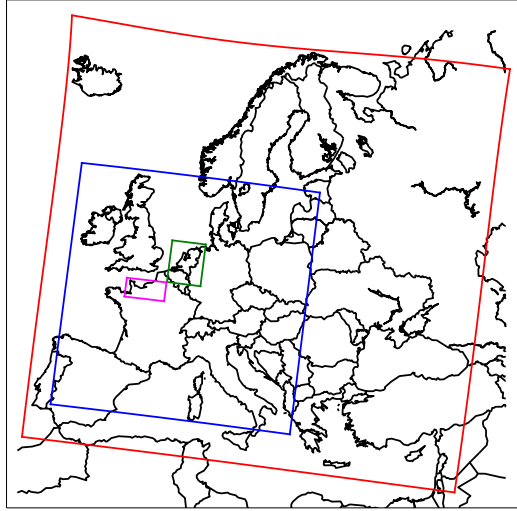
Figure 5.2: The four model domains used in WRF-Chem. Red indicates the outer borders of our simulation (36 km×36 km), while green and magenta indicate the borders of the domains used for our sample results (4 km×4 km).

uate the production if it was distributed linearly with height and pressure. The cosmogenic production is inversely proportional to the solar activity and as such is going to change periodically. In 2010, however, the solar activity was at its minimum in the 11-year solar cycle and the cosmogenic production was at its maximum. Our flux data was available only for the year 2010 and we have used it also for the following years, keeping in mind that the actual cosmogenic production following 2010 is likely smaller than what we have modeled. We use the 2010 fluxes for all three years also for the ocean disequilibrium flux. The biospheric disequilibrium flux, however, we scale with the instantaneous temperature, which will result in this flux scaling with the ecosystem respiration in each separate year just as the biospheric respiration flux (Bozhinova et al., 2014). We evaluate the importance of these additional terms later in our discussion. With these changes, the regional CO_2 budget is now described as:

$$CO_{2obs} = CO_{2bg} + CO_{2ff} + CO_{2p} + CO_{2r} \qquad (5.1)$$

Here the CO_2 concentrations (in ppm) of different origin are indicated with subscript as follow: fossil fuels (ff), biospheric photosynthesis (p), biospheric respiration (r), background (bg), and the total observed at the location (obs). For our domain, the background

Table 5.1: Information on the separate tracers used in this study

Tracer type	Term or Code	Data Source	Description
Background	CO_{2bg}	CarbonTracker	Background CO_2
Biosphere	CO_{2r}	SiBCASA	Ecosystem respiration of CO_2
Biosphere	CO_{2p}	SiBCASA	Photosynthetic uptake of CO_2
Biosphere	$^{14}CO_{2bio}^{dis}$	Miller et al. (2012)	Biospheric disequilibrium of $^{14}CO_2$
Ocean	$^{14}CO_{2o}^{dis}$	Miller et al. (2012)	Oceanic disequilibrium of $^{14}CO_2$
Cosmogenic	$^{14}CO_{2c}$	Miller et al. (2012)	Cosmogenic production of $^{14}CO_2$
Fossil fuels	CO_{2ff}, SNAP 1	IER	Energy production sector.
Fossil fuels	CO_{2ff}, SNAP 2	IER	Non-industrial combustion.
Fossil fuels	CO_{2ff}, SNAP 3	IER	Combustion in manufacturing.
Fossil fuels	CO_{2ff}, SNAP 4	IER	Production processes.
Fossil fuels	CO_{2ff}, SNAP 7	IER	Road transportation.
Fossil fuels	CO_{2ff}, rest	IER	Rest of the fossil fuel emissions.
Nuclear	$^{14}CO_{2n}$, SFR	AREVA	Spent-fuel reprocessing emissions.
Nuclear	$^{14}CO_{2n}$, PWR	IAEA	Pressurized water reactors.
Nuclear	$^{14}CO_{2n}$, BWR	IAEA	Boiling water reactors.
Nuclear	$^{14}CO_{2n}$, AGR	IAEA	Advanced gas-cooled reactors.
Nuclear	$^{14}CO_{2n}$, MAG	IAEA	Magnox reactors.
Nuclear	$^{14}CO_{2n}$, LWG	IAEA	Light-water-cooled reactors.
Nuclear	$^{14}CO_{2n}$, rest	IAEA	Other nuclear reactors emissions.

term (CO_{2bg}) is considered to include the changes in total CO_2 due to forest fires, ocean gas exchange and stratospheric intrusions, which are not explicitly resolved in our modeling framework. Some of the latter contribute to the change in the atmospheric $\Delta^{14}CO_2$ and these we express by their $^{14}CO_2$-only fluxes, as follows:

$$
\begin{aligned}
\Delta_{obs}CO_{2obs} &= \Delta_{bg}(CO_{2bg} + CO_{2p} + CO_{2r}) + \Delta_{ff}CO_{2ff} + \\
&+ \quad ^{14}\Delta(^{14}CO_{2bio}^{dis} + {}^{14}CO_{2o}^{dis} + {}^{14}CO_{2n} + {}^{14}CO_{2c})
\end{aligned}
\tag{5.2}
$$

In this equation, the Δ symbol indicates the $\Delta^{14}CO_2$ signature (in ‰) of CO_2 concentrations of different origin. In addition to the sources described before, the $^{14}CO_2$ concentrations due to biospheric and ocean disequilibrium, nuclear and cosmogenic origin are indicated by the symbols $_{bio}^{dis}$, $_o^{dis}$, $_n$ and $_c$, respectively. The $^{14}\Delta$ stands for the Δ signature of a pure $^{14}CO_2$ flux and Δ_{ff} = -1000 ‰ as fossil fuel is entirely devoid of $^{14}CO_2$. For our domain, we use Δ_{bg} time series from the monthly observed $\Delta^{14}CO_2$ at the high alpine station Jungfraujoch (3580 m. asl., Switzerland, data for the period courtesy to I. Levin and S. Hammer, University of Heidelberg). The importance of this choice and arguments behind it are elaborated later in our results and general discussion.

It is important to note that the term "background" here represents the general atmospheric CO_2 levels at the start of the simulation. They change over time due to long-range transport, as modeled with CarbonTracker Europe inverse modeling system, and stay close to the ob-

served values at background sites for these years (Peters et al., 2010). Thus, CO_{2bg} is the only tracer with initial and boundary conditions. All other tracers are prescribed with emissions only and they represent the quantities recently added to the atmosphere within our domain, where recently refers to the period since the start of our simulations. We use separate tracers for the different anthropogenic emission categories and nuclear reactor types in order to distinguish their influence in our samples. All tracers used in this study are listed in Table 5.1.

5.3   Results

Our ^{14}C analysis of the plants from 79 locations sampled over three years reveal sometimes strong gradients from one sampling location to the next. Table A1 summarizes the ^{14}C analysis results for the individual plants and locations. In 2012, the statistics on the repeated analyses for many samples reduce the estimated error on the mean down to ~1.4‰. However, systematic errors during the measurement procedure cannot be eliminated with averaging over multiple analyses, and a more realistic lower limit for the measurement uncertainty on our samples is ~1.8‰(H. A. J. Meijer, personal correspondence). With that measurement uncertainty our 2010 samples from the northern regions of the Netherlands do not contain interpretable gradients from location-to-location. Similarly, the large $\Delta^{14}CO_2$ difference found between the three samples taken at the same location (#9.1, 9.2 and 9.3) are still consistent with random errors in our method. To see whether gradients in sample means from other locations are consistent with the expected fossil fuel and nuclear gradients, we next analyze the means of sampled plants spatially.

The view over the full spatial domain shows that our measurements can be used to identify urbanized or industrialized areas by their considerably depleted $\Delta^{14}CO_2$ signature, or areas where nuclear $^{14}CO_2$ is significantly enriching the atmosphere. The clear separation between samples from different regions is visualized in Figure 5.3, where we note the different color scales on the different maps and different years. Our study is amongst the first to characterize the atmospheric $\Delta^{14}CO_2$ through annual plants in Europe at this scale, and our results show expected patterns between background and polluted areas similar to ones observed by Palstra et al. (2008) in wine-ethanol, or by Riley et al. (2008) for California, or across the USA (Hsueh et al., 2007). To better compare the observed large-scale gradients we next group the samples from the Netherlands into four distinct regions, namely North, Central, South and Randstad (previously indicated in Figure 5.1), and additionally group the samples from Germany and France.

We find differences between the sampled regions that are consistent between the years. Figure 5.4 shows these regional gradients on top of the continuing depletion of atmospheric $\Delta^{14}CO_2$ of approximately –5‰/year. This is best seen in our plant samples for the three
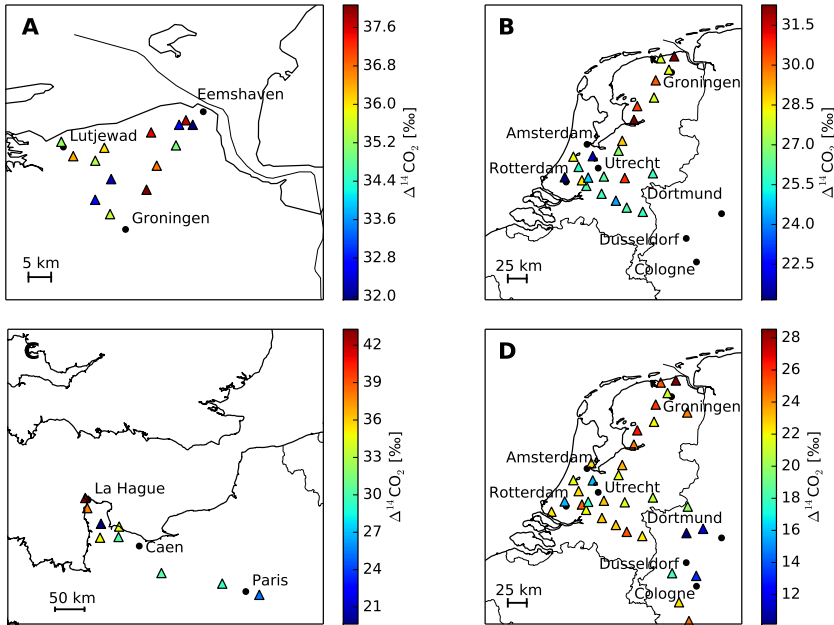
Figure 5.3: Sampling locations and ^{14}C analysis results for the 79 maize leaf samples gathered in (A) 2010, (B) 2011, (C and D) 2012. Plant samples gathered in urbanized and highly industrialized areas in the Netherlands, Germany and France stand out with more depleted $\Delta^{14}CO_2$, while the ones gathered near La Hague show enrichment due to nuclear $^{14}CO_2$ influence. Note the different color scales in each plot.

consecutive years for the North region.The samples from 2011 and 2012 demonstrate a gradient from the cleaner (North) to the most polluted (Randstad) region in the Netherlands, and a further depletion towards the German Ruhr-area. Despite the large variability between individual samples this behavior is consistent in the regional means for the two years. The annual downward trend is clearly an important component of an analysis that spans multiple years like ours, even more so because its magnitude is comparable to the largest gradients within the Netherlands. We therefore first evaluate how the plants capture the trend in the background compared to the traditional atmospheric sampling strategy.

Our plant samples from three sites in the North region of the Netherlands show an annual $\Delta^{14}CO_2$ depletion in line with the observed atmospheric $\Delta^{14}CO_2$ depletion at a set of European background sites. This is shown in Figure 5.5 where our plant samples are additionally in very good agreement with the atmospheric observations at Lutjewad in 2011 and 2012. In
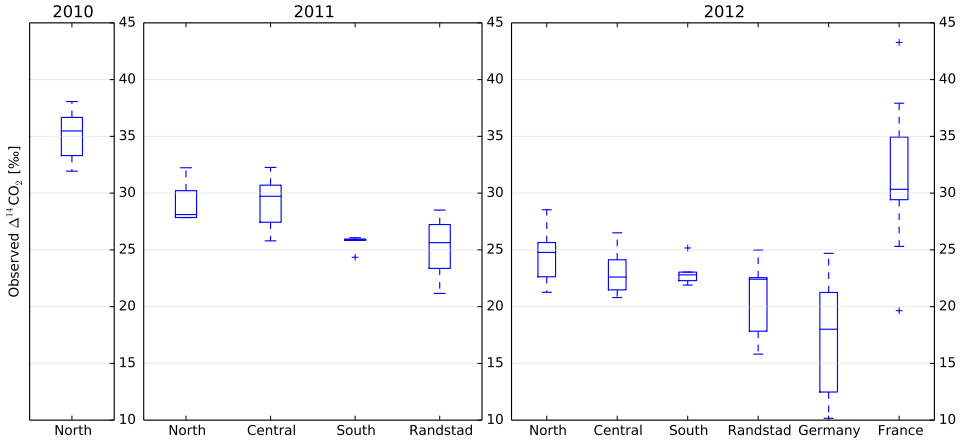
Figure 5.4: Sample results grouped by their respective region in the Netherlands, Germany or France. In regions sampled in consecutive years we can see the downwards trend of the atmospheric $\Delta^{14}CO_2$. The regions with expected cleaner air show consistently higher values than the ones associated with urbanized or industrial pollution. The samples from France are enriched compared to the samples from the Netherlands and Germany, even from previous years. Here the whisker on the boxplot represents the ranges for the bottom 25% and the top 25% of the data values, excluding outliers.

contrast, the year 2010 seems to have had a very high background $\Delta^{14}CO_2$ in the atmospheric records at both Lutjewad and Mace Head compared to our plant samples and to other European sites. These suggest an atmospheric depletion from 2010 to 2011 of more than 14‰ at these locations, which for now remains unexplained. We do note that there is also considerable variation of almost 7‰ in the atmospheric background $\Delta^{14}CO_2$ observations across Europe within each year. This confirms the results of Turnbull et al. (2009b) who noted the importance and difficulty of choosing a $\Delta^{14}CO_2$ background when analyzing regional samples. For our further analysis we nevertheless want to use a background $\Delta^{14}CO_2$, either as the Δ^{14}_{bg} term for our model (see Equation 2), or to subtract from our plant samples to remove the year-to-year depletion and bring out regional patterns across all our samples. We therefore chose to use Jungfraujoch as our background site in this study, because the observed $\Delta^{14}CO_2$ there has a consistent year-to-year depletion of close to 5‰ and fall well within the range of other observations. We will comment more on this choice in our discussion. With the background $\Delta^{14}CO_2$ defined we can proceed to compare our observations to the simulated gradients from our modeling framework.

Our model can generally capture the trend and gradient in the observed $\Delta^{14}CO_2$ be-
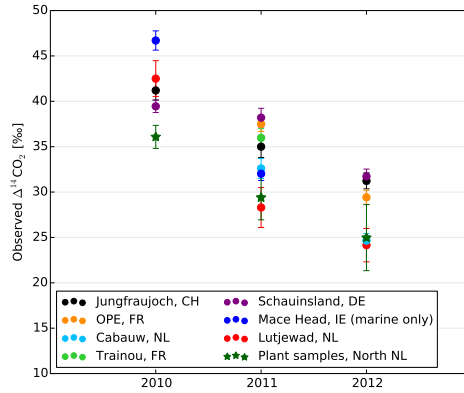
Figure 5.5: Interannual comparison between repeated observations from the north region of the Netherlands and the atmospheric observations at several sites in the region averaged for the period of plant growth. The plant samples show downward trend comparable with European background measurements and especially in 2011 and 2012 very good comparability to the nearest atmospheric observations at Lutjewad. It is important to note the large spread in the different atmospheric observations and also the very variable magnitude of the change that can occur between consecutive years (Mace Head 2010-2011,Schauinsland 2010-2011). The observational data used here is courtesy to CIO, Groningen University (Lutjewad site); I. Levin and S. Hammer, University of Heidelberg (Jungfraujoch, Schauinsland, Mace Head, Cabauw sites); and M. Schmidt, LSCE France (OPE and Trainou sites).

tween years and regions. Most of the model results agree well with the observed values in Figure 5.6, especially when considering the sample uncertainty. In panel A the model-to-observation RMSD is 3.24‰, when we exclude the effect of the 8 largest outliers (the outliers themselves are still shown in the figure). This mismatch becomes smaller when we look at the relative $\Delta^{14}CO_2$ signatures (panel B), where the RMSD is 2.78‰, with the same outlier treatment. In comparison, the combined measurement uncertainty of our plant samples varies from 1.8‰ to 3.0‰ depending on the number of analysis repetitions and limitations due to systematic errors. This shows the ability of our model to simulate the relative plant $\Delta^{14}CO_2$ signatures. The observed gradients in panel A seem to be affected strongly by the annual trend in the background and after removing it most of the observed values in panel B fall in a very narrow range of gradients. We should note again the strong effect the chosen background site could have in panel A for the model-to-observation mismatch, but we will elaborate on this in our discussion. We will focus our further analysis on the relative $\Delta^{14}CO_2$ signatures and take another look at the regional modeled and observed gradients.

Plants can capture large scale gradients, despite that on the smaller scale (<100 km)
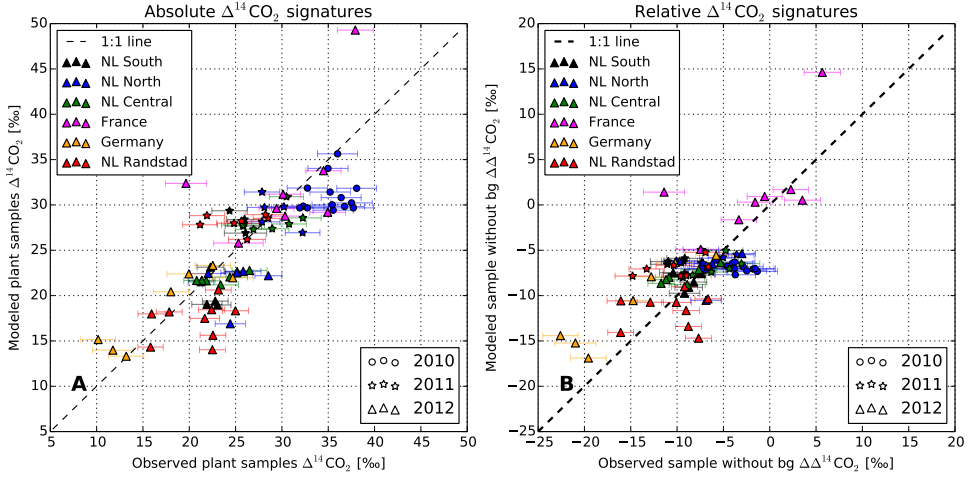
Figure 5.6: Comparison between modeled and observed plant samples for the different years and regions. In panel A) we show the absolute signatures and here the modeled values were obtained by using observed $\Delta^{14}CO_2$ at Jungfraujoch as a background (Δ_{bg}). This is in contrast to panel B) where we show the relative signatures and where the Jungfraujoch Δ_{bg} averaged over the period of plant growth is subtracted from each observed plant samples. In both panels the result for the location of La Hague is outside the scale.
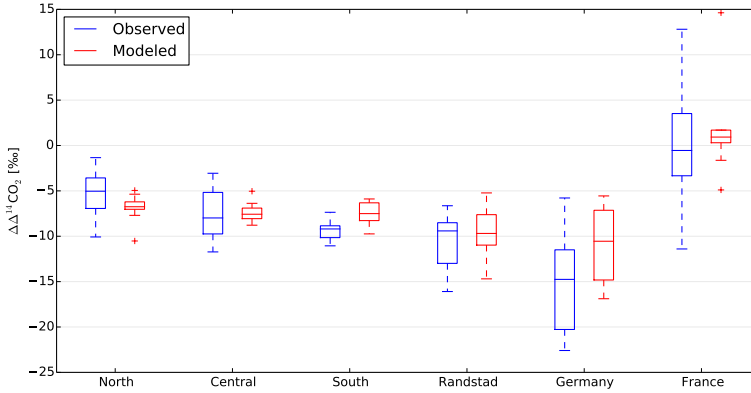
Figure 5.7: $\Delta^{14}CO_2$ signatures relative to the Jungfraujoch Δ_{bg} grouped depending on the region. The variability in observed samples is not always captured by the model even though usually there is agreement between the regional median values. The gradients between different regions are still visible, however, for most of the Netherlands, the relative signatures overlap considerably.

Figure 5.8: Model analysis of the additional enriching or depleting influences for each sampled location and year, where the sum of all contributions indicates the modeled plant samples. The small but consistent nuclear enrichment is found throughout the Netherlands in all years. It's effects are diminished for Germany, but greatly increased for France, where ratio between nuclear to fossil fuel influence is strongly reversed. With the exception of France, the strongest signals are connected with the energy production, followed by road transport.

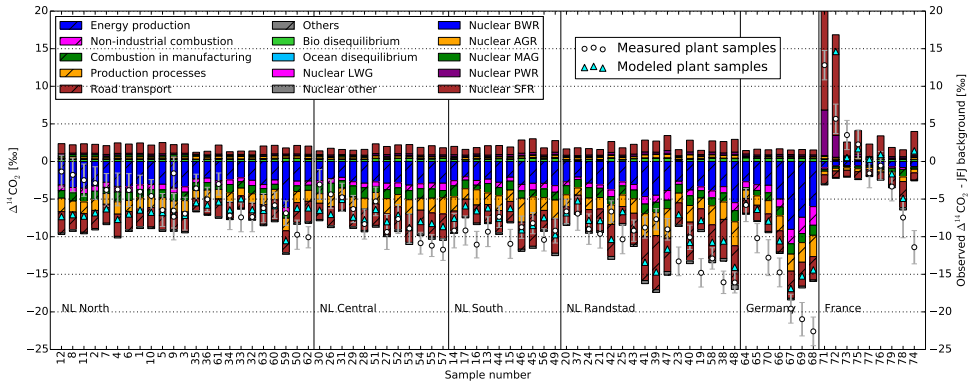distinguishing between noise and signal can be challenging. This is seen in Figure 5.7, where the averages over larger regions are presented. For the North, Central and South regions in the Netherlands, however, model results largely overlap indicating that we should look at the larger scale to find significant gradients. We should note that after the de-trending the modeled variability in most of the regions does not match the observed one, but large part of it could be noise due to random errors in the observations. Since the scatter between the observed samples within a region is considerable, we will examine the modeled results for that scale in more detail later on.

Within the different regions in our study we find better model representation in larger areas. Significant correlations were found within Germany (r=0.94, n=7, p=0.002), France (r=0.70, n=9, p=0.04), and with much smaller, but still significant numbers for the whole Netherlands (r=0.43, n=63, p=0.0004) and the Randstad-Central-North trajectory (r=0.49, n=53, p=0.0002). These results shows that the model captures large scale gradients, but test on the smaller scale did not reveal significant correlations in almost all of the individual regions within the Netherlands. The only exception (the Central region, r=0.81, n=12, p=0.002) can possibly be connected with the magnitude of the gradient, which is larger as this region is situated between the polluted Randstad and cleaner North regions. With this note in mind, we will inspect the individual samples within each region and what is causing the observed and modeled gradients there.

According to our model results, the plant $\Delta^{14}CO_2$ depletion in the Netherlands and Ger-

many is driven mainly by three categories of fossil fuel emissions (energy production, road traffic, and production processes), however, small enrichment from nuclear $^{14}CO_2$ and biospheric disequilibrium is present throughout all samples. Figure 5.8 shows the simulated composition of the $\Delta^{14}CO_2$ signature in maize leaves for each of our samples. Given the size of the gradients within a region it is clear that verifying the emissions from a single fossil fuel category (e.g. road traffic) will not be possible with plant samples. Furthermore, in most of France the enrichment due to nuclear $^{14}CO_2$ (especially from the spent-fuel reprocessing plant in La Hague) is so large that fossil fuel monitoring through $\Delta^{14}CO_2$ in plants will not be feasible. Near Paris (#78) the ratio between nuclear and fossil fuel influences is more favorable for such observations, but it will require careful evaluation of the nuclear $^{14}CO_2$ that is advected to the area.

5.4   Discussion

In this work we included several terms in the simulation of atmospheric $^{14}CO_2$ budget that were identified but not included in our previous study (Bozhinova et al., 2014) and we will first reflect on their possible influence on the plant samples we gathered. Our results show that in our domain the biospheric disequilibrium should be taken into account as its total contribution in our modeled plant samples varied up to 0.5‰ (Figure 5.8), while the influence of the ocean disequilibrium is negligible. These terms were considerably larger in previous decades and will continue to shrink in the future as the atmosphere-biosphere-ocean $\Delta^{14}CO_2$ equilibrates the excess ^{14}C that was produced in the atmosphere during the atmospheric bomb tests in the last century (Levin et al., 2010). The influence of cosmogenic production was at least 1000 times smaller than the biospheric disequilibrium. This was not only because the major part of the stratosphere is above the top of our model since these results were similar for our secondary tracer where the production was distributed linearly with the pressure. This is consistent with the study of Turnbull et al. (2009b), which showed that cosmogenic production has a significant influence only for the $\Delta^{14}CO_2$ observations obtained above 7000 m altitude.

The choice of background site for the atmospheric $\Delta^{14}CO_2$ (Δ_{bg}) plays an important role in the interpretation of our results. In Equations 1 and 2 we describe a framework in which air masses with initial CO_2 content of CO_{2bg} and $\Delta^{14}CO_2$ signature of Δ_{bg} travel through the domain and are influenced by the various local CO_2 and $^{14}CO_2$ sources. For a single instantaneous measurement this would require obtaining Δ_{bg} upwind from the sampling location. However, for integrated air and plant samples the upwind region will vary throughout the sampling period. This is why researchers prefer to use instead "clean air" samples from approximately the same time as Δ_{bg}, preferably from high-altitude sites which would be close

proxies for the free tropospheric air (Turnbull et al., 2009b). As described earlier, we chose to use the monthly mean observations from the site Jungfraujoch as this Δ_{bg} time series, as they were available for all three years of our study, and were most consistent with the observed annual decrease in the plant samples from our "clean" North region in the Netherlands. Choosing a site with a different decline in these three years (for example Schauinsland, where there is very little decline between 2010 and 2011) would cause the model results to get different year-to-year variations than observed in our plant samples. Partly, this is because adding a monthly constant background signature to the high resolution model results (Figure 5.6A) is more likely to incur additional errors than when subtracting a monthly background from the integrated plant samples. This underlies our choice to subtract Δ_{bg} from our observed samples (Figure 5.6B).

In terms of plant growth, size of the region sampled, regional $\Delta^{14}CO_2$ background and the relative importance of the nuclear $^{14}CO_2$ emissions in the region, the samples from France differ most significantly from all other. However, with the exception of the three samples closest to the tip of Normandy (#71, 72, 74) the rest of the observed samples are represented well by the model, as shown in Figure 5.6. From the three anomalous samples, sample #74 is a definite outlier in the observational results (see Figure 5.3C, Figure 5.8), with the lowest signature measured in our campaign in France, which also includes samples from the fossil-fuel polluted vicinity of Paris. We cannot find the reason behind this one measured low value in either the emission maps or regional information, but they were consistent in all the individual target reanalyses for this location. In this case the modeled sample agrees with the other observed samples in the region, while sample #74 is far below it.

The two samples closest to the Spent Fuel Reprocessing Plant (SFRP) in La Hague (#71 and #72) show enrichment in their $\Delta^{14}CO_2$ signature compared to the background of Jungfraujoch in both model and observations. The modeled results overpredict the observations quite considerably in the case of sample #71 (200+‰ modeled vs 43‰ observed, outside the scale in all figures). Our results, however, are not inconsistent with other plant and air measurements from this area. In a study conducted for the period 1997-1999, Fontugne et al. (2004) found similar and even more enriched $\Delta^{14}CO_2$ signatures in furze (flowering plants in the *Fabaceae* family), with large variability between neighboring samples on a spatial resolution of less than a kilometer. This indicates that to resolve the plume close to the source, our model would need a very fine resolution to capture the processes that currently occur at sub-grid scale. The current domain resolution of $4\,km \times 4\,km$ is too coarse to capture the gradients created by the nuclear point source of La Hague's SFRP in the grid cells immediately surrounding it. Furthermore, we should note that in reality the temporal emission pattern from this site is not continuous as implemented in the model, but emissions occur about 10 to 15 times a day with each release lasting for 30 to 40 minutes. Since we compare with observations from plants, which integrate signals over a larger period, this difference

will have relatively small effect, but it will be more important if comparing to observations with higher temporal resolution.

We evaluated the uncertainty in our modeled plant results that is introduced when the modeled plant development differs from the observed. For this purpose we used the additional developmental dates provided by our cooperating farmers (Table S1 - General sample information) to vary the day of emergence and recalculate the plant signature depending on if the flowering date (where available) was modeled well by our plant growth model or not. The resulting spread from the "control" signatures used in the Results section can be considered an evaluation of the plant growth modeling error. The lower and higher estimates exceeded an absolute value of 1‰ for 15 (<20%) of our samples, with only 8 (~10%) of all cases exceeding 2‰. We should note that this is not the total model uncertainty, which in the case of atmospheric transport modeling is more difficult to estimate, but its size is already comparable to the intrinsic measurement uncertainty of our observations.

Our results agree with previous plant sampling studies (Hsueh et al., 2007; Riley et al., 2008; Palstra et al., 2008) that revealed regional fossil fuel emission patterns, and we further develop the model interpretation of the observed plant samples. This new modeling framework, however, is still unable to reproduce the variability in observed $\Delta^{14}CO_2$ in polluted areas with a high spatial resolution, which was also the case in the study by Riley et al. (2008). Plant samples can be useful for the investigation of point sources (Turnbull et al., 2014a), but not all studies yet try to quantify the effect of the variable plant growth and its effect on the $\Delta^{14}CO_2$ signature of the assimilated CO_2. An additional complication when dealing with perennial plants (Park et al., 2013; Sakurai et al., 2013b; Baydoun et al., 2015) could be the re-allocation of carbon assimilated from previous seasons for the initialization and maintenance of the current season growth.

Finally, we address the general use of plant samples of $\Delta^{14}CO_2$ in monitoring strategies of fossil fuel emissions. Without doubt, the information obtained from plant samples is unique and valuable since there is currently no alternative that allows us to easily obtain measurements outside established observational sites. The ease of sampling and ability to quickly gather such information from a large area are considerable strengths of this approach. However, even when plant samples are obtained systematically such that we can account for instance for the effects of the plant growth and development rate, the interpretation of an integrated sample over such a long period introduces additional uncertainty. This is because of our inability to completely reconstruct the sampling kernel in our current crop models, as well as to simultaneously simulate the vertical structure of the atmospheric boundary layer during crop growth. The inherent measurement uncertainty in the ^{14}C analysis further complicates the quantitative analysis and we currently doubt whether regular plant sampling campaigns are a cost effective way to monitor fossil fuel emissions. An improvement in measurement precision to less than 1.0‰ could change this view though.

Other current monitoring strategies hold better promise. For example, combining continuous CO_2 and CO observations with integrated weekly or bi-weekly observations of atmospheric $\Delta^{14}CO_2$ (van der Laan et al., 2010; Vogel et al., 2010, 2013b) allows an estimate of the fossil fuel CO_2 addition on a high temporal resolution. Although this method also has its challenges related to the constancy of emission factors over time and space, the time series generated this way allow a better evaluation of relative emissions strengths and transport patterns across the domain of interest than integrated plant samples. In addition, a range of chemical species measured in flask samples can help identify the influence of some specific anthropogenic sources (Turnbull et al., 2011a; Miller et al., 2012). The combination of these methods, their implementation in existing observational networks and the expansion of the observational network should in our opinion therefore receive higher priority when designing a fossil fuel monitoring methodology. Nevertheless, targeted regional plant sample gathering could provide limited information where other observational infrastructure is not yet available, where typical gradients in atmospheric $\Delta^{14}CO_2$ are not yet known, or where regional gradients are expected to exceed the current measurement precision by a very large margin.

5.5 Conclusions

We have presented three years of plant-sampled $\Delta^{14}CO_2$ observations obtained throughout the Netherlands, Germany and France, which show the distinct influence of fossil fuel CO_2 and nuclear enrichment on the atmospheric $\Delta^{14}CO_2$ on the regional scale. We find measurable differences between various sampled regions, however their true gradients are difficult to evaluate directly due to the large year-to-year draw-down in the average atmospheric $\Delta^{14}CO_2$ and large inherent measurement uncertainty in the observations. The gradients are captured well by plant samples, which agree well with the available European direct atmospheric measurements, even though the observed spread in the latter between stations and between years can be substantial.

Our model results for the simulated plant samples compare well with the observed deviation from the regional background values with RMSD = 2.78‰ when the 8 largest outliers are excluded. This deviation is comparable with the combined measurement uncertainty of the plant samples, which varies from 1.8 to 3.0‰. We found significant correlations in all large (>100 km) regions sampled in our campaigns, which indicates that on this scale our model captures well the observations. On smaller scales the model generally is not able to reproduce the measured variability, with the notable exception of the Central region of the Netherlands (r=0.81). This region is located between the urbanized and industrialized region of Randstad and the much cleaner region in the north of the Netherlands with possibly the largest regional gradients in $\Delta^{14}CO_2$ in the country. In-depth tracer analysis of our modeling

results shows that depletion in our plant $\Delta^{14}CO_2$ samples are driven mainly by emissions by energy production, road traffic and production processes. This largely differs for the samples obtained in France, where nuclear enrichment dominates over the fossil fuel signals. Nevertheless, given the size of the gradients within regions, plant samples cannot be used to target specific emission categories.

5.6   Appendix A

Table A1: The ^{14}C analysis results from each sampling location used in this study. Here $\Delta^{14}C$ is the weighted average and $\pm\Delta^{14}C$ refers to the error on this mean* for each location. Number of analyses refers to the total number of subsamples analyzed and used for these statistics. For the complete results and other metadata from each sampling location, please see the supplementary materials.

* *Sometimes the estimated measurement uncertainty is quite small (<1.8‰), but this does not account for the systematic errors inherent to the measurement equipment and process. As such, 1.8‰ is likely the lower limit of our instrumental precision, regardless of the number of analysed samples. Such cases are marked with * in this table.*

Sample Nr.	Lat	Lon	Sampling Date	Average $\Delta^{14}C[\permil]$	$\pm\Delta^{14}C[\permil]$	Number of Analyses
Netherlands, 2010						
1	53.394	6.360	30-7-2010	35.2	2.2	4
2	53.365	6.399	3-8-2010	36.4	2.2	4
3	53.318	6.523	3-8-2010	32.3	2.2	4
4	53.248	6.517	3-8-2010	35.5	2.2	4
5	53.277	6.469	4-8-2010	32.8	2.2	4
6	53.355	6.471	4-8-2010	35.4	2.2	4
7	53.380	6.502	5-8-2010	36.0	2.2	4
8	53.409	6.657	5-8-2010	37.5	2.2	4
9.1	53.423	6.750	5-8-2010	31.9	3.1	2

Table A1: (continued)

Sample Nr.	Lat	Lon	Sampling Date	$\Delta^{14}C[‰]$	$\pm\Delta^{14}C[‰]$	Number of Analyses
9.2	53.423	6.750	5-8-2010	37.7	2.2	4
9.3	53.423	6.750	5-8-2010	32.7	2.3	4
10	53.382	6.739	5-8-2010	35.0	2.2	4
11	53.343	6.674	5-8-2010	36.8	2.1	4
12	53.295	6.638	5-8-2010	38.1	2.2	4
Netherlands, 2011						
13	51.559	5.965	22-8-2011	25.8	2.0	4
14	51.610	5.660	22-8-2011	26.1	2.3	3
15	51.694	5.453	22-8-2011	24.4	1.9	4
16	51.777	5.180	22-8-2011	25.9	1.7*	5
17	51.872	4.888	30-8-2011	26.0	1.9	4
19	51.973	4.473	23-8-2011	21.2	1.9	4
20	51.938	4.803	23-8-2011	28.5	1.6*	6
21	52.098	4.739	24-8-2011	25.6	1.9	4
23	52.225	5.011	24-8-2011	21.9	1.9	4
24	51.983	5.225	25-8-2011	26.2	2.0	4
25	51.970	4.924	30-8-2011	24.8	1.9	4
26	51.963	5.626	30-8-2011	30.8	1.9	3
27	52.017	6.169	31-8-2011	25.8	2.3	3
28	52.289	5.511	31-8-2011	26.9	2.0	4
29	52.408	5.584	31-8-2011	29.0	1.8	5
30	52.656	5.816	1-9-2011	32.3	2.0	4
31	52.820	5.882	1-9-2011	30.5	1.9	4
32	52.920	6.213	1-9-2011	27.8	2.0	4
33	53.388	6.356	1-9-2011	27.9	1.9	4
34	53.249	6.516	2-9-2011	28.1	1.9	4
35	53.408	6.625	2-9-2011	32.2	1.9	4
36	53.125	6.251	15-9-2011	30.2	1.6*	4
37	52.219	4.637	15-9-2011	28.2	2.2	3
Netherlands, 2012						
38	52.225	5.011	27-8-2012	15.9	1.5*	8
39	52.431	4.984	27-8-2012	22.5	1.4*	8
40	52.228	4.636	27-8-2012	21.7	1.6*	6
41	52.098	4.739	27-8-2012	22.6	1.4*	8
42	51.938	4.803	27-8-2012	25.0	1.4*	8
43	51.983	5.225	27-8-2012	23.1	1.4*	8
44	51.610	5.660	28-8-2012	25.2	1.4*	8
45	51.694	5.453	28-8-2012	22.8	1.4*	8

Table A1: (continued)

Sample Nr.	Lat	Lon	Sampling Date	$\Delta^{14}C[‰]$	$\pm\Delta^{14}C[‰]$	Number of Analyses
46	51.778	5.187	28-8-2012	23.0	1.5*	7
47	51.850	4.220	28-8-2012	22.4	1.4*	8
48	51.974	4.472	28-8-2012	15.8	1.4*	8
49	51.874	4.885	28-8-2012	21.9	1.6*	6
50	52.920	6.213	30-8-2012	22.0	1.9	4
51	52.820	5.883	30-8-2012	26.5	1.9	4
52	52.651	5.813	30-8-2012	24.4	1.9	4
53	52.408	5.584	30-8-2012	23.4	1.9	4
54	52.289	5.511	30-8-2012	21.8	1.4*	8
55	51.963	5.626	6-9-2012	21.4	1.4*	8
56	51.559	5.957	6-9-2012	22.3	1.5*	8
57	52.017	6.169	6-9-2012	20.8	1.4*	8
58	51.970	4.924	10-9-2012	17.8	1.4*	8
59	53.023	6.868	11-9-2012	24.4	1.6*	6
60	53.388	6.356	11-9-2012	25.1	1.7*	5
61	53.409	6.657	11-9-2012	28.5	1.5*	7
62	53.261	6.488	11-9-2012	21.3	1.4*	8
63	53.125	6.251	11-9-2012	25.8	1.9	4
Germany, 2012						
64	50.447	6.806	14-9-2012	24.7	2.2	3
65	50.764	6.631	14-9-2012	22.5	1.9	4
66	51.111	6.512	14-9-2012	18.0	1.9	4
67	51.073	6.967	14-9-2012	13.2	1.9	4
68	51.585	6.800	15-9-2012	10.2	1.9	4
69	51.631	7.120	15-9-2012	11.8	2.2	4
70	51.900	6.836	15-9-2012	20.0	2.4	4
France, 2012						
71	49.680	-1.911	3-9-2012	43.3	1.9	4
72	49.543	-1.803	3-9-2012	37.9	1.9	4
73	49.163	-1.331	3-9-2012	34.9	1.9	4
74	49.367	-1.391	4-9-2012	19.6	2.2	3
75	49.391	-0.949	4-9-2012	34.5	1.9	4
76	49.239	-0.905	4-9-2012	30.1	1.9	4
77	48.864	0.292	4-9-2012	30.3	1.9	4
78	48.848	2.682	5-9-2012	25.3	2.7	2
79	48.902	1.763	5-9-2012	29.4	1.9	4

6
General discussion and outlook

6.1 Introduction

The work within this thesis should be placed in the larger context of the continuous attempts to construct a fossil fuel CO_2 emissions monitoring and verification network. Considering the EU's persistence in the reduction of its emission levels (Friedlingstein et al., 2014), verifying the current fossil fuel CO_2 emissions and identifying the successful emission-reduction policies can be extremely helpful in applying these in other regions of the world. Pacala et al. (2010) also outlined how helpful systematic $\Delta^{14}CO_2$ observations can be to reduce the uncertainty in the regional fossil fuel emissions estimates.

   The goal of this thesis work is to evaluate plant-sampled $\Delta^{14}CO_2$ as a source of quantitative information on the atmospheric fossil fuel CO_2 concentrations and emissions. This research is needed because ^{14}C is one of the most useful tracers that can separate between natural and anthropogenic fluxes of CO_2, but its atmospheric observations are still too few. Plant samples can potentially provide such observations as they integrate the atmospheric $\Delta^{14}CO_2$ in their biomass over the growing season. Hsueh et al. (2007) showed that annual plants are good qualitative indicator of the regional fossil fuel CO_2 concentrations in North America. Nevertheless, plant CO_2 assimilation patterns differ from the usually constant collection rate in traditional integrated samples and these differences should be addressed before any atmospheric model-plant data comparisons can be accurately interpreted.

   We address our first research question (*How accurate can we model the $\Delta^{14}CO_2$ signa-*

ture of an annual crop?) by evaluating how plant growth influences the $\Delta^{14}CO_2$ signature in annual plants in Chapter 3. We found that the $\Delta^{14}CO_2$ signature created with a crop growth model differs measurably (>1‰) from the atmospheric average or from the signature calculated by using environmental proxies for plant growth. This confirms that this effect should be accounted for when plant-sampled $\Delta^{14}CO_2$ is compared to modeled values. A simple approximation for crop growth, such as the GPP estimate used by Riley et al. (2008), will not work for all plant samples, as the phenological development in some species controls the period of growth for the different plant parts. Different periods of sampling the atmospheric $\Delta^{14}CO_2$ creates gradients between the final signatures of samples from different plant parts, and this effect cannot be assessed without using a crop model that simulates both the plant growth, development and carbon allocation.

Plants assimilate atmospheric CO_2 in a fundamentally different way than atmospheric samplers. Correct interpretation will require an additional modeling step, and as such it will incorporate additional uncertainty to the $\Delta^{14}CO_2$ extracted from plant data. The complete uncertainty associated with the calculation of the plant $\Delta^{14}CO_2$ signature is yet to be evaluated, as it depends both on the crop growing pattern and the atmospheric $\Delta^{14}CO_2$ temporal evolution over the simulated location. As we show in Chapter 4, the differences in the atmospheric $\Delta^{14}CO_2$ due to pollutant transport will superimpose on the growth-related gradients between plant parts. The possible covariance between the two effects is likely to be site-specific, for example if the wind direction associated with more beneficial for plant growth weather conditions at specific location is also downwind from an industrialized area with strong fossil fuel CO_2 emissions. Nevertheless, in this thesis we evaluate the size of the separate elements that will contribute to this uncertainty, e.g. the sensitivity of the modeled plant $\Delta^{14}CO_2$ to the input weather, or the sensitivity to the exact shape of the modeled averaging kernel.

In this thesis, we focused on verifying the $\Delta^{14}CO_2$ signals we find in annual plants and the atmosphere on the regional scale. For this purpose, we conducted modeling and experimental studies of the atmospheric $\Delta^{14}CO_2$ signature and the various anthropogenic sources that influence it. Our first two studies (Chapter 3 and Chapter 4) model the weather and transport of tracers for the period between April and September 2008, as this was the closest period for which we had available tracer data to use as initial and boundary conditions. In Chapter 5, we investigate the periods between April and September in 2010, 2011, and 2012, as these periods were the growing seasons for the crop fields from which we collected samples in our regional campaigns. Our study area is positioned in Europe and we chose to use samples of maize leaves, but our methodology can be applied in other regions and for different plant species as well.

In Chapter 4 we evaluate our modeling framework against the available atmospheric observations in order to address our second research question (*What modeling framework is required to simulate the regional $^{14}CO_2$ budget?*). We focused our interest on the European

landscape, as it offers a unique opportunity to verify our observational methods and we could investigate our atmospheric modeling results. The region has a complex structure of its anthropogenic emissions with large heterogeneity in the fossil fuel CO_2 emissions (shown previously in Fig. 1.2 on page 13) and large diversity in the anthropogenic (both fossil fuel and nuclear) emission sources. Still, the bottom-up reported anthropogenic emissions for Europe have relatively small uncertainty and there is a observational network in place to monitor the atmospheric concentrations of CO_2 and other tracer gases. Our results concerning the contribution of the different anthropogenic terms in the atmospheric $\Delta^{14}CO_2$ budget is important in view of the future expansion of the $\Delta^{14}CO_2$ observational network. We find that in large regions within France and Great Britain nuclear $^{14}CO_2$ emissions are of the same or even larger importance for the atmospheric $\Delta^{14}CO_2$ as the fossil fuel CO_2 emissions. Our results are consistent with the previous study by Graven and Gruber (2011) and outline at a finer spatial resolution the areas where the estimation of fossil fuel CO_2 from $\Delta^{14}CO_2$ requires a correction to account for the nuclear influence, similar to the method used in Vogel et al. (2013a).

Our final research question (*Are plant samples a feasible source of new information for the anthropogenic CO_2 emissions on the regional scale?*) we address within Chapter 5 of this thesis with our own plant sampling campaign set up in Western Europe. This study evaluates the skill of our modeling framework to reproduce plant $\Delta^{14}CO_2$ samples in our European domain with its complex anthropogenic emissions. Additional to the analysis of the direct ^{14}C results, we use our $\Delta^{14}CO_2$ modeling framework (Chapter 4) and our method to calculate the plant $\Delta^{14}CO_2$ (Chapter 3) to evaluate the signals recorded in the samples. This important step is necessary to evaluate the information that can be gained from plant samples about the fossil fuel signals in the atmospheric $\Delta^{14}CO_2$.

Our model-plant comparison in Chapter 5 revealed that our modeling framework reproduced with statistically significant correlation the $\Delta^{14}CO_2$ gradients in the larger regions sampled during our campaign. The spread (RMSD) in our modeling results was of similar size to the instrumental precision of the $\Delta^{14}CO_2$ plant samples (overall <2.8‰). This value is equivalent to the change in current atmospheric $\Delta^{14}CO_2$ that can be attributed to ~1.0 ppm of fossil fuel CO_2. Observations of fossil fuel CO_2 with this precision can be an asset in future fossil fuel monitoring strategies, even though some of their limitations, as we will discuss in more details next.

6.2 Fossil fuel monitoring strategy

This thesis shows that plant samples can be used quantitatively to evaluate the atmospheric $\Delta^{14}CO_2$ signatures similarly to an integrated air sample. They have the advantages of growing

in both rural and urban areas and the ability to provide information about the spatial gradients between atmospheric observational sites. Here, the ^{14}C measurement precision and the gradient in the atmospheric $\Delta^{14}CO_2$ are the factors that limit the spatial resolution at which our modeling framework can provide interpretation for the signals found in plant samples. We found that in most of our small (<100km) sampled regions the model could not reproduce the gradient observed in the plant samples. The only exception was a region between the rural north and the urbanized south of the Netherlands, where the atmospheric $\Delta^{14}CO_2$ gradient is the largest over the country. In comparison, our framework was able to produce good correlation between modeled and observed samples in all large (>100km) regions in Chapter 5.

The presence of $^{14}CO_2$ emissions from the nuclear industry affects the fossil fuel CO_2 recalculation from both atmospheric and plant $\Delta^{14}CO_2$ observations. In our Chapter 4 we evaluate the magnitude of its influence and similarly to the study for Europe by Graven and Gruber (2011) and for Canada by Vogel et al. (2013a) we find that without correction for its enriching effect fossil fuel CO_2 estimated from atmospheric $\Delta^{14}CO_2$ would be severely underestimated. This is particularly important for Western France and Great Britain, where the strongest sources of nuclear $^{14}CO_2$ emissions in our domain are located.

Nuclear production of $^{14}CO_2$ has relatively unknown temporal patterns and variable emission rates, but well-know emission locations. Usually each site has an individual and dedicated environmental monitoring program that collects $^{14}CO_2$ observations from the biosphere to assess radiation exposure. Using a modeling framework like ours it could be possible to interpret such observational record and constrain the uncertainties connected with the nuclear emissions. It is quite remarkable that in the interpretation of our plant samples (Chapter 5) our model and observations capture the very different character of the atmospheric $\Delta^{14}CO_2$ signatures over France, and over the Netherlands and Germany. Considering that in France the energy production relies far less on fossil fuels and on close to 75% of nuclear power, we showed that this difference can be captured in studies of the atmospheric transport.

Plant samples integrate over longer periods and as such their temporal resolution is coarse even compared to atmospheric $\Delta^{14}CO_2$ samples that integrate the atmospheric signals over weekly or bi-weekly periods. Nevertheless, they can be a valuable addition to a setup that investigates the emissions of a single source (Turnbull et al., 2014a) as plant samples are easy to obtain down-wind and/or up-wind as long as you have the appropriate meteorological observations for the past period.

Recently, atmospheric $\Delta^{14}CO_2$ samples have been used to also identify the biogenic fraction of industrial CO_2 emissions (Palstra and Meijer, 2014). The so-called biofuel and biogas differ in their impact on the atmospheric $\Delta^{14}CO_2$ from fossil fuel and natural gas emissions. The biogenic fuels and gas will be produced from carbon that has been more recently in the atmosphere, and as such their $\Delta^{14}CO_2$ signature does not differ as much as the signature of

the very old fossil fuels. However, it is likely that they will still be considered anthropogenic CO_2 emissions in the country reported inventories. As the use of these fuels has been increasing in the past decade, $\Delta^{14}CO_2$ and $^{13}CO_2$ observations could provide additional constraint on their estimated fraction from the total anthropogenic CO_2 emissions.

Fossil fuel monitoring is already well developed in North America through organized observational networks of measurements of CO_2 concentration and fluxes from dedicated observational sites, tall towers and aircraft measurements. The largest networks are operated by Environment Canada and the Earth System Research Laboratory (NOAA), but other laboratories also run small networks of multiple observational sites. In Europe, the Integrated Carbon Observation System (ICOS) infrastructure is setting up a dense network of atmospheric and flux measurements with an initial configuration of 23 observational sites and plans for further expansion (Kadygrov et al., 2015). In such networks, observations of atmospheric CO_2 and $\Delta^{14}CO_2$ alone or combined with CO observations with a higher temporal resolution (among others van der Laan et al., 2010; Vogel et al., 2010; Turnbull et al., 2011a) can provide the information required to identify fossil fuel CO_2 on the regional scale or even to attribute the different fossil fuel sources in the emissions of an urban area (Turnbull et al., 2014b). Currently, this is likely the most promising method that provides both accuracy and high temporal resolution of the fossil fuel CO_2 estimates. In Chapter 5 we conclude that plant samples are unlikely to be able to compete with this method and stand alone as a source of systematic $\Delta^{14}CO_2$ observations. Their strengths, however can still be used through organized intensive sampling campaigns to complement more accurate observational techniques by providing additional spatial information, or to provide observational data in remote regions that lack observational infrastructure.

6.3 Plant sampling methods

In this thesis we explore the observational challenges connected with using plants as samplers for atmospheric $\Delta^{14}CO_2$. Plant samples have multiple advantages connected with the ease of sample collection and their spatial availability in most places on the planet. Their disadvantages lie in the interpretation of the $\Delta^{14}CO_2$ signature of the samples, as they assimilate CO_2 differently from continuous atmospheric samplers, which collect at a constant rate. In Chapter 3, we show that these differences can be substantial and a bias will be introduced in the estimation of the atmospheric $\Delta^{14}CO_2$ unless the crop growth is accounted for.

During the planning of a plant sampling campaign, practical concerns arise about the species and plant parts that will be sampled. The plant phenology plays a key role as the various plant parts accumulate biomass sometimes during very different periods, and in many plant species part of the assimilated carbohydrates are stored as reserves in one organ to be

used later for the growth of another. Unless this process can be accounted for and sufficiently verified, the interpretation of $\Delta^{14}CO_2$ signature from such plant organs will carry a larger uncertainty which varies largely between plant species. For the annual crops used in this thesis (maize and wheat) at harvest up to 15% of dry mass accumulated in the storage organs was from reallocated starch reserves, as discussed in Chapter 3. The effect of translocation on the sampled $\Delta^{14}CO_2$ signature can be more significant in perennial crops and trees, where the reallocated carbon will have the signature of earlier years. Consequently, the difference with the current atmosphere can be significant due to the large annual draw-down of the atmospheric $\Delta^{14}CO_2$.

Sampling campaigns that obtain observations of $\Delta^{14}CO_2$ from plant material have been used to evaluate the fossil fuel CO_2 distribution and transport in North America (Hsueh et al., 2007; Riley et al., 2008; Pataki et al., 2010), Western Europe (Palstra et al., 2008; Capano et al., 2013; Sakurai et al., 2013a), Lebanon (Baydoun et al., 2015), Korea (Park et al., 2013), Japan and Bolivia (Sakurai et al., 2013b), Mexico (Beramendi-Orosco et al., 2013), and many other places. There are more studies, which use plant samples but investigate purely the enrichment effects due to nuclear $^{14}CO_2$ emissions (Šturm et al., 2012; Wang et al., 2012, 2013). Even though most studies mention that plant observations are representative of only small time period, the majority of these do not attempt to combine the information of the plant growth and the observed $\Delta^{14}CO_2$ and derive their results through a simple calculation (similar to Eq. 1.6 on page 17). With our analysis framework it will be possible to use these previously obtained plant samples around the world to revisit their $\Delta^{14}CO_2$ results as part of a larger network.

There are already plant models that aim to simulate directly the ^{14}C cycle within the plant. We found that the models used by Aulagnier et al. (2012) have too simple carbon allocation and they use only few compartments to represent different type of plant biomass. As a result, they will not be able to represent correctly the signature of a sample from, for example, only leaves, and comparison to actual plant samples will become impractical as it will require a representative carbon sample from an entire plant biomass. Our SUCROS results in Chapter 3 for the different growing periods of leaves and stem in maize, show that it was important to represent these two plant organs with separate compartments. Still, such models offer the possibility of implementing carbon isotopic cycles directly in the plant/biospheric model as part of a larger modeling framework as for example, the implementation of the stable isotopes ($^{12,13}C$) in the SiBCASA biospheric model presented by van der Velde et al. (2014b).

There are some obvious limitations to the use of plant samples as observations of the atmosphere. For example, they account only for the daytime atmospheric $\Delta^{14}CO_2$ signature, and most species have a single growing season within a year. Usually this period will coincide with the summer season, when the fossil fuel emissions could be less intense (as shown previously on Fig. 2.2 on page 35) and are distributed over a deeper atmospheric boundary

layer. A sampling strategy that involves crops with successive growing periods could be used to obtain observations over a longer time period during the year. If the carbon relocation in perennial plants can be modeled sufficiently accurate , dendrochronological samples from trees that provide information over multiple years (Beramendi-Orosco et al., 2013; Park et al., 2013; Capano et al., 2013) can be properly interpreted and included in modeling comparisons.

In this thesis, we used a relatively simple crop growth model to simulate annual crops and used information supplied by the farmers to constrain the phenology of our simulations (Chapter 5). The model-to-data mismatch was of the same magnitude as the measurement precision of the observed plant samples (~2.8‰). As such it becomes difficult to further evaluate the skill of our model, as we are within the "noise" range of the plant measurements. Our method of constructing averaging kernels could be applied to even more complex model representations that are already available and aim at forecasting the crop yield and growing season, for example the MARS Crop Yield Forecasting System for Europe (Institute for Environment and Sustainability, Joint Research Center) in Europe. This system employs the WOFOST crop model, which is from the same family of models as SUCROS, but this more advanced model uses crop and soil management information and includes the effects of nutrient-limited conditions on the plant growth. Further on, we believe farmer information about the observed plant phenological development, as the one we used in our study, could be used more often to constrain the plant development, growth and yield.

6.4 Atmospheric transport modeling

The atmospheric modeling framework, which we presented in Chapter 4 and later upgraded in Chapter 5, covers an extensive part of the CO_2 and $^{14}CO_2$ regional cycle. We have verified it against available CO_2 and $\Delta^{14}CO_2$ observations and we use it to evaluate the contribution of different terms from the $\Delta^{14}CO_2$ budget for the final signatures observed over Europe. We found that many of the extra terms added to the system in Chapter 5 provided negligible contributions for the regional $\Delta^{14}CO_2$ budget, as previously evaluated in Chapter 4. Still, in other regions these terms may be of larger importance.

A similar small term, which is not considered in our current framework is the accumulation of the atmospheric $\Delta^{14}CO_2$ signature in the biospheric carbon pool of our WRF-Chem model. In our atmospheric model the biospheric uptake and respiration fluxes are assumed to have the signature of the background air (Δ_{bg}), with the exception of the disequilibrium influence on the respiration term. In contrast, in the work of Riley et al. (2008), the plants assimilate carbon with the signature of the current atmosphere (Δ_{air} in Eq. 2.1 on page 40), thus allowing short-term changes in the atmospheric $\Delta^{14}CO_2$ to affect the biosphere in WRF-Chem. A $\Delta^{14}CO_2$ biospheric storage like this will reflect that the local biosphere fluxes with

the atmosphere have the signature of the atmospheric $\Delta^{14}CO_2$ most commonly observed at the location, and will be equivalent to a spatially-explicit short-term disequilibrium flux. We should stress, that this accumulation of $\Delta^{14}CO_2$ in the biosphere as represented in our atmospheric transport model is entirely separate from SUCROS-based offline calculation of the $\Delta^{14}CO_2$ accumulation in particular crop.

In Chapter 5 we discussed the representation of emission plumes in our mesoscale model. This issue is of particular importance when one attempts to compare observations to model results for a location that in real world is exposed to a large point source. In our model, such sources are recalculated as area sources of a single grid box and this will bias a model-data comparison for these observing locations. A higher horizontal resolution will likely solve the severity of the problem, but eventually it comes down to resolving the actual plume rather than degrading the emissions to the model grid in mesoscale models. Still, we require a mesoscale model to adequately forecast the weather during the plant growing season. In Chapter 3 we found that the weather of a particular growing season was one of the most important factors determining the $\Delta^{14}CO_2$ signals that accumulate in plant biomass.

For our fossil fuel-based emissions, effective heights are included in the IER data. These height estimates are based on the stack height, average flue gas temperature, flue gas flow rate and velocity (Pregger et al., 2007; Pregger and Friedrich, 2009). An improvement in the emissions from nuclear-based sources would include the effective height of the emissions using that same methodology, rather than only the average height of the emission stacks, as it is in our current framework. Most of the nuclear $^{14}CO_2$ emissions enter the atmosphere with the water vapor released by the cooling towers of the power plant, and as such their effective emission height will be higher, resulting in the $^{14}CO_2$ being mixed vertically and transported further away from the source. For future applications it is recommended to estimate the effective emission heights with a plume model for a selection of atmospheric stability cases and to use the average effective height for each location in our modeling framework. The difference in our results between Chapter 4 (only surface emissions) and Chapter 5 (supplied emission heights) were largest in the lowest 200 m of the atmosphere and as most atmospheric observations are obtained below this height, it is a key point when comparing model and observations. The difference between using the stack height and the effective emission height, however, will likely have more subtle effects on the tracer concentrations as the typical cooling towers in the nuclear industry are already quite tall (>250m).

Finally, it might be useful to include the absolute $^{14}CO_2$ tracer in modeling systems which already include $^{13}CO_2$ and the processes that result in isotopic fractionation (van der Velde et al., 2014b). This would be an alternative for the common methodology used in this thesis to model atmospheric $\Delta^{14}CO_2$. The transport of all C-isotopes and their absolute quantities will allow us to calculate $\Delta^{14}CO_2$ in the system and comparison to observations. The large advantage would be, that such system will become independent from the background

$\Delta^{14}CO_2$ observations and the uncertainties connected with the choice of the regional background site, as we discussed in Chapter 5. A secondary advantage would be that background observations, usually long time-series of $\Delta^{14}CO_2$, will be available to evaluate or constrain the modeled carbon isotopic ratios. However, such a system will require much more additional input information about the initial state and boundary conditions (if it is not a global system) of all carbon isotopes, which is not required with the $\Delta^{14}CO_2$-approach we implemented. Moreover, additional uncertain fractionation processes (e.g. during the diffusive uptake in the stomata) need to be included.

6.5 Future work: Inversions

The work in this thesis describes a sampling strategy for collecting annual plant samples and a modeling framework that aims at reproducing, through "forward" modeling, the $\Delta^{14}CO_2$ signature that was measured. Our immediate motivation is to evaluate the uncertainties connected with the use of plant samples as observations of the atmospheric $\Delta^{14}CO_2$. Beyond the scope of our work lies the future: using $\Delta^{14}CO_2$ observations for the verification of anthropogenic fossil fuel CO_2 emissions.

For example, van der Laan et al. (2010) estimated the regional fossil fuel emissions for the Netherlands using atmospheric observations of CO, $\Delta^{14}CO_2$, and ^{222}Rn. Peylin et al. (2011) recalculated fossil fuel CO_2 from $\Delta^{14}CO_2$ observations and compared it to modeled estimates to evaluate the uncertainties connected with different fossil fuel inventories and atmospheric transport models. A step further would be to use CO_2 and $\Delta^{14}CO_2$ observations in an "inversion" model to independently estimate current anthropogenic CO_2 emission inventories.

Atmospheric CO_2 inversion modeling combines the knowledge about the atmospheric transport and mixing processes (by using a forward atmospheric model) with a prior estimate of the surface fluxes of different sources and sinks of CO_2. The resulting CO_2 fields are sampled at the times and locations of available observations, and then compared to the observational data. The information about the model-data mismatch can be used to tune multiple scaling factors that control the surface fluxes and the new estimate for the surface emissions is used for the next forward simulation (Peters et al., 2007). After several iterations, the surfaces fluxes are optimized to produce minimum model-observation mismatch.

Current fossil fuel CO_2 inversions are complicated by the incomplete understanding of the natural emissions of CO_2 (Pacala et al., 2010). Most CO_2 inversion models assume that fossil fuel emissions are well-known and that variability in the observed CO_2 mole fractions can be entirely attributed to the uncertain biospheric CO_2 flux. Recently, van der Velde et al. (2014a) showed that including $^{13}CO_2$ observations in CO_2-inversion model provides additional constraints to the system to identify the role of the biospheric fluxes from other

natural sources and sinks. In a similar manner, $^{14}CO_2$ observations would provide means to separate fossil fuel and non-fossil fuel CO_2 contributions.

Using inversion system on the regional scale poses more challenges, but a high-resolution mesoscale model will allow such system to interpret and use more of the available atmospheric observations, which are not used in current global systems (Ahmadov et al., 2009). Our modeling framework, with its CO_2 and $\Delta^{14}CO_2$ information could be part of such inversion system. There are hardly enough observations yet to use as constrains, but while the current $\Delta^{14}CO_2$ observational network is expanding, plant samples could be used to fill the gaps in the current sampling grid. This will lower the uncertainty in flux estimates in regions that have few to none regular atmospheric observations. The work in this thesis outlined and quantified the challenges and uncertainties connected with the quantitative use of $\Delta^{14}CO_2$ observations in both atmosphere and plants.

References

Aerts-Bijma, A. T., Meijer, H. A. J., and van der Plicht, J.: AMS sample handling in Groningen, Nuclear Instruments and Methods in Physics Research Section B: Beam Interactions with Materials and Atoms, 123, 221–225, 1997.

Aerts-Bijma, A. T., van der Plicht, J., and Meijer, H. A. J.: Automatic AMS Sample Combustion And CO_2 Collection, Radiocarbon, 43, 293–298, 2001.

Ahmadov, R., Gerbig, C., Kretschmer, R., Rödenbeck, C., Bousquet, P., and Ramonet, M.: Comparing high resolution WRF-VPRM simulations and two global CO_2 transport models with coastal tower measurements of CO_2, Biogeosciences, 6, 807–817, 2009.

Anderson, E., Libby, W., Weinhouse, S., Reid, A., Kirshenbaum, A., and Grosse, A.: Natural Radiocarbon from Cosmic Radiation, Physical Review, 72, 931–936, 1947.

Andres, R., Boden, T., and Higdon, D.: A new evaluation of the uncertainty associated with CDIAC estimates of fossil fuel carbon dioxide emission, Tellus B, 66, doi:10.3402/tellusb.v66.23616, 2014.

Arora, V. and Gajri, P.: Assessment of a crop growth-water balance model for predicting maize growth and yield in a subtropical environment, Agricultural Water Management, 46, 157–166, 2000.

Aulagnier, C., Dizès, S. L., Maro, D., Hébert, D., Lardy, R., Martin, R., and Gonze, M.-A.: Modelling the transfer of ^{14}C from the atmosphere to grass: A case study in a grass field near AREVA-NC La Hague, Journal of environmental radioactivity, 112, 52–59, 2012.

Baydoun, R., Samad, O. E., Nsouli, B., and Younes, G.: Measurement of Radiocarbon Content in Leaves near a Cement Factory in Mount Lebanon, Radiocarbon, 57, [in press], doi:10.2458/azu_rc.57.18108, 2015.

Beramendi-Orosco, L., Hernandez-Morales, S., Gonzalez-Hernandez, G., Constante-Garcia, V., and Villanueva-Diaz, J.: Dendrochronological Potential of Fraxinus uhdei and

Its Use as Bioindicator of Fossil CO_2 Emissions Deduced from Radiocarbon Concentrations in Tree Rings, Radiocarbon; Vol 55, No 2–3 (2013), 55, 834–840, doi:10.2458/azu_js_rc.55.16240, 2013.

Boden, T. A., Marland, G., and Andres, R. J.: Global, Regional, and National Fossil-Fuel CO_2 Emissions, doi:10.3334/CDIAC/00001_V2010, 2010.

Boons-Prins, E. R., de Koning, G. H. J., van Diepen, C. A., and de Vries, F. W. T. P.: Crop specific simulation parameters for yield forecasting across the European Community, Simulation Reports CABO-TT 32. CABO- DLO, DLO Winand Staring Centre, JRC, Wageningen., 1993.

Bozhinova, D., Combe, M., Palstra, S. W. L., Meijer, H. A. J., Krol, M. C., and Peters, W.: The importance of crop growth modeling to interpret the $\Delta^{14}CO_2$ signature of annual plants, Global Biogeochemical Cycles, 27, 792–803, doi:10.1002/gbc.20065, 2013.

Bozhinova, D., van der Molen, M. K., van der Velde, I. R., Krol, M. C., van der Laan, S., Meijer, H. A. J., and Peters, W.: Simulating the integrated summertime $\Delta^{14}CO_2$ signature from anthropogenic emissions over Western Europe, Atmos. Chem. Phys., 14, 7273–7290, 2014.

Brouwer, R.: Some aspect of the equilibrium between overground and underground plant parts, Jaarb. IBS, Wageningen, pp. 31–39, 1963.

Burchuladze, A., Chudy, M., Eristavi, I., Pagava, S., Povinec, P., Sivo, A., and Togonidze, G.: Anthropogenic ^{14}C variations in atmospheric CO_2 and wines, vol. 31, pp. 771–776, 1989.

Capano, M., Altieri, S., Marzaioli, F., Sirignano, C., Pignatelli, O., Martinelli, N., Passariello, I., Sabbarese, C., Ricci, P., Gigli, S., and Terrasi, F.: Widespread Fossil CO_2 in the Ansanto Valley (Italy): Dendrochronological, ^{14}C, and ^{13}C Analyses on Tree Rings, Radiocarbon, 55, 1114–1122, doi:10.2458/azu_js_rc.55.16237, 2013.

Chen, F. and Dudhia, J.: Coupling an Advanced Land Surface–Hydrology Model with the Penn State–NCAR MM5 Modeling System. Part I: Model Implementation and Sensitivity, Mon. Wea. Rev., 129, 569–585, doi:10.1175/1520-0493(2001)129<0569:CAALSH>2.0.CO;2, 2001.

Ciais, P., Paris, J. D., Marland, G., Peylin, P., Piao, S. L., Levin, I., Pregger, T., Scholz, Y., Friedrich, R., Rivier, L., Houwelling, S., and Schulze, E. D.: The European carbon balance. Part 1: fossil fuel emissions, Global Change Biology, 16, 1395–1408, doi:10.1111/j.1365-2486.2009.02098.x, 2010.

Ciais, P., Dolman, A., Bombelli, A., Duren, R., Peregon, A., Rayner, P., Miller, C., Gobron, N., Kinderman, G., Marland, G., Gruber, N., Chevallier, F., Andres, R., Balsamo, G., Bopp, L., Bréon, F.-M., Broquet, G., Dargaville, R., Battin, T., Borges, A., Bovensmann, H., Buchwitz, M., Butler, J., Canadell, J., Cook, R., DeFries, R., Engelen, R., Gurney, K., Heinze, C., Heimann, M., Held, A., Henry, M., Law, B., Luyssaert, S., Miller, J., Moriyama, T., Moulin, C., Myneni, R., Nussli, C., Obersteiner, M., Ojima, D., Pan, Y., Paris, J.-D., Piao, S., Poulter, B., Plummer, S., Quegan, S., Raymond, P., Reichstein, M., Rivier, L., Sabine, C., Schimel, D., Tarasova, O., Valentini, R., Wang, R., van der Werf, G., Wickland, D., Williams, M., and Zehner, C.: Current systematic carbon-cycle observations and the need for implementing a policy-relevant carbon observing system, Biogeosciences, 11, 3547–3602, 2014.

Combe, M.: Modeling $^{12}CO_2$ and $^{14}CO_2$ fixation in common Dutch crops: the example of spring wheat, Wageningen University, Wageningen, the Netherlands, MSc. thesis, 75p., 2010.

Combe, M., de Arellano, J. V.-G., Ouwersloot, H., Jacobs, C., and Peters, W.: Two perspectives on the coupled carbon, water and energy exchange in the planetary boundary layer, Biogeosciences, 12, 103–123, 2015.

Coniglio, M., Correia, J., Marsh, P., and Kong, F.: Verification of Convection-Allowing WRF Model Forecasts of the Planetary Boundary Layer Using Sounding Observations, Wea. Forecasting, 28, 842–862, doi:doi: 10.1175/WAF-D-12-00103.1, 2013.

de Foy, B., Burton, S., Ferrare, R., Hostetler, C., Hair, J., Wiedinmyer, C., and Molina, L.: Aerosol plume transport and transformation in high spectral resolution lidar measurements and WRF-Flexpart simulations during the MILAGRO Field Campaign, Atmospheric Chemistry and Physics, 11, 3543–3563, 2011.

de Wekker, S. F. J., Steyn, D. G., Fast, J. D., Rotach, M. W., and Zhong, S.: The performance of RAMS in representing the convective boundary layer structure in a very steep valley, Environmental Fluid Mechanics, 5, 35–62, 2005.

Djuricin, S., Pataki, D. E., and Xu, X.: A comparison of tracer methods for quantifying CO_2 sources in an urban region, Journal of Geophysical Research-Atmospheres, 115, D11 303, doi:10.1029/2009JD012236, 2010.

Dudhia, J.: Numerical study of convection observed during the Winter Monsoon Experiment using a mesoscale two-dimensional model, Journal of the Atmospheric Sciences, 46, 3077–3107, 1989.

EEA, 2001: Joint EMEP/CORINAIR Atmospheric Emission Inventory Guidebook, Third edition, Copenhagen: European Environment Agency, available online at http://www.eea.europa.eu/publications/EMEPCORINAIR, 2001.

Ek, M., Mitchell, K., Lin, Y., Rogers, E., Grunmann, P., Koren, V., Gayno, G., and Tarpley, J.: Implementation of NOAH land surface model advances in the National Centers for Environmental Prediction operational mesoscale Eta model, Journal of Geophysical Research-Atmospheres, 108, 8851, doi:10.1029/2002JD003296, 2003.

Fontugne, M., Maro, D., Baron, Y., Hatté, C., Hebert, D., and Douville, E.: ^{14}C sources and distribution in the vicinity of La Hague nuclear reprocessing plant; Part I, Terrestrial environment., Radiocarbon, 46, 2004.

Francey, R. J., Trudinger, C. M., van der Schoot, M., Law, R. M., Krummel, P. B., Langenfelds, R. L., Paul Steele, L., Allison, C. E., Stavert, A. R., Andres, R. J., and Rödenbeck, C.: Atmospheric verification of anthropogenic CO_2 emission trends, Nature Clim. Change, 3, 520–524, doi:http://dx.doi.org/10.1038/nclimate1817, 2013.

Friedlingstein, P., Houghton, R., Marland, G., Hackler, J., Boden, T., Conway, T., Canadell, J., Raupach, M., Ciais, P., and Quéré, C. L.: Update on CO_2 emissions, Nature Geoscience, 3, 811–812, 2010.

Friedlingstein, P., Andrew, R., Rogelj, J., Peters, G., Canadell, J., Knutti, R., Luderer, G., Raupach, M., Schaeffer, M., van Vuuren, D., and Quere, C. L.: Persistent growth of CO_2 emissions and implications for reaching climate targets, Nature Geosci, 7, 709–715, doi:Review, 2014.

Galmarini, S., Bianconi, R., Addis, R., Andronopoulos, S., Astrup, P., Bartzis, J. C., Bellasio, R., Buckley, R., Champion, H., Chino, M., D'Amours, R., Davakis, E., Eleveld, H., Glaab, H., Manning, A., Mikkelsen, T., Pechinger, U., Polreich, E., Prodanova, M., Slaper, H., Syrakov, D., Terada, H., and van der Auwera, L.: Ensemble dispersion forecasting - Part II: Application and evaluation, Atmospheric Environment, 38, 4619–4632, 2004.

Galmarini, S., Kioutsioukis, I., and Solazzo, E.: E pluribus unum: ensemble air quality predictions, Atmospheric Chemistry and Physics Discussions, 13, 581–631, 2013.

Gamnitzer, U., Karstens, U., Kromer, B., Neubert, R. E. M., Meijer, H. A. J., Schroeder, H., and Levin, I.: Carbon monoxide: A quantitative tracer for fossil fuel CO_2?, Journal of Geophysical Research-Atmospheres, 111, D22 302, doi:10.1029/2005JD006966, 2006.

Gerbig, C., Körner, S., and Lin, J. C.: Vertical mixing in atmospheric tracer transport models: error characterization and propagation, Atmos. Chem. Phys., 8, 591–602, 2008.

Godwin, H.: Half-life of radiocarbon, Nature, 195, 984, 1962.

Goudriaan, J.: A simple and fast numerical method for the computation of daily totals of crop photosynthesis, Agr Forest Meteorol, 38, 249–254, 1986.

Goudriaan, J. and van Laar, H.: Modelling potential crop growth processes : textbook with exercises, Kluwer Academic Publishers, Dordrecht, The Netherlands, monograph, 1994.

Goudriaan, J. and van Laar, H. H.: Relations between leaf resistance, CO_2-concentration and CO_2-assimilation in maize, beans, Lalang grass and sunflower, Photosynthetica, 12, 241–249, 1978.

Graven, H. D. and Gruber, N.: Continental-scale enrichment of atmospheric $^{14}CO_2$ from the nuclear power industry: potential impact on the estimation of fossil fuel-derived CO_2, Atmospheric Chemistry and Physics, 11, 12 339–12 349, doi:10.5194/acp-11-12339-2011, 2011.

Graven, H. D., Guilderson, T. P., and Keeling, R. F.: Observations of radiocarbon in CO_2 at La Jolla, California, USA 1992-2007: Analysis of the long-term trend, Journal of Geophysical Research-Atmospheres, 117, D02 302, doi:10.1029/2011JD016533, 2012a.

Graven, H. D., Guilderson, T. P., and Keeling, R. F.: Observations of radiocarbon in CO_2 at seven global sampling sites in the Scripps flask network: Analysis of spatial gradients and seasonal cycles, Journal of Geophysical Research-Atmospheres, 117, D02 303, doi:10.1029/2011JD016535, 2012b.

Grell, G., Peckham, S., Schmitz, R., McKeen, S., Frost, G., Skamarock, W., and Eder, B.: Fully coupled "online" chemistry within the WRF model, Atmospheric Environment, 39, 6957–6975, 2005.

Griffin, K., Anderson, O., Gastrich, M., Lewis, J., Lin, G., Schuster, W., Seemann, J., Tissue, D., Turnbull, M., and Whitehead, D.: Plant growth in elevated CO_2 alters mitochondrial number and chloroplast fine structure, Proceedings of the National Academy of Sciences of the United States of America, 98, 2473–2478, 2000.

Guérif, M. and Duke, C.: Calibration of the SUCROS emergence and early growth module for sugar beet using optical remote sensing data assimilation, European Journal of Agronomy, 9, 127–136, 1998.

Gurney, K., Mendoza, D., Zhou, Y., Fischer, M., Miller, C., Geethakumar, S., and Can, S. D.: High resolution fossil fuel combustion CO_2 emission fluxes for the United States, Environmental Science and Technology, 43, 5535–5541, 2009.

Hariprasad, K., Srinivas, C., Singh, A., Rao, S. V. B., Baskaran, R., and Venkatraman, B.: Numerical simulation and intercomparison of boundary layer structure with different PBL schemes in WRF using experimental observations at a tropical site, Atmospheric Research, 145–146, 27–44, 2014.

Hesshaimer, V.: Tracing the global carbon cycle with bomb radiocarbon, Univ. of Heidelberg, Heidelberg, Germany, URL `http://www.ub.uni-heidelberg.de/archiv/1094`, ph.D. thesis, 1997.

Hong, S.-Y., Noh, Y., and Dudhia, J.: A new vertical diffusion package with an explicit treatment of entrainment processes, Mon Weather Rev, 134, 2318–2341, 2006.

Hsueh, D. Y., Krakauer, N. Y., Randerson, J. T., Xu, X., Trumbore, S. E., and Southon, J. R.: Regional patterns of radiocarbon and fossil fuel-derived CO_2 in surface air across North America, Geophysical Research Letters, 34, L02 816, doi:10.1029/2006GL027032, 2007.

Hu, X.-M., Nielsen-Gammon, J., and Zhang, F.: Evaluation of Three Planetary Boundary Layer Schemes in the WRF Model, J. Appl. Meteor. Climatol., 49, 1831–1844, doi:doi:10.1175/2010JAMC2432.1, 2010.

Hu, X.-M., Klein, P., and Xue, M.: Evaluation of the updated YSU planetary boundary layer scheme within WRF for wind resource and air quality assessments, J. Geophys. Res. Atmos., 118, 10,490–10,505, 2013.

Indermuhle, A., Stocker, T., Joos, F., Fischer, H., Smith, H., Wahlen, M., Deck, B., Mastroianni, D., Tschumi, J., Blunier, T., Meyer, R., and Stauffer, B.: Holocene carbon-cycle dynamics based on CO_2 trapped in ice at Taylor Dome, Antarctica, Nature, 398, 121–126, doi:10.1038/18158, 1999.

IPCC: Climate Change 2013: The Physical Science Basis. Contribution of Working Group I to the Fifth Assessment Report of the Intergovernmental Panel on Climate Change, Cambridge University Press, Cambridge, United Kingdom and New York, NY, USA, doi:10.1017/CBO9781107415324, URL `www.climatechange2013.org`, 2013.

Jacobs, C., van den Hurk, B., and de Bruin, H.: Stomatal behaviour and photosynthetic rate of unstressed grapevines in semi-arid conditions, Agr Forest Meteorol, 80, 111–134, 1996.

Janjić, Z.: The Step-Mountain Eta Coordinate Model: Further Developments of the Convection, Viscous Sublayer, and Turbulence Closure Schemes, Mon. Wea. Rev., 122, 927–945, doi:10.1175/1520-0493(1994)122<0927:TSMECM>2.0.CO;2, 1994.

Kadygrov, N., Broquet, G., Chevallier, F., Rivier, L., Gerbig, C., and Ciais, P.: On the potential of ICOS atmospheric CO_2 measurement network for the estimation of the biogenic CO_2 budget of Europe, Atmos. Chem. Phys. Discuss., 15, 14 221–14 273, 2015.

Kalnay, E., Kanamitsu, M., Kistler, R., Collins, W., Deaven, D., Gandin, L., Iredell, M., Saha, S., White, G., and Woollen, J.: The NCEP/NCAR 40-year reanalysis project, Bulletin of the American Meteorological Society, 77, 437–471, 1996.

Keeling, C. D.: Atmospheric carbon-dioxide in 19th-century, Science, 202, 1109–1109, 1978.

Keeling, C. D., Whorf, T. P., Wahlen, M., and van der Plicht, J.: Interannual extremes in the rate of rise of atmospheric carbon dioxide since 1980, Nature, 375, 666–670, 1995.

Kleczek, M. A., Steeneveld, G.-J., and Holtslag, A. A. M.: Evaluation of the Weather Research and Forecasting Mesoscale Model for GABLS3: Impact of Boundary-Layer Schemes, Boundary Conditions and Spin-Up, 152, 213–243, 2014.

Koffi, E., Rayner, P., Scholze, M., Chevallier, F., and Kaminski, T.: Quantifying the constraint of biospheric process parameters by CO_2 concentration and flux measurement networks through a carbon cycle data assimilation system, Atmospheric Chemistry and Physics Discussions, 12, 24 131–24 172, 2012.

Kooistra, L., Bergsma, A., Chuma, B., and de Bruin, S.: Development of a dynamic web mapping service for vegetation productivity using earth observation and in situ sensors in a sensor web based approach, Sensors, 9, 2371–2388, doi:10.3390/s90402371, 2009.

Kuc, T., Rozanski, K., Zimnoch, M., Necki, J., and Korus, A.: Anthropogenic emissions of CO_2 and CH_4 in an urban environment, Applied Energy, 75, 193–203, 2003.

Lee, S.-H., Kim, S.-W., Trainer, M., Frost, G. J., Mckeen, S. A., Cooper, O. R., Flocke, F., Holloway, J. S., Neuman, J. A., Ryerson, T., Senff, C. J., Swanson, A. L., and Thompson, A. M.: Modeling ozone plumes observed downwind of New York City over the North Atlantic Ocean during the ICARTT field campaign, Atmospheric Chemistry and Physics, 11, 7375–7397, doi:10.5194/acp-11-7375-2011, 2011.

LeQuere, C., Roedenbeck, C., Buitenhuis, E. T., Conway, T. J., Langenfelds, R., Gomez, A., Labuschagne, C., Ramonet, M., Nakazawa, T., Metzl, N., Gillett, N., and Heimann, M.: Saturation of the Southern Ocean CO_2 sink due to recent climate change, Science, 316, 1735–1738, doi:10.1126/science.1136188, 2007.

Levin, I. and Hesshaimer, V.: Radiocarbon-a unique tracer of global carbon cycle dynamics, Radiocarbon, 42, 69–80, 2000.

Levin, I. and Karstens, U.: Inferring high-resolution fossil fuel CO_2 records at continental sites from combined $^{14}CO_2$ and CO observations, Tellus B, 59, 245–250, 2007.

Levin, I. and Kromer, B.: Twenty years of atmospheric $^{14}CO_2$ observations at Schauinsland station, Germany, Radiocarbon, 39, 205–218, 1997.

Levin, I. and Rödenbeck, C.: Can the envisaged reductions of fossil fuel CO_2 emissions be detected by atmospheric observations?, Naturwissenschaften, 95, 203–208, 2008.

Levin, I., Munnich, K., and Weiss, W.: The effect of anthropogenic CO_2 and ^{14}C sources on the distribution of ^{14}C in the atmosphere, Radiocarbon, 22, 379–391, 1980.

Levin, I., Schuchard, J., Kromer, B., and Munnich, K. O.: The continental European Suess effect, Radiocarbon, 31, 431–440, 1989.

Levin, I., Kromer, B., Schmidt, M., and Sartorius, H.: A novel approach for independent budgeting of fossil fuel CO_2 over Europe by $^{14}CO_2$ observations, Geophys. Res. Lett, 30, 2194, doi:10.1029/2003GL018477, 2003.

Levin, I., Hammer, S., Kromer, B., and Meinhardt, F.: Radiocarbon observations in atmospheric CO_2: Determining fossil fuel CO_2 over Europe using Jungfraujoch observations as background, Science of the Total Environment, The, 391, 211–216, 2008.

Levin, I., Naegler, T., Kromer, B., Diehl, M., Francey, R. J., Gomez-Pelaez, A. J., Steele, L. P., Wagenbach, D., Weller, R., and Worthy, D. E.: Observations and modelling of the global distribution and long-term trend of atmospheric $^{14}CO_2$, Tellus B, 62, 26–46, doi:10.1111/j.1600-0889.2009.00446.x, 2010.

Levin, I., Kromer, B., and Hammer, S.: Atmospheric $\Delta^{14}CO_2$ trend in Western European background air from 2000 to 2012, Tellus B; Vol 65 (2013), 65, doi:http://dx.doi.org/10.3402/tellusb.v65i0.20092, 2013.

Libby, W.: Atmospheric helium three and radiocarbon from cosmic radiation, Physical Review, 1946.

Lin, J. C. and Gerbig, C.: Accounting for the effect of transport errors on tracer inversions, Geophysical Research Letters, 32, L01 802, 2005.

Lopez, M., Schmidt, M., Delmotte, M., Colomb, A., Gros, V., Janssen, C., Lehman, S., Mondelain, D., Perrussel, O., Ramonet, M., Xueref-Remy, I., and Bousquet, P.: CO, NO_X and $^{13}CO_2$ as tracers for fossil fuel CO_2: results from a pilot study in Paris during winter 2010, Atmos. Chem. Phys., 13, 7343–7358, 2013.

Manohar, S., Meijer, H., and Herber, M.: Radon flux maps for the Netherlands and Europe using terrestrial gamma radiation derived from soil radionuclides, Atmospheric Environment, 81, 399–412, 2013.

Marland, G.: Uncertainties in accounting for CO_2 from fossil fuels, Journal of Industrial Ecology, 2008.

Marland, G. and Rotty, R.: Carbon dioxide emissions from fossil fuels: a procedure for estimation and results for 1950–1982, Tellus B, 36B, 232–261, 1984.

Marland, G., Boden, T. A., and Andres, R. J.: Global, Regional, and National Fossil Fuel CO_2 Emissions, in: Trends: A Compendium of Data on Global Change, Carbon Dioxide Information Analysis Center, Oak Ridge National Laboratory, U.S. Department of Energy, Oak Ridge, Tenn., U.S.A., URL http://cdiac.ornl.gov/trends/emis/overview, 2008.

McCartney, M., Baxter, M. S., and Scott, E. M.: Carbon-14 discharges from the nuclear fuel cycle: 1. Global effects, Journal of environmental radioactivity, 8, 143–155, 1988a.

McCartney, M., Baxter, M. S., and Scott, E. M.: Carbon-14 discharges from the nuclear fuel cycle: 2. Local effects, Journal of environmental radioactivity, 8, 157–171, 1988b.

Meesters, A. G. C. A., Tolk, L. F., Peters, W., Hutjes, R. W. A., Vellinga, O. S., Elbers, J. A., Vermeulen, A. T., van der Laan, S., Neubert, R. E. M., Meijer, H. A. J., and Dolman, A. J.: Inverse carbon dioxide flux estimates for the Netherlands, Journal of Geophysical Research D: Atmospheres, 117, 2012.

Meijer, H. A. J., van der Plicht, J., Gislefoss, J. S., and Nijdal, R.: Comparing long-term atmospheric ^{14}C and ^{3}H records near Groningen, The Netherlands with Fruholmen, Norway and Izaña, Canary Islands ^{14}C stations, Radiocarbon, 37, 39–50, 1995.

Meijer, H. A. J., Smid, H., Perez, E., and Keizer, M. G.: Isotopic characterisation of anthropogenic CO_2 emissions using isotopic and radiocarbon analysis, Physics and Chemistry of the Earth, 21, 483–487, 1996.

Miller, J. B., Lehman, S. J., Montzka, S. A., Sweeney, C., Miller, B. R., Karion, A., Wolak, C., Dlugokencky, E. J., Southon, J., Turnbull, J. C., and Tans, P. P.: Linking emissions of fossil fuel CO_2 and other anthropogenic trace gases using atmospheric $^{14}CO_2$, Journal of Geophysical Research D: Atmospheres, 117, 2012.

Mlawer, E., Taubman, S., Brown, P., Iacono, M., and Clough, S.: Radiative transfer for inhomogeneous atmospheres: RRTM, a validated correlated-k model for the longwave, Journal of Geophysical Research D: Atmospheres, 102, 16 663–16 682, 1997.

Monteith, J. L.: Evaporation and the Environment, 19th Symposia of the Society for Experimental Biology, pp. 205–234, 1965.

Mook, W. G. and van der Plicht, J.: Reporting ^{14}C activities and concentrations, Radiocarbon, 41, 227–239, 1999.

Naegler, T. and Levin, I.: Closing the global radiocarbon budget 1945–2005, J. Geophys. Res, 111, doi:10.1029/2005JD006758, 2006.

Naegler, T. and Levin, I.: Observation-based global biospheric excess radiocarbon inventory 1963–2005, Journal of Geophysical Research-Atmospheres, 2009a.

Naegler, T. and Levin, I.: Biosphere-atmosphere gross carbon exchange flux and the $\delta^{13}CO_2$ and $\Delta^{14}CO_2$ disequilibria constrained by the biospheric excess radiocarbon inventory, Journal of Geophysical Research-Atmospheres, 114, doi:10.1029/2008JD011116, 2009b.

Nakanishi, M. and Niino, H.: An improved Mellor-Yamada Level-3 model with condensation physics: Its design and verification, Boundary-Layer Meteorology, 112, 1–31, 2004.

Nakanishi, M. and Niino, H.: An improved Mellor-Yamada Level-3 model: Its numerical stability and application to a regional prediction of advection fog, Boundary-Layer Meteorology, 119, 397–407, 2006.

NCEP: U.S. National Centers for Environmental Prediction Final (FNL) Operational Model Global Tropospheric Analyses, continuing from July 1999, Dataset ds083.2 published by the CISL Data Support Section at the National Center for Atmospheric Research, Boulder, CO, available online at http://dss.ucar.edu/datasets/ds083.2/., updated daily.

Nydal, R.: Further investigation on the transfer of radiocarbon in nature, J. Geophys. Res., 73, 3617–3635, 1968.

Nydal, R. and Gislefoss, J.: Further application of bomb ^{14}C as a tracer in the atmosphere and ocean, Radiocarbon, 38, 389–406, 1996.

Olivier, J. G. J. and Berdowski, J. J. M.: Global emissions sources and sinks, in: Berdowski, J., Guicherit, R. and B.J. Heij, "The Climate System", pp. 33–78, Balkema Publishers/Swets & Zeitlinger Publishers, Lisse, The Netherlands, 2001.

Olivier, J. G. J. and Peters, J. A. H. W.: Uncertainties in global, regional and national emission inventories. In: van Ham, J., A.P.M. Baede, R. Guicherit and J.F.G.M. Williams-Jacobse (eds.):'Non-CO_2 greenhouse gases: scientific understanding, control options and policy aspects. Proceedings of the Third International Symposium, Maastricht, Netherlands, 21-23 January 2002', Millpress Science Publishers, Rotterdam. ISBN 90-77017-70-4, pp. 525–540, 2002.

Olsen, S. and Randerson, J.: Differences between surface and column atmospheric CO_2 and implications for carbon cycle research, J. Geophys. Res., 109, D02 301, 2004.

Pacala, S., Breidenich, C., and Brewer, P. G.: Verifying greenhouse gas emissions: Methods to support international climate agreements, National Research Council of the National Academies, National Academies Press, Washington, DC., Committee on Methods for Estimating Greenhouse Gas Emissions, Board on Atmospheric Sciences and Climate Division on Earth and Life Studies, 2010.

Palstra, S. and Meijer, H.: Biogenic Carbon Fraction of Biogas and Natural Gas Fuel Mixtures Determined with 14C, Radiocarbon, 56, 7–28, 2014.

Palstra, S. W. L., Karstens, U., Streurman, H., and Meijer, H. A. J.: Wine ethanol ^{14}C as a tracer for fossil fuel CO_2 emissions in Europe: Measurements and model comparison, Journal of Geophysical Research-Atmospheres, 113, doi:10.1029/2008JD010282, 2008.

Park, J., Hong, W., Park, G., Sung, K., Lee, K., Kim, Y., Kim, J., Choi, H., Kim, G., and Woo, H.: A Comparison of Distribution Maps of $\Delta^{14}C$ of 2010 and 2011 in Korea, Radiocarbon, 55, 841–847, doi:10.2458/azu_js_rc.55.16307, 2013.

Pataki, D. E., Randerson, J. T., Wang, W., Herzenach, M. K., and Grulke, N. E.: The carbon isotope composition of plants and soils as biomarkers of pollution, 2010.

Penning de Vries, F. W. T. and van Laar, H. H.: Simulation of plant growth and crop production, Centre for Agricultural Publishing and Documentation (Pudoc), Wageningen, the Netherlands, URL `http://edepot.wur.nl/167315`, monograph, 1982.

Penning de Vries, F. W. T., Jansen, D. M., ten Berge, H. F. M., and Bakema, A.: Simulation of ecophysiological processes of growth in several annual crops, Centre for Agricultural Publishing and Documentation (Pudoc), Wageningen, URL `http://edepot.wur.nl/108856`, monograph, 1989.

Peters, W., Jacobson, A. R., Sweeney, C., Andrews, A. E., Conway, T. J., Masarie, K., Miller, J. B., Bruhwiler, L. M. P., Petron, G., Hirsch, A. I., Worthy, D. E., van der Werf, G. R., Randerson, J. T., Wennberg, P. O., Krool, M., and Tans, P. P.: An atmospheric perspective on North American carbon dioxide exchange: CarbonTracker, Proceedings of the National Academy of Sciences, 104(48), 18 925–18 930, 2007.

Peters, W., Krol, M. C., van der Werf, G. R., Houweling, S., Jones, C. D., Hughes, J., Schaefer, K., Masarie, K. A., Jacobson, A. R., Miller, J. B., Cho, C. H., Ramonet, M., Schmidt, M., Ciattaglia, L., Apadula, F., Helta, D., Meinhardt, F., di Sarra, A. G., Piacentino, S., Sferlazzo, D., Aalto, T., Hatakka, J., Strom, J., Haszpra, L., Meijer, H. A. J., van der Laan,

S., Neubert, R. E. M., Jordan, A., Rodo, X., Morgui, J. A., Vermeulen, A. T., Popa, E., Rozanski, K., Zimnoch, M., Manning, A. C., Leuenberger, M., Uglietti, C., Dolman, A. J., Ciais, P., Heimann, M., and Tans, P. P.: Seven years of recent European net terrestrial carbon dioxide exchange constrained by atmospheric observations, Global Change Biology, 16, 1317–1337, doi:10.1111/j.1365-2486.2009.02078.x, 2010.

Peylin, P., Houweling, S., Krol, M., Karstens, U., Rödenbeck, C., Geels, C., Vermeulen, A., Badawy, B., Aulagnier, C., Pregger, T., Delage, F., Pieterse, G., Ciais, P., and Heimann, M.: Importance of fossil fuel emission uncertainties over Europe for CO_2 modeling: Model intercomparison, Atmospheric Chemistry and Physics, 11, 6607–6622, 2011.

Pillai, D., Gerbig, C., Ahmadov, R., Roedenbeck, C., Kretschmer, R., Koch, T., Thompson, R., Neininger, B., and Lavric, J. V.: High-resolution simulations of atmospheric CO_2 over complex terrain - representing the Ochsenkopf mountain tall tower, Atmospheric Chemistry and Physics, 11, 7445–7464, doi:10.5194/acp-11-7445-2011, 2011.

Pino, D., de Arellano, J. V.-G., Peters, W., Schröter, J., van Heerwaarden, C., and Krol, M.: A conceptual framework to quantify the influence of convective boundary layer development on carbon dioxide mixing ratios, Atmospheric Chemistry and Physics, 12, 2969–2985, 2012.

Pregger, T. and Friedrich, R.: Effective pollutant emission heights for atmospheric transport modelling based on real-world information, Environmental Pollution, 157, 552–560, 2009.

Pregger, T., Scholz, Y., and Friedrich, R.: Documentation of the Anthropogenic GHG Emission Data for Europe Provided in the Frame of CarboEurope GHG and CarboEurope IP, Final Report CarboEurope-IP, 2007.

Quéré, C. L., Peters, G., Andres, R., Andrew, R., Boden, T., Ciais, P., Friedlingstein, P., Houghton, R., Marland, G., Moriarty, R., Sitch, S., Tans, P., Arneth, A., Arvanitis, A., Bakker, D., Bopp, L., Canadell, J., Chini, L., Doney, S., Harper, A., Harris, I., House, J., Jain, A., Jones, S., Kato, E., Keeling, R., Goldewijk, K. K., Körtzinger, A., Koven, C., Lefèvre, N., Maignan, F., Omar, A., Ono, T., Park, G.-H., Pfeil, B., Poulter, B., Raupach, M., Regnier, P., Rödenbeck, C., Saito, S., Schwinger, J., Segschneider, J., Stocker, B., Takahashi, T., Tilbrook, B., van Heuven, S., Viovy, N., Wanninkhof, R., Wiltshire, A., and Zaehle, S.: Global carbon budget 2013, Earth Syst. Sci. Data, 6, 235–263, 2014.

Randerson, J., Enting, I., Schuur, E., Caldeira, K., and Fung, I. Y.: Seasonal and latitudinal variability of troposphere D 14 CO 2: Post bomb contributions from fossil fuels, oceans, the stratosphere, and the terrestrial biosphere, Global Biogeochem. Cycles, 16, 1112, doi:10.1029/2002GB001876, 2002.

Raupach, M., Marland, G., Ciais, P., Quéré, C. L., Canadell, J., Klepper, G., and Field, C.: Global and regional drivers of accelerating CO_2 emissions, Proceedings of the National Academy of Sciences, 104, 10 288–10 293, doi:10.1073/pnas.0700609104, 2007.

Ridgwell, A., Zondervan, I., Hargreaves, J., Bijma, J., and Lenton, T.: Assessing the potential long-term increase of oceanic fossil fuel CO_2 uptake due to CO_2-calcification feedback, Biogeosciences, 4, 481–492, 2007.

Riley, W., Hsueh, D., Randerson, J., Fischer, M. L., Hatch, J. G., Pataki, D. E., Wang, W., and Goulden, M. L.: Where do fossil fuel carbon dioxide emissions from California go? An analysis based on radiocarbon observations and an atmospheric transport model, J. Geophys. Res, 113, doi:10.1029/2007JG000625, 2008.

Roberts, M. and Southon, J.: A preliminary determination of the absolute $^{14}C/^{12}C$ ratio of OX-I, Radiocarbon, 49, 441–445, 2007.

Ronda, R., de Bruin, H., and Holtslag, A.: Representation of the canopy conductance in modeling the surface energy budget for low vegetation, Journal of Applied Meteorology, 40, 1431–1444, 2001.

Sakurai, H., Namai, S., Inui, E., Tokanai, F., Kato, K., Takahashi, Y., Sato, T., Kikuchi, S., Arai, Y., Masuda, K., Shibata, K., and Kuriyama, Y.: Measuring ^{14}C Concentration in Wine to Monitor Global Distribution of ^{14}C, Radiocarbon, 55, 1827–1833, doi:10.2458/azu_js_rc.55.16370, 2013a.

Sakurai, H., Tokanai, F., Kato, K., Takahashi, Y., Sato, T., Kikuchi, S., Inui, E., Arai, Y., Masuda, K., Miyahara, H., Mundia, C., and Tavera, W.: Latest ^{14}C Concentrations of Plant Leaves at High Altitudes in the Northern and Southern Hemispheres: Vertical Stability of Local Suess Effect, Radiocarbon, 55, 1573–1579, doi:10.2458/azu_js_rc.55.16273, 2013b.

Schaefer, K., Collatz, G. J., Tans, P., Denning, A. S., Baker, I., Berry, J., Prihodko, L., Suits, N., and Philpott, A.: Combined Simple Biosphere/Carnegie-Ames-Stanford Approach terrestrial carbon cycle model, J Geophys Res-Biogeo, 113, G03 034, doi:10.1029/2007JG000603, 2008.

Shibata, S., Kawano, E., and Nakabayashi, T.: Atmospheric $^{14}CO_2$ variations in Japan during 1982-1999 based on ^{14}C measurements of rice grains, Appl Radiat Isotopes, 63, 285–290, doi:10.1016/j.apradiso.2005.03.011, 2005.

Shiga, Y., Michalak, A., Gourdji, S., Mueller, K., and Yadav, V.: Detecting fossil fuel emissions patterns from subcontinental regions using North American in situ CO_2 measurements, Geophys. Res. Lett., 41, 2014GL059 684, 2014.

Singels, A., van den Berg, M., Smit, M., Jones, M., and van Antwerpen, R.: Modelling water uptake, growth and sucrose accumulation of sugarcane subjected to water stress, Field Crops Research, 117, 59–69, 2010.

Skamarock, W., Klemp, J., Dudhia, J., Gill, D. O., Barker, D. M., Duda, M. G., Huang, X.-Y., Wang, W., and Powers, J. G.: A description of the Advanced Research WRF Version 3, NCAR Technical Note, NCAR/TN-475+STR, 2008.

Smith, H., Fischer, H., Wahlen, M., Mastroianni, D., and Deck, B.: Dual modes of the carbon cycle since the Last Glacial Maximum, Nature, 400, 248–250, doi:10.1038/22291, 1999.

Spitters, C.: Separating the diffuse and direct component of global radiation and its implications for modeling canopy photosynthesis Part II. Calculation of canopy photosynthesis, Agr Forest Meteorol, 38, 231–242, 1986.

Spitters, C., Toussaint, H., and Goudriaan, J.: Separating the diffuse and direct component of global radiation and its implications for modeling canopy photosynthesis Part I. Components of incoming radiation, Agr Forest Meteorol, 38, 217–229, 1986.

Steeneveld, G.-J., Mauritsen, T., Bruijn, E. D., and de Arellano, J. V.-G.: Evaluation of limited-area models for the representation of the diurnal cycle and contrasting nights in CASES-99, Journal of Applied Meteorology and Climatology, 47, 869–887, 2008.

Stephens, B. B., Gurney, K. R., Tans, P. P., Sweeney, C., Peters, W., Bruhwiler, L., Ciais, P., Ramonet, M., Bousquet, P., Nakazawa, T., Aoki, S., Machida, T., Inoue, G., Vinnichenko, N., Lloyd, J., Jordan, A., Heimann, M., Shibistova, O., Langenfelds, R. L., Steele, L. P., Francey, R. J., and Denning, A. S.: Weak northern and strong tropical land carbon uptake from vertical profiles of atmospheric CO_2, Science, 316, 1732–1735, doi:10.1126/science.1137004, 2007.

Sterk, H. A. M., Steeneveld, G. J., and Holtslag, A. A. M.: The role of snow-surface coupling, radiation, and turbulent mixing in modeling a stable boundary layer over Arctic sea ice, J. Geophys. Res. Atmos., 118, 1199–1217, 2013.

Strain, B. and Cure, J.: Direct effects of increasing carbon dioxide on vegetation, vol. DOE/ER-0238, U.S. Dep. of Energy, Washington, D.C., U.S., 1985.

Stuefer, M., Freitas, S. R., Grell, G., Webley, P., Peckham, S., Mckeen, S. A., and Egan, S. D.: Inclusion of ash and SO_2 emissions from volcanic eruptions in WRF-Chem: development and some applications, Geosci. Model Dev., 6, 457–468, doi:10.5194/gmd-6-457-2013, 2013.

Stuiver, M. and Polach, H.: Discussion: reporting of ^{14}C data, Radiocarbon, 19, 355–363, 1977.

Stuiver, M. and Quay, P.: Atmospheric ^{14}C changes resulting from fossil fuel CO_2 release and cosmic ray flux variability, Earth Planet. Sci. Lett, 53, 349–362, 1981.

Šturm, M., Vreča, P., and Bronić, I. K.: Carbon isotopic composition (δ^{13}C and ^{14}C activity) of plant samples in the vicinity of the Slovene nuclear power plant, Journal of environmental radioactivity, 110, 24–29, 2012.

Suess, H.: Radiocarbon concentration in modern wood, Science, 122, 415–417, 1955.

Svetlik, I., Povinec, P. P., Molnar, M., Vana, M., SIVO, A., and Bujtas, T.: Radiocarbon in the air of central Europe: Long-term investigations, Radiocarbon, 52, 823–834, 2010.

Szegvary, T., Conen, F., and Ciais, P.: European ^{222}Rn inventory for applied atmospheric studies, Atmospheric Environment, 43, 1536–1539, 2009.

Tans, P. P., Fung, I. Y., and Takahashi, T.: Observational constraints on the global atmospheric CO_2 budget, Science, 247, 1431–1438, 1990.

Thoning, K. and Tans, P.: Atmospheric carbon dioxide at Mauna Loa Observatory. 2. Analysis of the NOAA GMCC data, 1974-1985, J. Geophys. Res., 94, 8549–8565, 1989.

Tie, X., Madronich, S., Li, G., Ying, Z., Weinheimer, A., Apel, E., and Campos, T.: Simulation of Mexico City plumes during the MIRAGE-Mex field campaign using the WRF-Chem model, Atmospheric Chemistry and Physics, 9, 4621–4638, 2009.

Tolk, L. F., Peters, W., Meesters, A. G. C. A., Groenendijk, M., Vermeulen, A. T., Steeneveld, G. J., and Dolman, A. J.: Modelling regional scale surface fluxes, meteorology and CO_2 mixing ratios for the Cabauw tower in the Netherlands, Biogeosciences, 6, 2265–2280, 2009.

Turnbull, J., Miller, J., Lehman, S., and Tans, P.: Comparison of $^{14}CO_2$, CO, and SF_6 as tracers for recently added fossil fuel CO_2 in the atmosphere and implications for biological CO_2 exchange, Geophysical Research Letters, 33, doi:10.1029/2005GL024213, 2006.

Turnbull, J., Miller, J., Lehman, S., and Hurst, D.: Spatial distribution of $^{14}CO_2$ across Eurasia: measurements from the TROICA-8 expedition, Atmos. Chem. Phys, 2009a.

Turnbull, J., Rayner, P., Miller, J., Naegler, T., Ciais, P., and Cozic, A.: On the use of $^{14}CO_2$ as a tracer for fossil fuel CO_2 : Quantifying uncertainties using an atmospheric transport model, J. Geophys. Res., 114, D22 302, doi:10.1029/2009JD012308, 2009b.

Turnbull, J., Karion, A., Fischer, M. L., Faloona, I., Guilderson, T., Lehman, S. J., Miller, B. R., Miller, J. B., Montzka, S., Sherwood, T., Saripalli, S., Sweeney, C., and Tans, P. P.: Assessment of fossil fuel carbon dioxide and other anthropogenic trace gas emissions from airborne measurements over Sacramento, California in spring 2009, Atmospheric Chemistry and Physics, 11, 705–721, doi:10.5194/acp-11-705-2011, 2011a.

Turnbull, J., Tans, P., Lehman, S., Baker, D., Conway, T., Chung, Y., Gregg, J., Miller, J., Southon, J., and Zhou, L.-X.: Atmospheric observations of carbon monoxide and fossil fuel CO_2 emissions from East Asia, Journal of Geophysical Research D: Atmospheres, 116, 2011b.

Turnbull, J., Guenther, D., Karion, A., Sweeney, C., Anderson, E., Andrews, A., Kofler, J., Miles, N., Newberger, T., Richardson, S., and Tans, P.: An integrated flask sample collection system for greenhouse gas measurements, Atmos. Meas. Tech., 5, 2321–2327, 2012.

Turnbull, J. C., Keller, E. D., Baisden, T., Brailsford, G., Bromley, T., Norris, M., and Zondervan, A.: Atmospheric measurement of point source fossil CO_2 emissions, Atmos. Chem. Phys., 14, 5001–5014, 2014a.

Turnbull, J. C., Sweeney, C., Karion, A., Newberger, T., Lehman, S. J., Tans, P. P., Davis, K. J., Lauvaux, T., Miles, N. L., Richardson, S. J., Cambaliza, M. O., Shepson, P. B., Gurney, K., Patarasuk, R., and Razlivanov, I.: Towards quantification and source sector identification of fossil fuel CO_2 emissions from an urban area: Results from the INFLUX experiment, J. Geophys. Res. Atmos., 120, doi:10.1002/2014JD022555, 2014b.

van der Laan, S., Karstens, U., Neubert, R. E. M., van der Laan-Luijkx, I. T., and Meijer, H. A. J.: Observation-based estimates of fossil fuel-derived CO_2 emissions in the Netherlands using ^{14}C, CO and [222]Radon, Tellus B, 62, 389–402, doi:10.1111/j.1600-0889.2010.00493.x, 2010.

van der Molen, M. K. and Dolman, A. J.: Regional carbon fluxes and the effect of topography on the variability of atmospheric CO_2, J. Geophys. Res., 112, D01 104, 2007.

van der Plicht, J., Wijma, S., Aerts-Bijma, A. T., Pertuisot, M. H., and Meijer, H. A. J.: Status report: The Groningen AMS facility, Nuclear Instruments and Methods in Physics Research Section B: Beam Interactions with Materials and Atoms, 172, 58–65, 2000.

van der Stricht, S. and Janssens, A.: Radioactive effluents from nuclear power stations and nuclear fuel reprocessing sites in the European Union, 2004-08, Radiation Protection, 2010.

van der Velde, I. R., Miller, J. B., Schaefer, K., van der Werf, G. R., Krol, M. C., and Peters, W.: Terrestrial cycling of 13CO$_2$ by photosynthesis, respiration, and biomass burning in SiBCASA, Biogeosciences, 11, 6553–6571, 2014a.

van der Velde, I. R., Miller, J. B., Schaefer, K., van der Werf, G. R., Krol, M. C., and Peters, W.: Towards multi-tracer data-assimilation: biomass burning and carbon isotope exchange in SiBCASA, Biogeosciences Discuss., 11, 107–149, 2014b.

van Ittersum, M., Leffelaar, P., van Keulen, H., Kropff, M., Bastiaans, L., and Goudriaan, J.: On approaches and applications of the Wageningen crop models, European Journal of Agronomy, 18, 201–234, 2003.

van Laar, H. H., Goudriaan, J., and van Keulen, H.: SUCROS97: simulation of crop growth for potential and water-limited production situations; as applied to spring wheat, vol. 14, DLO Research Institute for Agrobiology and Soil Fertility and The C.T. de Wit Graduate School for Production Ecology, Wageningen, The Netherlands, URL `http://books.google.com/books?id=d3g6HQAACAAJ&printsec=frontcover`, 1997.

Vay, S. A., Tyler, S. C., Choi, Y., Blake, D. R., Blake, N. J., Sachse, G. W., Diskin, G. S., and Singh, H. B.: Sources and transport of Δ^{14}C in CO$_2$ within the Mexico City Basin and vicinity, Atmospheric Chemistry and Physics, 9, 4973–4985, 2009.

Vermeulen, A. T., Hensen, A., Popa, M. E., van den Bulk, W. C. M., and Jongejan, P. A. C.: Greenhouse gas observations from Cabauw Tall Tower (1992-2010), Atmospheric Measurement Techniques, 4, 617–644, 2011.

Vilà-Guerau de Arellano, J., Gioli, B., Miglietta, F., Jonker, H. J. J., Baltink, H. K., Hutjes, R. W. A., and Holtslag, A. A. M.: Entrainment process of carbon dioxide in the atmospheric boundary layer, J. Geophys. Res, 109, doi:10.1029/2004JD004725, 2004.

Vogel, F., Hammer, S., Steinhof, A., Kromer, B., and Levin, I.: Implication of weekly and diurnal ^{14}C calibration on hourly estimates of CO-based fossil fuel CO$_2$ at a moderately polluted site in southwestern Germany, Tellus, Series B: Chemical and Physical Meteorology, 62, 512–520, 2010.

Vogel, F., Levin, I., and Worthy, D.: Implications for Deriving Regional Fossil Fuel CO$_2$ Estimates from Atmospheric Observations in a Hot Spot of Nuclear Power Plant ^{14}CO$_2$ Emissions, Radiocarbon; Vol 55, No 2–3 (2013), doi:10.2458/azu_js_rc.55.16347, 2013a.

Vogel, F. R., Tiruchittampalam, B., Theloke, J., Kretschmer, R., Gerbig, C., Hammer, S., and Levin, I.: Can we evaluate a fine-grained emission model using high-resolution atmospheric transport modelling and regional fossil fuel CO$_2$ observations?, Tellus B; Vol 65 (2013), 2013b.

Wang, L., Zhang, Y., Wang, K., Zheng, B., Zhang, Q., and Wei, W.: Application of Weather Research and Forecasting Model with Chemistry (WRF/Chem) over northern China: Sensitivity study, comparative evaluation, and policy implications, Atmospheric Environment, doi:http://dx.doi.org/10.1016/j.atmosenv.2014.12.052, 2014.

Wang, Z., Xiang, Y., and Guo, Q.: ^{14}C Levels in Tree Rings Located near Qinshan Nuclear Power Plant, China, Radiocarbon; Vol 54, No 2 (2012), 2012.

Wang, Z., Xiang, Y., and Guo, Q.: Terrestrial distribution of ^{14}C in the vicinity of Qinshan nuclear power plant, China, Radiocarbon, 55, 59–66, 2013.

Watson, A. J., Schuster, U., Bakker, D. C. E., Bates, N. R., Corbiere, A., Gonzalez-Davila, M., Friedrich, T., Hauck, J., Heinze, C., Johannessen, T., Kortzinger, A., Metzl, N., Olafsson, J., Olsen, A., Oschlies, A., Padin, X. A., Pfeil, B., Santana-Casiano, J. M., Steinhoff, T., Telszewski, M., Rios, A. F., Wallace, D. W. R., and Wanninkhof, R.: Tracking the Variable North Atlantic Sink for Atmospheric CO_2, Science, 326, 1391–1393, doi:10.1126/science.1177394, 2009.

Willmott, C.: Some comments on the evaluation of model performance, Bulletin of the American Meteorological Society, 63, 1309–1313, 1982.

Xevi, E., Gilley, J., and Feyen, J.: Comparative study of two crop yield simulation models, Agricultural Water Management, 30, 155–173, 1996.

Zhang, L., van der Werf, W., Cao, W., Li, B., Pan, X., and Spiertz, J.: Development and validation of SUCROS-cotton: A potential crop growth simulation model for cotton, NJAS - Wageningen Journal of Life Sciences, 56, 59–83, 2008.

Summary

Anthropogenic fossil fuel CO_2 emissions are a major topic of research because they increase the atmospheric CO_2 mole fractions. This in turn affects the global greenhouse gas budget and the radiative forcing to the Earth's climate system. Research into atmospheric CO_2 variations on the regional scale is hampered by the challenge of assigning the observed CO_2 abundances to the fractions of biogenic and anthropogenic origin. Atmospheric ^{14}C observations can provide the additional information needed for this challenge, and plant samples provide observations that integrate the atmospheric $^{14}C/C$ ratios ($\Delta^{14}C$) over the growing season of the plant. This thesis describes systematic research into the $^{14}CO_2$ budget on the regional scale. Key components for the quantitative interpretation of plant and atmospheric $\Delta^{14}C$ samples are the effect of weather on CO_2 assimilation in plants and CO_2 from anthropogenic but non-fossil origin that can interfere with the estimation of fossil fuel CO_2 emissions to the atmosphere.

Plant samples provide the opportunity for cost-effective sampling without earlier investment or specialized infrastructure. Such information can be of great value in data assimilation systems, as it will provide uncertainty constraints in regions where CO_2 atmospheric observations are scarce or non-existent. If fossil fuel CO_2 is the only influence on the observed atmospheric $\Delta^{14}C$ signature, its mole fractions can be estimated in relatively simple method and subsequently the emission estimation will be less uncertain. In many regions, however, there are additional sources of $^{14}CO_2$ that offset the effect fossil fuel emissions have on the observed $\Delta^{14}C$. The research questions investigated in this thesis target the different steps required to use plant samples quantitatively to estimate atmospheric fossil fuel CO_2 abundances.

In Chapter 3 we address our first research question *How accurate can we model the $\Delta^{14}CO_2$ signature of an annual crop?* We evaluate the importance of plant growth on the resulting plant-sampled $\Delta^{14}C$ through a modeling study that includes temporal, but not spatial variations in the atmospheric $\Delta^{14}C$ signature. We introduce a process-based model of plant growth (SUCROS), which simulates CO_2 assimilation into the dry matter of different plant organs and the plant development through the growing season. We use the simulated daily growth as a weighting function (averaging kernel) for the atmospheric $\Delta^{14}C$ signature

as it is accumulated into the plant biomass. We assess the differences when using simpler proxies of plant growth to create the averaging kernel, or when comparing to the direct atmospheric average. We find that the growing pattern simulated by the model cannot be sufficiently replicated by simpler environmental variables and will result in a measurable ($>1‰$) gradient between the atmosphere and the different plant parts sampled. Furthermore, our results show that even small weather variations similar to those observed over the Netherlands over a single growing season, can result in a measurable difference in the Δ^{14}C signature of the sampled plant biomass. As this study lacks spatial variability in the atmospheric Δ^{14}C time-series supplied over the modeled area it was unclear if the covariation between weather patterns and atmospheric transport might result in the amplification of these spatial gradients.

Chapter 4 is dedicated to simulating the regional atmospheric $\Delta^{14}CO_2$ budget over Western Europe in order to address our next research question *What modeling framework is required to simulate the regional $^{14}CO_2$ budget?* We present the WRF-Chem model, which we use to simultaneously simulate the regional weather and the transport of CO_2 and $^{14}CO_2$ tracers that we have tagged according to their sources. We use atmospheric observations of CO_2 and $\Delta^{14}CO_2$ available in the region to verify the skill of our modeling framework. We evaluate the contribution of different anthropogenic terms in the budget and find that in Western Europe, the fossil fuel signal competes with $^{14}CO_2$ emissions from the nuclear industry. These two sources have opposite effects on the atmospheric $\Delta^{14}CO_2$ signature. Our results for the magnitude of both terms compare well with previously published results, but our framework allows us to evaluate them at higher spatial and temporal resolution. Nevertheless, since most of the available $\Delta^{14}CO_2$ observations are of lower temporal resolution, these findings will require further verification. Building on our previous work, we now find that the gradients between the modeled atmospheric samples and plant samples, created by the combined effect of weather on the plant growth and atmospheric transport, are mostly within the measurement precision of $\pm 2‰$ of a single measurement. Locally, they can exceed this threshold considerably, which implies that accounting for the effect of plant growth in some parts of the region is critical if plant samples are to be used to verify fossil fuel emissions in these areas.

With the study described in Chapter 5 we target our last research question *Are plant samples feasible source of new information for the anthropogenic CO_2 emissions on the regional scale?* We present the results of an experimental campaign in which we collected samples from maize leaves from Western Europe during the summers of 2010 – 2012. We present our sampling strategy and the results from the ^{14}C analysis of the samples. We find that the signatures of the collected plant samples in the region are realistic given the spread in available atmospheric $\Delta^{14}CO_2$ observations. We also find measurable differences between distinct sampled regions with different emissions, such as the north of the Netherlands, the Dutch Randstad, the German Ruhrgebiet, and the French region near La Hague. The mea-

surement uncertainty and the large annual draw-down in the atmospheric $\Delta^{14}CO_2$ make these results difficult to evaluate quantitatively on their own. We interpret the observed plant samples through their comparison with the $\Delta^{14}CO_2$ signature of the modeled plant samples. The spread in our modeled results is similar to the measurement uncertainty inherent in the observations and we find that our model correlates well with the observations over the larger (>100km) sampled regions. Only one of our smaller regions, located between the Randstad and the Dutch North, shows significant correlation between the modeled and observed plant samples, which shows that on the smaller scales (<100km) the model is not able to reproduce the observed variability. Our model suggests that only a few source categories contributed to the $\Delta^{14}CO_2$ gradients in the investigated region, but due to the small magnitude of the gradients and the limited measurement precision, plant samples are not yet useful to verify specific emission categories.

The results discussed in this thesis aim at quantitative interpretation of $\Delta^{14}CO_2$ of plant samples as an integrated observation of the atmospheric $\Delta^{14}CO_2$ signature. The thesis evaluates the magnitude of influence of different $\Delta^{14}CO_2$ budget terms over the European domain, and highlights the importance of the plant growth representation when investigating spatial gradients of plant-sampled $\Delta^{14}CO_2$.

SUMMARY

Samenvatting

Antropogene CO_2-emissies uit fossiele brandstof zijn een belangrijk onderzoeksonderwerp, omdat ze de atmosferische CO_2-concentraties verhogen. Deze beïnvloeden op hun beurt het globale broeikasgasbudget en de stralingsforcering op het klimaatsysteem van de Aarde. Onderzoek naar atmosferische CO_2-veranderingen op de regionale schaal is ingewikkeld omdat toename in de geöbserveerde CO_2-concentraties verdeeld moeten worden over de biogene en antropogene bijdrage.

Atmosferische ^{14}C-metingen kunnen die extra informatie bevatten die nodig is voor deze uitdaging. Plantenmonsters leveren metingen op die de atmosferische ^{14}C/C-verhoudingen (Δ^{14}C) integreren over het groeiseizoen van de plant. Deze dissertatie beschrijft systematisch onderzoek naar het [14]CO_2-budget op regionale schaal. De belangrijkste componenten voor de kwantitatieve interpretatie van plantmonsters en van atmosferische metingen van Δ^{14}C zijn het effect van weer op CO_2-assimilatie in planten, en CO_2 van antropogene oorsprong anders dan fossiele brandstoffen, omdat die kunnen interfereren met de schatting van de CO_2-emissies uit fossiele brandstoffen.

Plantmonsters bieden een relatief goedkope meetmethode zonder investering of specialistische infrastructuur. De informatie die het oplevert kan van grote waarde zijn voor data-assimilatiesystemen, omdat de onzekerheid kan beperken in gebieden waar atmosferische CO_2-metingen zeldzaam zijn of helemaal niet bestaan. Als CO_2 uit fossiele brandstof als enige de gemeten atmosferisch Δ^{14}C-signatuur beïnvloedt, kan de molfracties geschat worden met een relatief eenvoudige methode en vervolgens zal de emissieschatting minder onzeker zijn. Echter, in veel gebieden zijn er extra bronnen van [14]CO_2 die het effect van fossiele brandstof op de gemeten Δ^{14}C compenseren. De in deze dissertatie onderzochte onderzoeksvragen richten zich op de verschillende stappen die nodig zijn om plantmonsters kwantitatief te gebruiken om atmosferische fossiele brandstof CO_2-budgetten te schatten.

In Hoofdstuk 3 behandelen we onze eerste onderzoeksvraag *Hoe nauwkeurig kunnen we de $\Delta^{14}CO_2$-signatuur van een eenjarig gewas modelleren?* We evalueren het belang van de plantengroei op de gemeten Δ^{14}C in de plantenmonsters door middel van een modelstudie naar de temporele, maar niet de ruimtelijke variaties in de atmosferische Δ^{14}C-signatuur. We introduceren een proces-gebaseerd model voor plantengroei (SUCROS), welke de CO_2-

assimilatie in de droge stof van de verschillende plantorganen en de plantontwikkeling gedurende het groeiseizoen simuleert. We gebruiken de gesimuleerde dagelijkse groei als weegfunctie voor de atmosferische Δ^{14}C-signatuur. We beoordelen de verschillen die ontstaan wanneer eenvoudigere methoden van plantengroei gebruikt worden om de weegfunctie te construeren of wanneer vergeleken wordt met het directe atmosferische gemiddelde. Wij komen tot de conclusie dat het door het model gesimuleerde groeipatroon niet afdoende nagebootst kan worden door gebruik te maken van eenvoudigere omgevingsvariabelen en dat dit zal resulteren in een meetbare ($>1‰$) gradiënt tussen de atmosfeer en de verschillende plantendelen waarvan monsters worden genomen. Bovendien laten onze resultaten zien dat zelfs kleine weervariaties, vergelijkbaar met wat wordt waargenomen boven Nederland gedurende een enkel groeiseizoen, kan resulteren in een meetbaar verschil in de Δ^{14}C signatuur van de bemonsterde plantenbiomassa. Aangezien dit onderzoek geen ruimtelijke variabiliteit heeft in de atmosferische Δ^{14}C-tijdserie die wordt gebruikt in het gemodelleerde gebied, was het onduidelijk of the covariantie tussen weerpatronen en atmosferisch transport zou kunnen leiden tot versterking van deze ruimtelijke gradiënten.

Hoofdstuk 4 is gewijd aan het simuleren van het regionale atmosferische Δ^{14}CO$_2$-budget over West-Europa om onze volgende onderzoeksvraag te adresseren *Welk modelraamwerk is nodig om het regionale ^{14}CO$_2$-budget te simuleren?* We presenteren het WRF-Chem model, wat we gebruiken om gelijktijdig het regionale weer en het transport van CO$_2$ en ^{14}CO$_2$-tracers, die we gelabeld hebben naar hun bronnen, te simuleren. We gebruiken atmosferische CO$_2$- en Δ^{14}CO$_2$-metingen die beschikbaar zijn in het gebied om de resultaten van ons modelraamwerk te controleren. We evalueren hoe groot de bijdrage van verschillende antropogene termen in het budget zijn en komen tot de conclusie dat in West-Europa het signaal van de fossiele brandstof in de zelfde orde van grootte is als van de uitstoot van ^{14}CO$_2$ door de nucleaire industrie. Deze twee bronnen hebben een tegengestelde effecten op de atmosferische Δ^{14}CO$_2$-signatuur. De grootte van beide termen in onze resultaten zijn goed vergelijkbaar met eerder gepubliceerde resultaten, maar met ons raamwerk kunnen we ze met een fijnere ruimtelijke en temporele resolutie te bekijken. Toch zullen deze bevindingen verdere verificatie nodig hebben, omdat de meeste van de beschikbare Δ^{14}CO$_2$-metingen een grovere temporele resolutie hebben. Voortbouwend op ons eerdere werk, vinden we nu dat de gradiënten tussen de gemodelleerde atmosferische monsters en plantmonsters, veroorzaakt door het gecombineerde effect van het weer op de plantengroei en het atmosferisch transport, zich voornamelijk binnen de meetonzekerheid bevinden van $\pm 2‰$voor een enkele meting. Lokaal kunnen ze deze drempel aanzienlijk overstijgen, wat suggereert dat het cruciaal zou zijn om rekening te houden met het effect van plantengroei in sommige gebieden, vooral als plantmonsters gebruikt worden om de fossiele brandstofuitstoot op die plekken te verifiëren.

Met het in Hoofdstuk 5 beschreven onderzoek richten we ons op onze laatste onderzoeksvraag *Zijn plantmonsters een geschikte bron van nieuwe informatie voor de antropogene*

CO$_2$-uitstoot op de regionale schaal? We presenteren de resultaten van een meetcampagne waarbij we monsters van maisbladeren in heel West-Europa verzamelden gedurende de zomers van 2010 – 2012. We presenteren onze meetstrategie en de resultaten van de ^{14}C-analyse van de monsters. We vinden dat de signaturen van de verzamelde plantmonsters in de regio realistisch zijn gezien de spreiding in beschikbare atmosferische $\Delta^{14}CO_2$-metingen. We vinden ook meetbare verschillen tussen de monsters uit afzonderlijke regio's, zoals Noord-Nederland, de Nederlandse Randstad, het Duitse Ruhrgebied en de Franse regio nabij La Hague. De meetonzekerheid en sterke jaarlijkse afname in atmosferische $\Delta^{14}CO_2$ maken het moeilijk om deze resultaten kwantitatief onafhankelijk te evalueren. We interpreteren de gemeten plantmonsters door middel van vergelijking met de $\Delta^{14}CO_2$-signatuur van de gemodelleerde plantmonsters. De spreiding in onze modelresultaten is vergelijkbaar met de meetonzekerheid die inherent is aan de metingen en we vinden dat onze modelresultaten goed correleren met de metingen over de grotere (>100km) monsterregio's. Slechts een van onze kleinere gebieden, gelegen tussen de Randstad en Noord-Nederland, laat een significante correlatie zien tussen de gemodelleerde en gemeten plantmonsters, wat laat zien dat op de kleinere schalen (<100km) het model niet in staat is om de gemeten variabiliteit te reproduceren. Ons model suggereert dat slecht een paar broncategorieën bijdragen aan de $\Delta^{14}CO_2$-gradiënten in het onderzochte gebied, maar door de zwakte van de gradiënten en de beperkte meetprecisie zijn plantmonsters nog niet bruikbaar om specifieke emissiecategorieën te verifiëren.

De resultaten die in deze dissertatie besproken worden, richten zich op de kwantitatieve interpretatie van $\Delta^{14}CO_2$ in plantmonsters als een geïntegreerde meting van de atmosferische $\Delta^{14}CO_2$-signatuur. De dissertatie evalueert de mate van invloed van verschillende $\Delta^{14}CO_2$-budgettermen over het Europese gebied en benadrukt het belang van de beschrijving van plantengroei bij het onderzoeken van ruimtelijke gradiënten van $\Delta^{14}CO_2$ op basis van plantmonsters.

Acknowledgments

147

Maarten, it is safe to say that some of the most challenging and stressful moments of my PhD were connected with conversations between the two of us. As my first promotor, your questions and comments were always aimed at raising the quality on my work, my behavior and research. By pushing the bar a bit higher every time you challenged me to become a better scientist and a better professional, and I thank you for that. And while this journey took a bit longer than anticipated, I hope that you are happy with the result. I am really looking forward to your radiocarbon song.

Michiel, you joined my team of advisors a bit later, but your arrival couldn't have been at a better time. This is not only because of your invaluable help with the coding and the WRF model, but also because of your exceptionally encouraging and friendly demeanor. I remember the compliments that you made for my work at the time and what a boost that was for my motivation and confidence, even as I didn't believe them - they were almost outrageously over-the-top. I have always been too critical towards my own work, but you helped me see that one shouldn't only look at the shortcomings, but also at the larger picture of what was achieved. It was really fun and a pleasure working with you.

Next, I would like to give thanks to the staff of the Centre for Isotope Research at the University of Groningen for their help with the navigation in the complex sea of carbon isotopes and radiocarbon sampling and analysis. I am very grateful to prof. Harro Meijer for his valuable comments on my work and his support for the project, and to Bert Kers for his practical expertise with setting up our field experiments and for introducing me to Ludolf Rietema, the first farmer to participate in my sampling campaign. I will add here my thanks to Sander van der Laan (even though at the time that we met he had already left CIO) for helping me decipher the observational data from the Lutjewad station and the wonderful theories during our combined research. My deepest appreciation goes to my colleague and friend, Sanne Palstra, whose patience I have tested numerously in the past six years with a multitude of questions and discussions about the ^{14}C sampling and analysis. Even at the moment of writing these lines, she is taking care of my latest batch of experimental results. Sanne, thank you for your help and for all that you have taught me.

For five years at the Meteorology and Air Quality group I met and worked with so many interesting and wonderful people, that I doubt I will be able to express my gratitude to all by name. Even then, I will try. In my project I had to learn to work both with numerical and field experiments and in such a small, yet diverse group as the MAQ I managed to find support and help for both. More often than not, the one person that would have the practical solutions and answers was Kees, regardless if it was about looking for experimental parts, setting up

WRF or simply helping with a bicycle trouble. He would sit with me and sift through hundreds of lines of code to help me figure what went wrong with the compilation of my model. Once I managed to get past that, it would be Gert-Jan who would patiently listen through my questions and suggestions about how to run the model or read the data. Jordi helped me understand a bit better the land-surface interactions and the processes in the mixed boundary layer, and managed to plant the seed of suspicion about complicated "black-box" models. I want to take the time to note Ingrid van der Laan-Luijkx's constant smile despite all the small things that I was bothering her with. Regardless if it was a question about CO_2 or a request to proof-read my article, you were always there to help. Thank you!

Bert Holtslag, Bert van Hove, Reinder, Oscar, and Arnold: with you I had less interactions, but I remember that when I would come to either of you with questions you would always have time to advise and guide me to the answer. Bert Heusinkveld, you were always full of useful ideas about the practical parts of field experiments and my expedition to Germany for the sampling campaign in 2012 would not have been the same without yours and Joel's help. Lastly, from the staff of the MAQ I would like to thank Caroline, for her support and help with the organization of basically everything. If you didn't know how to do something, you always knew someone who does, and that made the planning of the sampling campaign and our seminar so much easier.

When I started my PhD there were a handful of other PhD students, but within a year our numbers more than doubled. By now most of you have graduated or moved away, but I would like to note what a pleasure it was to embark on this adventure with such unique companions. Even though every one of us had his (or hers) own project and research, we were all facing the same challenges and your support and help were as important for me, as it was to provide you with the same back when you needed it. I wish you all success in your new ventures and I hope our paths will cross once again. There were many things I could thank you for, but I will try to stay short, if that is at all possible.

Daniëlle, you were the only of our colleagues to have the time, desire, and courage to drive with me in 2011 for my sampling campaign, when I was a brand new driver with less than three months of a driving license and no experience whatsoever driving on the dutch roads. That really meant a lot to me and I want to thank you for being such an excellent co-pilot! Anneke, thank you for the Grondboren tournaments and the WE-Days and for being so enthusiastic about team sport activities. You really made me consider them in totally new and far more pleasant perspective. Natalie, thank you for the occasional help with WRF, but more so for the great company at coffee time, at PhD drinks and dinners. You were one of the people, I always knew would be happy to go out for one, even though we didn't have them as

often as I would have liked. Eduardo, thank you for the late afternoon talks in our PhD room that more often than not had nothing to do with science, but something to do with a video you shared and were watching.

Miranda and Marina, who would have expected that our original party committee would be so much fun, at least in the few years when we were free enough to do it. I want to thank you both also for bringing some homemade sweets at work in those first few months when we had started. I would have never started bringing cookies and cupcakes myself if it wasn't for your example and I think many other colleagues should thank you for that as well! Marina, with you we both struggled with WRF and arguably conquered it. Having someone to share my frustration with the model and rant about bugs and compilation errors was really priceless. Also, that kwarktaart is forever in my heart. Bram and Joost, we did not interact at work that much before you graduated, but I want to tell you that I remember vividly our last discussion and your support at that moment meant the world to me.

Ivar, I want to thank you and Magdalena for being such great neighbors and friends, for all the movie nights and dinners, for harboring my books after my move and especially for saving me that one time when I locked myself out! Who can forget that?! Michal, my sole East-European comrade, you were more than once a lifesaver for my sanity during these five years. You introduced me to few of the greatest friends I have met in the Netherlands, got me on a sailing boat, and even dared to visit Bulgaria with me. I think the next stop for our adventures ought be Poland... or Brazil!

I will close the MAQ-part of my acknowledgments with the appreciation for the two colleagues who provided me with scientific and emotional support, friendship, laughs and criticism, basically whenever and whatever was needed to get me where I am today: my paranymphs, Marie and Huug. There are so many stories of our exploits, so many precious moments and memories that bring warmth to my heart. We will always have the race to GrenobIe, our car adventures during the sampling campaign, the taxi-for-cookies service and the Star Trek marathons. I am falling short on words to express how important was your faith in me, especially in this last stretch far away from both of you. Being speechless is very unfamiliar to me, as you well know, so I will keep it simple. **Merci & Bedankt.**

To the many friends, who made my stay in Wageningen and the Netherlands so much more exciting, I thank you. To my Brazilian friends: Carlos, Helio, Felipe and Marina, thank you for the wonderful memories and I hope to visit you soon! To Célia Sapart and the IMAU choir, thank you for the joy of singing together. For once, I felt as if my loud and unbearable voice had a purpose. To my role-playing group and especially Katharina, thank you for

giving me the opportunity to release the stress from work by sailing with the most amazing pirate crew that ever existed. I was looking forward to our games for a whole week, every week.

Моята холандска история започна пролетта на 2007ма година когато научния ми ръководител от катедра "Метеорология и Геофизика" на Физическия Факултет на СУ, доцент Елисавета Пенева ми препрати обява за лятно училище в Холандия и ме насърчи да си потърся позиция за докторантура. Ели, благодаря ти от все сърце!

Преселвайки се, дори и само за няколко години, в напълно непозната страна, далеч от семейство и родина е плашещо и самотно начинание. Ива, ако не беше ти сигурно даже нямаше и да си помисля да избера точно тази страна и щях да изпусна толкова много. Благодаря ти за подкрепата, за дешифрирането на холандските нрави и порядки в онези първи месеци, когато редовно ти идвах на гости за уикенда в Ротердам. Благодаря ти за приятелството и търпението и за това, че години по-късно все още ме търпеше да ти се изсипя за уикенда в Амстердам почти без предупреждение.

На старите приятели обратно в България, които не ме забравиха и не се сърдеха когато се появявах от нищото само за няколко дни, веднъж-два пъти в годината. Знам, че изпуснах ужасно много рожденни дни и други, големи и малки събития. Благодаря ви за това, че когато се видим ме карате да се чувствам все едно никъде не съм ходила и през цялото време съм била с вас.

На новите приятели, с които пътищата ни се пресякоха във Вахенинген, благодаря ви за забавите, прекрасните български вечери и безбройните усмивки. На Митко и Иван, за помощта при местенето и за търпението по време на набезите към ИКЕА. На Надя и Марина за вечерите в International Club и всичките други партита. На Даниела и Слав Семерджиеви за разходките до Keukenhof и една друга по-невероятна история с ИКЕА. На Галина, Искра и многото други момичета, с които спретнахме най-страхотната Българска вечеря за IxESN Wageningen. Надали някога ще забравя поточната линия за рязане, белене, чистене и стъргане на тиква за тиквеник в хола ми. Благодаря ви толкова много за възможността да се чувствам у дома си далеч от дома.

И накрая искам да благодаря на цялото ми семейството за това, че нямаше момент, в който да не са ме подкрепяли въпреки решението ми да замина надалеч за толкова години. Мамо, без твоята твърда убеденост, че трябва да последвам

мечтата си надали дори бих се замислила за чужбина. Тате, без твоя пример в академичните среди тази мечта дори нямаше да я има. В крайна сметка и това поколение трябва да има проф. Божинов(а), нали? Благодаря ти, бабо Доре, за търпението с твърде редките ми обаждания и посещения. Бате, благодаря, че не ми натякваше колко лоша леля съм заради пропуснатите рожденни и именни дни и всички други празници. Рали, с теб се разделихме в София и събрахме в чужбина и оттогава пътищата ни се пресичат, разделят и пак събират. Благодаря ти за търпението към ужасната ти братовчедка, която твърде често беше твърде заета и стресирана. Успех с твоето собствено завършване и да видим къде ще ни отвее вятъра след това. Благодаря и на другите ми близки за съветите и пожеланията. Обичам ви!

Lastly, I would like give special thanks to the people that were crucial to the success of my sampling campaign. This list without doubt starts with Marie Combe, driving me around Groningen in the summer of 2010. It includes the people that helped me get used to driving in the Netherlands, when I got my own driving license: Daniëlle van Dinther and Dimitar Valev. This list is a way to include all of my friends, who would help me cut the sampled leaves and prepare them for laboratory work and I hope I am not missing someone there: Michal, Vyara, Maria and Nikolai. Lastly, in our last year of sampling we decided to travel to places, where I knew the language even less than I knew dutch and I was aided by my colleagues for the travel and interpretation to the farmers. In Germany, I was helped by Bert Heusinkveld and Joel Schröter. In France, I once again relied on the patient nature of Marie Combe. These summer adventures are forever staying with me as one of the most fun and pleasant experiments I have participated up to date. In no small part that is because of all the farmers that participated in my sampling campaigns. I was so very pleasantly surprised by your desire to cooperate with us and in the case with the dutch farmers, with your patience for my struggles with the dutch language.

From the Netherlands the farmers and businesses that cooperated with my study are Ludolf Rietema, J.T. Knook, A.M.M. Vermue, M. Kuipers, W. Telintel, Bos-Spoelman, J. Schoonderwoerd, J.A. Goense, S. van der Brug, R. Toren, W. Peters, Martijn van Raaij, Vof van der Velden-Bongers, Van der Doelen, Frank van Loon, L.M. de Groot, Arie Steenwijk, Ingrid Schmidt, Bert and Mieke Vergeer, Sjaak Kruiswijk, Kees Vroege, J.M. Spruit, Erik Daniels, Rene Luimes, F. A. M. Potters, Wim and Margret van den Bosch, Jos and Elsbeth Ruijter, Klaas and Gerrie Veenhouwer, Anne Marks, Jan van den Greft, Jaap-Klaas and Marga van Dijk, familie Lubrecht, familie van der Lely, and H. Mentink. The cooperating farmers from Germany are Alwin Wirz, Peter Hahn, Hartmut Steinfarz, Gisbert Münster, Reinhard Gossen, Hubert Franzen, and Norbert Oenning. And finally, the farmers from France are Jean-Pierre Audoir, Laurent Thomas, Pascal Raulline, Christian Jouanne, Jean-Jacques Coisnard, Patrick and Anne Feron, Thierry Fleury, Sylvain Mathieu, and Silvy and François Muret.

Thank you! Bedankt! Merci! Danke!

ACKNOWLEDGMENTS

Curriculum Vitae and Education certificate
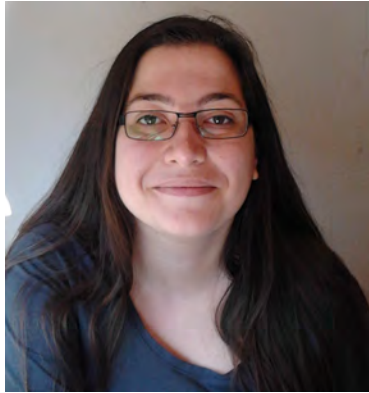
Denica Bozhinova

Education

Ph.D. in Meteorology and Air Quality
Wageningen University, Wageningen, the Netherlands
Thesis title: "Interpreting plant-sampled $\Delta^{14}CO_2$ to study regional anthropogenic CO_2 signals in Europe"

2009 – 2015

M.Sc. in Meteorology
Sofia University "St. Kliment Ohridski", Sofia, Bulgaria
Thesis title: "Analysis of the climate variability for the Balkan peninsula"

2006 – 2008

B.Sc. in Physics
Sofia University "St. Kliment Ohridski", Sofia, Bulgaria
Thesis title: "The phenomenon of El Niño and Southern Oscillation – behaviour and physical mechanism"

2002 – 2006

Workshops and trainings

- Atmospheric ^{14}C workshop at the International Radiocarbon Conference, Paris, France, 2012
- Scientific Writing Course at Wageningen University, Wageningen, the Netherlands, 2011
- Autumn School "Biogeochemistry and –physics of the lower atmosphere" organised by Cyprus Institute and Max Planck Institute for Chemistry, Paphos, Cyprus, 2010
- Environmental Research in Context, Research School for Socio-Economic and Natural Sciences of the Environment, Apeldoorn, the Netherlands, 2010
- Summer School "Physics of the Climate System" at Utrecht University, Utrecht, the Netherlands, 2007

Organized seminars

- "Climate-Carbon Interactions: From Science To Policy" Symposium, Wageningen University, Wageningen, the Netherlands, 2015

Publications and presentations

Journal publications

- **Bozhinova, D.**, Palstra, S.W.L., van der Molen, M. K., Krol, M. C., Meijer, H. A. J., and Peters, W.: *Three years of $\Delta^{14}CO_2$ observations from maize leaves in the Netherlands and Western Europe*, Radiocarbon, submitted and currently pending revisions.

- **Bozhinova, D.**, van der Molen, M. K., van der Velde, I.R., Krol, M. C., van der Laan, S., Meijer, H. A. J., and Peters, W.: *Simulating the integrated summertime $\Delta^{14}CO_2$ signature from anthropogenic emissions over Western Europe*, Atmos. Chem. Phys., vol. 14 (14) pp. 7273-7290, doi:10.5194/acp-14-7273-2014, 2014.

- **Bozhinova, D.**, Combe, M., Palstra, S.W.L., Meijer, H.A.J., Krol, M.C., Peters, W.: *The importance of crop growth modeling to interpret the $\Delta^{14}CO_2$ signature of annual plants*, Global Biogeochemical Cycles, vol. 27 (3), p. 792 - 803, doi:10.1002/gbc.20065, 2013.

Oral Presentations (selection)

- ***Invited speaker*** for the Geochemical Club Luncheon Seminar, University of East Anglia, United Kingdom: "*High-resolution modeling of $\Delta^{14}CO_2$ over Europe. Possibilities, limitations, and implications for $^{14}CO_2$ observations and fossil fuel CO_2 emissions verification*", March 2013.

- ***Presented*** "*High-resolution simulations of the $\Delta^{14}CO_2$ gradients from fossil fuels and nuclear power plants over Europe*" at American Geophysical Union: Fall meeting, San Francisco, California, USA, 2012.

- ***Presented*** "*Using plants as $\Delta^{14}CO_2$ samplers: the importance of crop growth modeling*" at Research School for Socio-Economic and Natural Sciences of the Environment Symposium: Modelling and observing earth system compartments, Wageningen, the Netherlands, 2011

- ***Presented*** "*Modeling ^{14}C exchange to estimate regional fossil fuel emissions*" at Buys Ballot Research School: Fall symposium, the Netherlands, 2010.

Poster Presentations (selection)

- "*Using annual plants as atmospheric $^{14}CO_2$ samplers for regional fossil fuel emissions estimates: crop modeling and intensive sampling approaches*", American Geophysical Union: Fall meeting, San Francisco, California, USA, 2010.

- "*Using annual plants as $^{14}CO_2$ samplers: A crop growth modeling perspective*", Autumn School of Biogeochemistry and -physics of the lower atmosphere. Paphos, Cyprus, 2010.

Netherlands Research School for the
Socio-Economic and Natural Sciences of the Environment

D I P L O M A

For specialised PhD training

The Netherlands Research School for the
Socio-Economic and Natural Sciences of the Environment
(SENSE) declares that

Denica Nikolaeva Bozhinova

born on 20 May 1984 in Sofia, Bulgaria

has successfully fulfilled all requirements of the
Educational Programme of SENSE.

Wageningen, 21 October 2015

the Chairman of the SENSE board

Prof. dr. Huub Rijnaarts

the SENSE Director of Education

Dr. Ad van Dommelen

The SENSE Research School has been accredited by the Royal Netherlands Academy of Arts and Sciences (KNAW)

KONINKLIJKE NEDERLANDSE
AKADEMIE VAN WETENSCHAPPEN

The SENSE Research School declares that **Ms Denica Bozhinova** has successfully fulfilled all requirements of the Educational PhD Programme of SENSE with a work load of 44 EC, including the following activities:

SENSE PhD Courses

o   Environmental Research in Context (2010)
o   Autumn School: Biogeochemistry and -physics of the lower atmosphere (2010)
o   Research in Context Activity: Co-organising Symposium on 'Climate-Carbon Interactions: From Science To Policy', Wageningen University (2015)

Other PhD and Advanced MSc Courses

o   Crop Ecology, Wageningen University (2010)
o   Mesoscale Meteorological Modelling, Wageningen University (2010)
o   Scientific writing, Wageningen University (2011)

External training at a foreign research institute

o   Training in handling of chemical materials, and pre- and post-processing of NaOH solution and plant material for 14C analysis, Centre for Isotope Research Laboratory, University of Groningen (2010)

Management and Didactic Skills Training

o   Supervising three MSc students with theses entitled 'Explaining black carbon observations at the Veenkampen station in Wageningen' (2013), 'Measurement and Modelling Ambient Air Quality in Arba Minch, Ethiopia' (2014), and 'NO$_x$ concentrations and exposure in Amsterdam and over Europe: First assessment based on joint high resolution WRF modelling and observations' (2014)

Oral Presentations

o   *Modelling ^{14}C exchange to estimate regional fossil fuel emissions*. Buys Ballot Research School: Fall Symposium, 27-29 October 2010, Callantsoog, The Netherlands
o   *Using plants as $\Delta^{14}CO_2$ samplers: the importance of crop growth modelling*. SENSE Symposium: Modelling and observing Earth System Compartments, 22 February 2011, Wageningen, The Netherlands
o   *High-resolution simulations of the $\Delta^{14}CO_2$ gradients from fossil fuels and nuclear power plants over Europe*. American Geophysical Union: Fall Meeting, 3-7 December 2012, San Francisco, United States
o   *High-resolution modelling of $\Delta^{14}CO_2$ over Europe: possibilities, limitations, and implications for $^{14}CO_2$ observations and fossil fuel CO_2 emissions verification*. Geochemical Club Luncheon Seminar, 4 March 2013, Norwich, United Kingdom

SENSE Coordinator PhD Education

Dr. ing. Monique Gulickx